



UNIVERSITÀ DEGLI STUDI DI NAPOLI

FEDERICO II

Facoltà di Ingegneria

Tesi di Dottorato di Ricerca in Ingegneria dei Sistemi Meccanici

XXVII Ciclo

**DISTRIBUTED POLYGENERATION IN LOAD
SHARING APPROACH**

Coordinatore del Corso

Ch.mo Prof. FABIO BOZZA

Relatore

Ch.mo Prof. MAURIZIO SASSO

Candidato

MICHELE CANELLI

INDEX

LIST OF PERSONAL PUBLICATIONS	4
INTRODUCTION.....	6
CHAPTER 1: Investigation on the performance of a micro-cogeneration system in different applications	19
1.1 System configuration	19
1.2 Modelling approach	24
1.2.1 Micro-cogenerator model	25
1.2.2 Thermal energy storage model	31
1.2.2.1 Mathematical model	35
1.2.2.2 Test facility.....	37
1.2.2.3 Calibration and validation of the model.....	39
1.2.2.4 Simulation of solar thermal heating system.....	53
1.2.3 Other components.....	57
1.3 3-E analysis.....	58
1.4 Optimal thermo-economic control of the MCHP system with load sharing application	61
1.4.1. User description.....	62
1.4.2. Operating system optimization	65
1.4.3. Discussion and results	71
1.5 Microcogeneration in buildings with low energy demand in load sharing application	74
1.5.1. Users description	75
1.5.1.1 Residential user	75
1.5.1.2 Office user.....	80
1.5.1.3. Load sharing.....	82
1.5.2. Discussion and results	85

1.6 Integration between electric vehicle charging and a micro-cogeneration system.....	93
1.6.1. User description.....	94
1.6.2. Discussion and results	100
CHAPTER 2: Dynamic simulations of hybrid energy systems in load sharing application	112
2.1 System configuration.....	112
2.2. Model description.....	116
2.3. Simulation inputs and control approach	119
2.3.1 Domestic hot water demand.....	119
2.3.2 Electric load profile	120
2.3.3 Equipment capacity	121
2.3.4 Control strategy	123
2.4. Energy, environmental and economic analysis methodologies.....	124
2.5. Discussion and results	125
CHAPTER 3: Energy planning by means Urban Energy Maps: CCHP for small urban districts	130
3.1 Energy planning of urban districts: methodology	131
3.2 Evaluations of building energy performances.....	132
3.3 Urban energy maps	136
3.4 The polygeneration equipment	139
3.5 Discussion and results.....	143
CONCLUSION	148
Nomenclature	153
Reference.....	160
LIST OF FIGURES.....	172
LIST OF TABLES.....	176

LIST OF PERSONAL PUBLICATIONS

- I. “Descrizione dei modelli dei sistemi fisici e degli algoritmi sviluppati per il controllo e l’ottimizzazione di micro_poligeneratori distribuiti. Validazione sperimentale ed analisi di sensitività”, G. Angrisani, M. Canelli, A. Rosato, C. Roselli, M. Sasso, S. Sibilio, Report Ricerca Sistema Elettrico RdS/2012/077, 2012, http://www.enea.it/it/Ricerca_sviluppo/documenti/ricerca-di-sistema-elettrico/efficienza-energetica-servizi/2011/077-rds-pdf
- II. “Optimal thermo-economic control of a micro-cogeneration system in thermal load sharing approach”, G. Angrisani, M. Canelli, A. Rosato, C. Roselli, M. Sasso, S. Sibilio, Proceeding of the 3rd edition of the International Conference on Microgeneration and Related Technologies, Naples 15-17 April 2013.
- III. “Load sharing with a local thermal network fed by a microcogenerator: Thermo-economic optimization by means of dynamic simulations”, G. Angrisani, M. Canelli, A. Rosato, C. Roselli, M. Sasso, S. Sibilio, Applied Thermal Engineering (2014), doi: 10.1016/j.applthermaleng.2013.09.055.
- IV. “Microcogeneration in buildings with low energy demand in load sharing application”, G. Angrisani, M. Canelli, C. Roselli, M. Sasso, submitted to Energy Conversion and Management.
- V. “Integration between electric vehicle charging and micro-cogeneration system”, G. Angrisani, M. Canelli, C. Roselli, M. Sasso, accepted from Energy Conversion and Management.
- VI. “Distributed generation systems for thermal and electrical demands of urban districts: experimental and numerical application to an italian historical center”, F. Ascione, M. Canelli, R.F. de Masi, M. Sasso, G.P. Vanoli, Proceeding of the 3rd edition of the International Conference on Microgeneration and Related Technologies, Naples 15-17 April 2013.
- VII. “Combined cooling, heating and power for small urban districts: An Italian case-study”, Ascione, F., Canelli, M., De Masi, R.F., Sasso, M., Vanoli, G.P, Applied Thermal Engineering (2014), doi: 10.1016/j.applthermaleng.2013.10.058

- VIII. "Calibration and validation of a thermal energy storage model: influence on simulation results", G. Angrisani, M. Canelli, C. Roselli, M. Sasso, *Applied Thermal Engineering* (2014), doi:10.1016/j.applthermaleng.2014.03.012.
- IX. "Dynamic simulations of hybrid energy systems in load sharing application", M. Canelli, E. Entchev, M. Sasso, L. Yang, M. Ghorab, *Applied Thermal Engineering* (2015), doi:10.1016/j.applthermaleng.2014.12.061
- X. "Thermodynamic analysis of compression/absorption heat pump", M. Canelli, C. Roselli, A. Russo, M. Sasso, submitted to ASME-ATI-UIT 2015 Conference on Thermal Energy Systems: Production, Storage, Utilization and the Environment, 17–20 May 2015, Napoli, Italy.
- XI. "Optimal operation of a District Heating power plant with Thermal Energy Storage", G. Gambino, M. Canelli, A. Russo, M. Himanka, M. Sasso, C. Del Vecchio, L. Glielmo, submitted to the 54th IEEE Conference on Decision and Control, 15-18 December 2015, Osaka, Japan.

INTRODUCTION

In European Union the final energy consumption in residential and commercial buildings represents around 40% of the total final energy use and it is responsible for 36% of Carbon Dioxide equivalent emissions [1]. In order to reach the climate and energy targets of European Union for 2020 and beyond [2] it is important to reduce the primary energy consumption in these two sectors. In the context of European Union targets the diffusion of distributed polygeneration systems can significantly contribute to reduction of emissions attributed to the residential and commercial sectors.

The term “polygeneration” represents the combined production of more than one energy vectors (i.e. electricity, heat, cooling, chemical products, etc.) from a single primary energy source. Most common is cogeneration, or Combined Heat and Power (CHP) [3], which involves the combined production of electric and thermal energy. The trigeneration systems, or Combined Cooling, Heating and Power (CCHP) [3], allow the simultaneous satisfaction of three energy requirements: electricity, cooling and heating. Throughout this thesis, the term polygeneration is used as a generalized term to refer to both cogeneration and trigeneration systems.

In general the term distributed generation (DG) refers to the use of stand-alone or grid connected small, modular electric generation devices which are located close to the users [4]. Therefore DG systems are generally located close to the power demand, on the customer side of the meter or on the distribution network. The system size ranging from few kilowatts to few megawatts [4].

The Figure A is useful to compare the DG system with respect to the centralized one, analyzing the traditional energy flow which, starting from required primary source, is converted, usually in a large plant, and then transmitted to the end-user to satisfy energy demands. In cases of DG, the energy flow is converted in a decentralized energy conversion plant, very close to the end-user, and then distributed to the final appliances. It is obvious as the transition from the centralized to decentralized system that is usually approached as DG allows reducing the losses due to distribution and/or transmission of working fluids or electricity and energy cycling losses [3]. On the other hand the miniaturization process leads to a reduction of the energy performance of the

conversion device due to the “size effect”. Therefore the DG does not always lead to energy savings and pollutant emissions reduction. Therefore, there is the need to support the diffusion of on-site small complex energy conversion devices based on polygeneration system. Consequently the term distributed polygeneration refers to a particular case of DG where the generation system is a polygenerator.

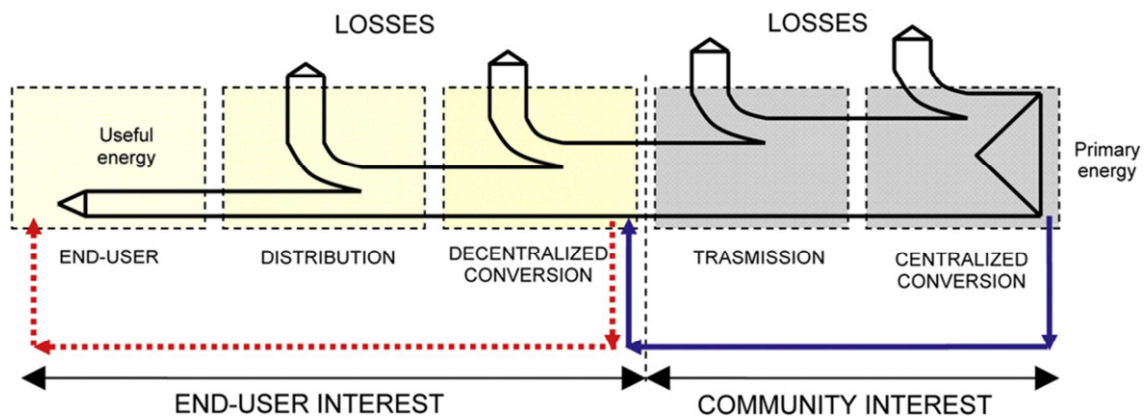


Figure A. Sankey diagram of energy conversion processes.

Most of this thesis work refers to distributed polygeneration systems characterized by a few kilowatts electric capacity. According to the European Directive 2004/8/EC [5], the prefix “micro-” (i.e. micro-cogeneration, micro-trigeneration, micro-polygeneration) refers to a device characterized by a power rating less than 50 kW_{el}, while different authors, in literature, refer to a limit of 15 kW_{el} [6][7][8].

The diffusion of micro-cogeneration (MCHP, Micro Combined Heat and Power) and micro-trigeneration (MCCHP, Micro Combined Cooling, Heating and Power) systems can significantly contribute to reduction of primary energy consumption and CO₂ emissions attributed to the residential and commercial sectors. In recent years different researches have been conducted on the analysis of MCHP and MCCHP based on different technologies.

In [9] the authors analyzed the energy, environmental and economic feasibility of micro-trigeneration system in a residential building under varying operating conditions. Results indicate that compared to separate generation, MCCHP has the potential to deliver

significant primary energy (17÷48%) and emission savings (up to 50%), although the extent of such savings are strongly dependent on the efficiency of the alternative separate generation available. The system's economic performance was highly susceptible to the operating conditions. Therefore this study highlighted the financial risks related to the installation of a MCCHP system in a residential sector.

In [10] the authors investigated on thermo-economic performance of different MCHP systems based on reciprocating internal combustion engines and Stirling engines. The analysis was performed in two European locations (Italy and Germany) and the results obtained highlighted a primary energy savings up to 27% (Italy) and 36% (Germany) and a pollutant emissions reduction up to 33% (Italy) and 35% (Germany). Moreover the study showed that the economic results strongly depend on the annual operational hours of the micro-cogeneration system.

In [11] an investigation about the energy, economic and environmental feasibility of a micro-cogeneration system for residential application was performed by means of dynamic simulations, considering thermal insulated residential buildings. The simulation results showed that the proposed system allows a reduction of primary energy consumption, carbon dioxide emissions and operating costs with respect to the conventional system. Moreover the duration diagram of the space heating load highlights the small operational hours of the MCHP system.

In [12] the energy performances of a micro-cogeneration system based on Polymer Electrolyte Fuel Cell (PEFC) are investigated. The MCHP system was installed in a residential building in Japan. The study highlighted how the primary energy saving of the proposed system with respect to a reference one strongly depends on the operation condition of the MCHP. The primary energy saving is in the range 1.3÷18.4% and depend on the electric and thermal energy requirements from the user.

In [13] the authors investigated on the energy and environmental performance of an internal combustion engine cogenerator in residential building located in different Canadian Regions. The primary energy saving analysis showed positive value for existing Canadian houses in all regions excluding Quebec due to the predominance of hydro generated electricity in that province. From environmental point of view, the MCHP

system is a favorable alternative with respect to conventional energy conversion systems in all of the houses in the five climatic regions of Canada.

In [14], a trigeneration system consisting of a micro-cogenerator that interacts with a desiccant-based air handling unit, equipped with a silica-gel desiccant wheel, has been analyzed. The system provides the air-conditioning service to a university room during summer and winter periods and thermal energy for domestic hot water production. The MCCHP leads to promising results, in terms of primary energy saving (7.7%) and equivalent carbon dioxide emissions reductions (15.3%). The economic analysis showed the high pay-back period for the trigeneration system.

All this study highlighted how the energy and the environmental benefits of micro-polygeneration systems in residential and commercial users cannot be disputed, but some obstacles could jeopardize the diffusion of these promising technologies. Firstly, the high specific investment cost (€/kW) of the micro-polygeneration system due to size effect and immature state of some technologies leads to long investment's payback period. In addition, the installation of polygeneration systems in residential or tertiary users bring about low operating hours per year of the system, and consequently high payback periods. This aspect is more obvious in Mediterranean area due to the relatively mild climatic conditions, which negatively affects the operating hours per year.

For the electricity network the advantages or disadvantages related to the DG depend on its penetration. With low and moderate use of distributed generation, costs can be saved while with very high penetration the network may even need to be reinforced [7].

Historically, distribution and transmission network are designed to transport power from central power plants to dispersed users. Broad diffusion of DG would change this concept, because electricity generation in distributed power plants implies a change in loads and currents in the electricity network. This aspect may affect system reliability, power quality, and congestion in the network [7]. As mentioned above, a high penetration of distributed polygeneration would have beneficial effects on the system, since currents in transformers, transmission and distribution line would be reduced. As a consequence, transmission and distribution losses are reduced and investments in this network might be deferred or suspended. However, increased market penetration of distributed polygeneration could also raise several challenges for network operators.

The capacity of equipment (transformers, power lines, fuses, switches, etc.) may not be suitable due to changed or reversed power flows [7]. With many distributed generators, the voltage could vary beyond established limits [7]. In some cases, protection of the distribution network may become more difficult with distributed generators. DG may, depending on the circumstances, either increase or decrease the power quality of the distribution network through, for example, transient voltage variations or harmonic voltage distortions [7].

In this thesis, in order to overcome or reduce some negative aspects related to the diffusion of distributed polygeneration different strategies are investigated. One interesting solution could be the load sharing approach [15], which consists in the introduction of a small electric and thermal micro-grid allowing the sharing of electric, thermal and cooling loads among a group of diversified end users. By sharing the load among different types of final users (residential, commercial, institutional, etc.) it is possible to increase the operating hours of the MCHP system. In moderate climatic conditions, like Italian ones, typically characterized by low thermal load and few hours of heating system operation the MCHP can achieve satisfying economic, energy and environmental performance. In fact, as an example, the thermal load of residential users typically occurs in the evenings and early mornings, while for commercial users it occurs during the day time hours. By coupling these two users it can be considered a single common energy conversion system to satisfy their thermal energy requirements, increasing its operating hours. In addition, the introduction of a small micro grid in load sharing approach could reduce the load flow between the micro grid and the distribution network increasing the percentage of self-consumed electricity. In this way the micro grid could function closely as "island" mode and reduce the impact of the large-scale diffusion of distributed generation.

Moreover the introduction of an Energy Service Company (ESCO) that manages a large number of systems distributed on the territory, often referred as Virtual Power Plant (VPP), could obtain some advantages. A VPP consists of a number of geographically distributed power generation units that are managed by a centralized control system [7]. The VPP could offer various ways of reducing costs and increasing revenues. Firstly, there are positive effects related to the managing of a high number of polygenerator

system, for instance, buying a number of MCHP units or service contracts could lead to volume discounts, as well as discount for fuel needs [7]. Therefore the ESCo can often purchase natural gas and additional electricity at lower cost compared to the single user. The ESCo could help the network operators providing ancillary service and obtaining economic advantage. Moreover the integration of several systems in one operational unit could lead to lower maintenance cost and minimize the fuel use due to optimized operation strategy. In case of VPP the electricity produced could be marketed differently because the specific transaction cost can be lowered and certain regularity requirement can be fulfilled (i.e. minimum capacity required to participate to the electricity market) [7]. The energy service company often manages the MCHP (or CHP) systems according to a thermo-economic optimization control, because it is interested in revenues maximization or cost minimization. Different study analyzed the optimal operation strategy of distributed polygeneration systems.

In [16], an optimal online operation strategy for MCHP systems, which is more efficient than the conventional pre-determined (either heat-led or electricity-led) operation strategies, is presented. A generic optimal online linear programming optimizer was developed for operating a MCHP system, capable of minimizing the daily operation costs.

In [17], an energy supply chain network based on residential-scale microgeneration systems is proposed, modeled and optimized. A mathematical programming framework is developed for the operational planning of such energy supply chain networks. The minimization of total costs constitutes the objective function. Additionally, an alternative micro-grid structure that allows the heat interchange within subgroups of the overall micro-grid is proposed.

In [18], an energy dispatch algorithm that minimizes the cost of energy (electricity from the grid and natural gas for the engine and the boiler), based on energy efficiency constrains for each component, is presented. A deterministic network flow model of a typical CHP system is developed as part of the algorithm. This algorithm was used in simulations of a case study on the operation of an existing MCHP system. The results from the simulation demonstrate the economic advantages resulting from optimal operation.

In [19], a general environmental methodology is applied to a district heating (DH) system with centralized heat pumps, cogeneration units and an auxiliary furnace, supplemented by decentralized heat pumps; it includes the thermodynamic, economic, and environmental models of the systems. Optimization results, in terms of synthesis, design and operation of the network, are presented in [20].

In [21], a numerical optimization method has been applied to a small-scale cogenerator, based on a micro-gas turbine and driven by the heat demand of a medium-size building located in the north of Portugal. The mathematical model yields a non-linear objective function, subject to physical constraints of system operation, and defined as the maximization of the annual worth of the CHP system. A purchase cost equation was used for each major plant component, taking into account size and performance variables.

Others possible solutions analyzed in this thesis are related to the increasing share of self-consumed electricity “produced” by the MCHP system. In this way it is possible to reduce the potential impact related to the large diffusion of distributed polygeneration systems and improve the economic performance of the MCHP. In order to increase the share of self-consumed electricity two different strategies are analyzed. The first consists in the careful selection of the user in which the MCHP system is installed, while the second relies on the interaction between the MCHP system and the electric vehicles (EVs) charging. As regard to the choice of user it is important to highlight that the European Union through the Directive 2010/31/EU [22] that integrates the 2002/91/EC [23] promotes the energy performance improvement in new buildings and existing buildings that are subject to major renovation. Furthermore the European Union is aware that the existing building stock represents the most important sector for potential energy savings, through the directive 2012/27/EU [24], and it established that the rate of building renovation needs to be increased. In this context, in a near future the building envelope will be more energy efficient with higher level of insulation compared to the present building stock. The reduction of the heating demand due to the improvement of the thermal characteristics of the building envelope requires a careful assessment of the benefits connected to the installation of MCHP systems in residential or tertiary sectors. The smaller thermal load with respect to the current building stock

leads to a reduction of the micro-cogenerator size, with negative effects on energy efficiency and specific investment costs [3]. As previously mentioned, the introduction of a small thermal micro-grid allows to match several type of users (residential, commercial, institutional, etc.) in order to increase the cumulative load and the operational hours of the MCHP system (load sharing approach). Therefore, in addition to analyze the choice of the users type (residential, commercial, tertiary, etc.), it is essential to evaluate the technical and economic feasibility of the installation of an MCHP system in a building with low thermal energy demand.

As regard to the second possibility, it is related on the interaction between the electric vehicle charging and an MCHP system. It should be pointed that transport sector is responsible for around 25% of European Union (EU) greenhouse gas emissions [25]. Road transport alone represents about 20% of the EU total emissions of carbon dioxide (CO₂). Furthermore, the emissions from transport sector strongly increased in the last years (37% between 1990 and 2007) due to the increased needs of mobility [25]. Due to the industrial delocalization, the emission weight associated to transport sector will increase in many EU countries. In addition to the global emissions, road transport is a significant contributor to air pollution in urban area (local impact). Recent researches consistently indicate that the declining quality of air in urban area causes serious health problems [26]. In the near future the diffusion of plug-in electric vehicles (EVs), which is already occurring in countries such as Japan [27], could play an important role in the reduction of the local impact related to the transport sector and improve air quality in urban area. The diffusion of EVs could help to reduce the almost-total dependence of the transport sector on oil and consequently on exporting countries. The electric mobility moves the energy demand from oil to electricity. A great advantage of electricity use in the transport sector is that it can be produced from any primary energy source. This offers the opportunity to use in road transport different high conversion efficiency technologies and/or renewable energy sources. So the emerging trend towards the electrification of transport sector clearly benefits from the increasing share of renewable electricity and from the growing average electric efficiency of the thermo-electric power plants mix. Furthermore, EVs have a significant lower cost per kilometer with respect to internal combustion engine vehicles [28].

Nevertheless the EVs battery charging will increase the electricity demand, so this technology could have a big impact on the electric network. Different researches highlight that, in high penetration of EVs scenario, the charging of the EVs is not applicable for the current distribution network.

In [29] the authors proposed a method to evaluate the impacts of uncoordinated plug-in EVs charging on the electric distribution grid during peak periods. The impact analysis was performed in terms of voltage violations, power losses and line loading, and implemented on a real distribution system in Canada. The authors showed that there are significant impacts on distribution networks due to EVs charging.

Ref. [30] analyzed the effect of wide penetrations of EVs on distribution and transmission network. The results showed that 100% penetration of electric vehicles may cause serious overloading of the medium voltage transformers.

In [31] the authors proposed a stochastic modeling technique for analyzing impacts of EVs charging demand on distribution network. Numerical results highlighted that smart charging could reduce security problems due to high diffusion of EVs. The smart charging of EVs allows customers and network operators to manage the charging profile in order to get technical and economic benefits; it can be considered as a specific demand side management of EVs.

In order to meet the growing load due to the diffusion of EVs, the construction of new infrastructures seems to be required. To avoid or at least contain the huge investment needed to reinforce the electric network and to reduce the negative effects on electric distribution network (transformers and line saturation, increase of electrical losses, voltage deviation, etc.), several studies investigated the advantages connected to a smart charging of EVs [32].

Some papers investigated the possible synergy between micro-cogeneration (MCHP, Micro Combined Heat and Power) and electric vehicle charging. In fact the introduction of MCHP systems allows reducing the impact of the EVs charging on the electric grid.

In [33] the authors analyzed the advantages related to the charging of an EV with an MCHP system in a single detached house in Ottawa (Canada). From this study, an increase of the self-consumed electricity due to the EV battery charging emerged. This aspect led to economic advantages related to a better economic valorization of the “produced” electricity.

In ref. [34] the performance of a fuel cell cogenerator system combined with a plug-in hybrid EV was analyzed by an optimal operation planning model based on mixed integer linear programming. The analysis was carried out in a country, like Japan, where the reverse power flow from residential MCHP to the electric grid is not allowed. The authors highlighted how the introduction of EV charging allows increasing the electric capacity factor of the MCHP.

Refs [35][36] analyzed the energy, environmental and economic performance of a residential building-integrated micro-cogeneration system. This study also analyzed the effect of the introduction of overnight EV charging, that allows an increase of energy performance in the case of electric load-following operation of MCHP; otherwise the EV charging slightly reduces the energy performance in the case of thermal load-following operation. Including the overnight charging of EV, the MCHP system provided better environmental and economic results in case of electric load-following operation.

All these studies analyze the effects of EV charging on the MCHP performance without considering the influence of the charging strategy on the whole system performance.

Another interesting solution analyzed in this thesis refers to the introduction of hybrid energy system that combine two or more energy conversion devices, or two or more fuels for the same device, that when integrated, overcome limitations inherent in either [37], [38]. Among them, the hybrid renewable energy systems are hybrid energy system that integrates the use of conventional and renewable energy sources [39]. The use of renewable energy sources offers notable energy and environmental benefits by reducing dependence on fossil fuel and carbon dioxide emissions to the atmosphere. Otherwise some technologies using random renewable energy source, such as solar or wind energy, requires some back-up generating capacity due to their intermittent nature. Therefore coupling different technologies based on renewable and conventional source is possible to use the strength and disadvantages of one source to counterbalance those of the other. In fact a hybrid renewable energy system combine the high primary energy saving and the emission reduction related to the use of a renewable energy source to the reliability of an energy system powered by a traditional energy vector (electricity, natural gas, etc.).

The last analyzed solution consists in the use of Urban Energy Maps (UEMs) to locate an urban area suitable for the introduction of a polygeneration system. An analytical methodology aimed to characterize the energy performance of a wide building stock is proposed for both winter and summer [40]. The method was applied to the entire historical center of Benevento (Italy) and the results of the methodology are transferred into Geographic Information Systems (GISs) in order to create the Urban Energy Maps. These thematic maps could assist planners and stakeholders in to identify energy, environmental and economic effects of energy improving measures. Therefore the UEMs are a suitable tool dedicated to local government, usable for advanced energy planning. Using this tool is immediate to obtain a visual identification of energy performances and criticalities and evaluate possible improvement measures, with reference to whole city districts. In this thesis the UEMs are utilized to investigate on the installation of CCHP system, designed for satisfying the overall energy demands of a city block, by means of proper heating, cooling and electrical energy nets.

The thesis has been divided into three chapters. In the first part of chapter 1 the analyzed micro-cogeneration system, which consists of a 6 kW_{el} MCHP system, a peak boiler and a Thermal Energy Storage (TES), was introduced. The analyzed system and its energy interaction with the end users was modelled by means a dynamic simulation software. The models of the main components and their calibration and validation procedure, which was based on experimental and literature data, were described too. After, the energy, environmental and economic performances of the analyzed MCHP system were evaluated in different conditions. In the first analyzed case, the end users consist of a residential and an office building in load sharing approach. The MCHP system was managed by means of a thermo-economic control function, aimed at minimizing the operation cost of the system. Simulations have been performed considering different scenarios in terms of climatic conditions and prices of energy vectors (in order to evaluate the effects of the introduction of ESCo); the results show that the thermal load sharing approach is an effective way to increase the operating hours of the MCHP system in moderate climatic conditions, like Italian ones, typically characterized by low thermal load and few hours of heating system operation, achieving satisfying economic, energy and environmental performance. In the second analyzed

case, the users consist of a residential and an office building characterized by a higher level of thermal insulation with respect to the current building stock. A load sharing strategy between a multifamily residential building and an office one is taken in account. Particular attention is given to the estimation of electric load of the different users as the economic profitability of an MCHP system is strongly influenced by the amount of self-consumed electricity. The results indicate that the installation of MCHP systems in buildings with low thermal energy demand in load sharing allows increasing the percentage of self-consumed electricity reducing the bidirectional electricity flow between the users and the external grid, reducing the impact on the grid itself due to the large diffusion of distributed generation systems. In the last section of chapter 1, the interaction between an MCHP system, the EV charging and a typical semidetached house is investigated by means of dynamic simulations. The analysis is carried out in two different locations (Torino and Napoli) in order to evaluate the effects of climatic conditions on the system performance. A parametric analysis with respect to the daily driving distance of the EV is carried out in order to highlight the effect of this parameter on the simulation results. Furthermore two EV charging strategies are analyzed in order to maximize the share of self-consumed electricity.

The results state that operating cost reductions of the proposed system with respect to the reference one up to 60% can be achieved. Moreover the optimized charging strategy, with respect to the normal one, allows decreasing the operating cost of a percentage up to 11%.

In the chapter 2 the introduction of micro-cogeneration hybrid energy systems in load sharing approach are investigated using dynamic simulations. Once the advantage of load sharing approach was demonstrated, the performances of two different hybrid systems in load sharing scenario were analyzed. The first hybrid system consists of a micro-cogenerator based on FC and a Ground Source heat Pump (GSHP) while the second consists of Photovoltaic Thermal (PVT) collectors and a GSHP. Therefore both the hybrid systems are based on a MCHP and a GSHP, but only the latter represents a renewable hybrid energy system due to the presence of PVT collectors. The performances of these two systems were also compared to a stand-alone GSHP system in order to analyze the advantages of hybrid systems to a single GSHP system.

Finally, in the chapter 3 the use of UEMs to localize an urban area suitable for the introduction of a polygeneration system is investigated. Firstly a methodology able to estimate the energy demand of the existing building stock is presented. Secondly, the methodology was applied to the historical centre of Benevento in order to characterize its energy performance. Subsequently, the study highlighted the potentiality of UEMs in order to design a polygeneration system and a district heating and cooling network able to meet the energy requirements of a cluster of users.

Part of the research activities reported in this thesis was performed during the research period held at CanmetENERGY Research Centre, Natural Resources Canada, in Ottawa (Ontario, Canada).

This thesis work reports the main research activities results performed during the PhD period, that are also published in international journals and conferences as reported in the list of personal publications.

CHAPTER 1: Investigation on the performance of a micro-cogeneration system in different applications

In this chapter, the performances of a micro-cogeneration system that consists of an MCHP, a TES and a peak boiler are analyzed by means dynamic simulations. In particular, in section 1.1 the system configuration and the physical characteristics of the main components are described. After, in the section 1.2, the modelling approach is introduced starting from dynamic simulation software (TRNSYS) overview. Subsequently the models of the main components and their calibration and validation procedure are analyzed. In section 1.3 the typical 3-E simplified approach (Energy, Environmental and Economic approach) and the main assumption about the definition of the parameters used in the energy, environmental and economic analysis are presented. In subsequent sections the performances of the analyzed MCHP system are evaluated in different conditions (type of users, climatic condition). In particular in section 1.4 the end users consist of a residential and an office building in load sharing approach. The MCHP system is managed by means of a thermo-economic control function, aimed at minimizing the operation cost of the system. Simulations have been performed considering different scenarios in terms of climatic conditions and prices of energy vectors (in order to evaluate the effects of the introduction of ESCo). In section 1.5, the users consist of a multifamily residential building and an office one in load sharing approach. Both the buildings are characterized by a low thermal energy demand with respect to the current building stock. Finally in section 1.6 the interaction between an MCHP system, the EV charging and a typical semidetached house is investigated considering different climatic conditions and two EV charging strategies.

1.1 System configuration

The analyzed MCHP system consists of three main components (Figure 1.1):

- micro-cogenerator;
- thermal energy storage;
- peak boiler.

In Figure 1.1 the configuration of the analyzed system is showed.

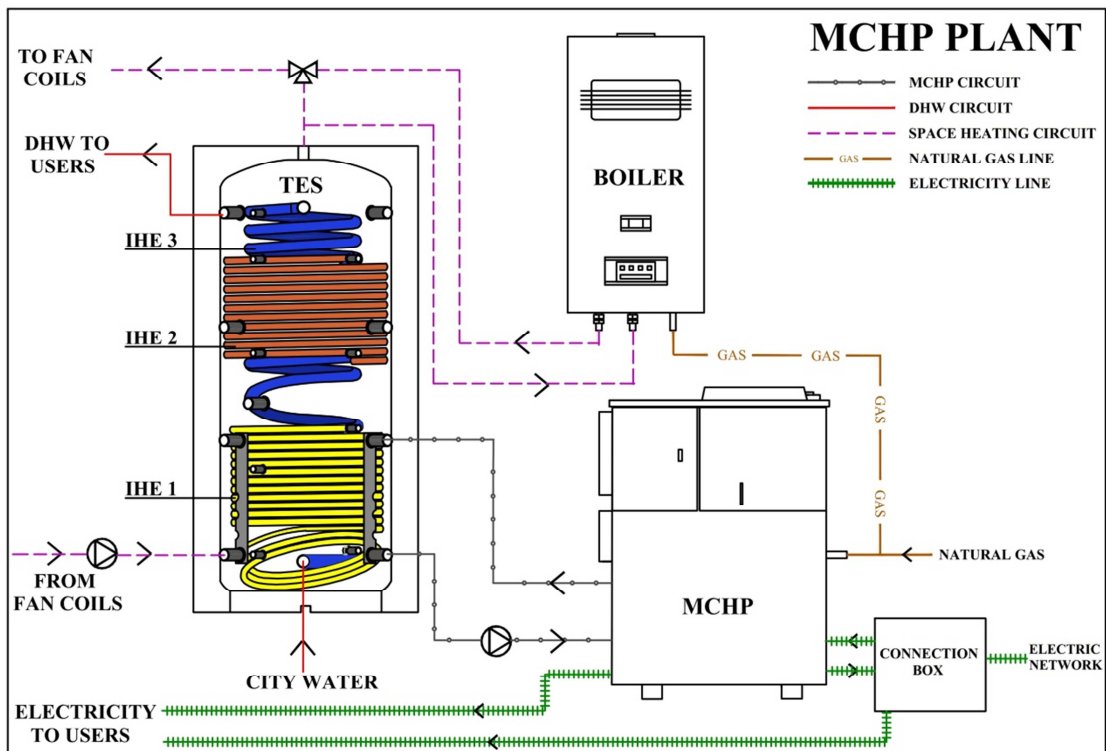


Figure 1.1. System configuration.

The installed MCHP is manufactured by AISIN-SEIKI, a Japanese TOYOTA group company, model GECC60A2N (Figure 1.2) [41].



Figure 1.2. The AISIN-SEIKI micro-cogenerator.

It is based on a reciprocating internal combustion engine fuelled by natural gas. The main characteristics of the MCHP are reported in Table 1.1 [41]. It has a nominal electric power of 6.0 kW and a nominal thermal power of 11.7 kW. Despite its compact design, the MCHP has high rated performance: Primary Energy Ratio (PER, namely the ratio of the useful thermal and electric energy supplied to the end-user to the primary energy input) of 85.0%, electrical efficiency of 28.8% and thermal efficiency of 56.2%.

Table 1.1. MCHP manufacturer data [41].

Power [kW]	Input	20.8
	Electric	6.0
	Thermal	11.7
Efficiencies [%]	Electric	28.8
	Thermal	56.2
	PER	85.0
Fuel	Natural gas	
Weight [kg]	465	
Size [mm]	Height	1500
	Width	1100
	Depth	660
Engine	Displacement [cm ³]	952
	Rotational speed [rpm]	1600-1800
Generator	Permanent magnet, synchronous generator with 16 pole	
Sound level [dBA]	54	

Figure 1.3 shows the heat recovery circuit of the AISIN MCHP system. The thermal energy is recovered from the engine jacket and the exhaust gas and it is transferred to the water in a brazed plate heat exchanger. Two thermostatic valves manage the operation of the MCHP cooling circuit. If the cooling fluid temperature is lower than 55°C the plate heat exchanger is by-passed (2) in order to ensure a rapid engine warm-up. Otherwise if the cooling fluid temperature is higher than 75°C part of it flows in the radiator (7) in order to disperse the exceeding heat and preserve the engine operation. In a normal operation mode (cooling fluid temperature between 55°C and 75°C) the engine coolant outlet from the engine (1) crosses the plate heat exchanger (5) and then the radiator is bypassed (6). In each operation condition the engine coolant exit to the thermostatic valve (3) crosses the exhaust gas heat exchanger (4) and flows in to the reciprocating internal combustion engine.

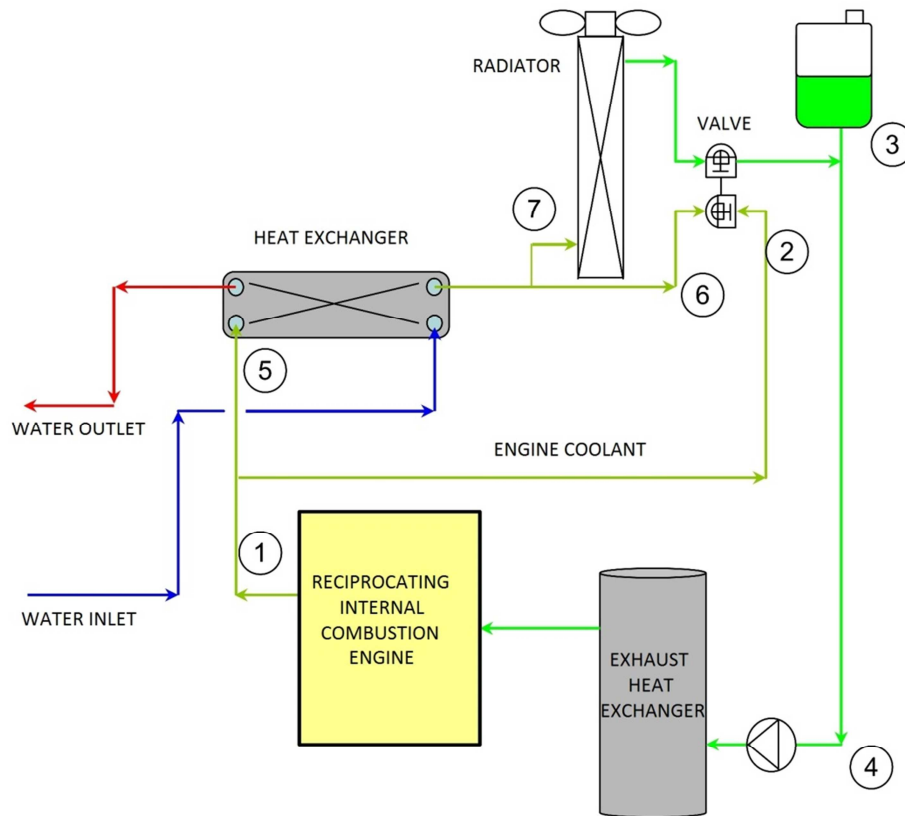


Figure 1.3. Thermal recovery circuit of the AISIN MCHP.

The MCHP can operate in two modes: “electric” led and “heat” led. In the first case it can deliver a variable electrical power from 0.3 kW to 6.0 kW in order to follow the electric load of the user; in the second case the system can operate only at full electric and thermal load with ON/OFF regulation. In the analyzed case the MCHP operates in “heat” led mode at full electric power; therefore, the MCHP is turned on and off according to the temperature of the TES. According to the supply temperature of the MCHP (65°C maximum), and in order to limit the use of the peak boiler, the temperature inside the TES is kept in the range 50-55°C. In particular the MCHP is turned off when the temperature inside the TES is greater than 55°C and it is turned on when the temperature drops below 50°C. The choice of TES operation temperature is also related to the supply temperature of fan coils (50-55°C) installed in the end users. If the electricity output to the MCHP system is greater than the electricity user demand a part of it is sold to the electric network.

The MCHP system is sized in order to meet the base of the user thermal load, while the peak loads are met by means a peak boiler fuelled by natural gas. Therefore the size of this component (peak boiler) depends on the thermal load of the final user; for this reason, in the following sections, a different peak boiler sizes will be introduced for each application.

The TES is a typical sensible heat storage using water as storage medium (Figure 1. 4).



Figure 1. 4. Analyzed thermal energy storage.

The storage tank is built from carbon steel, with a capacity of 1,000 liters. It has three heat exchangers: two of them, placed in the lower and upper part of the storage, are carbon steel heat exchangers that can interact with external energy conversion devices. The third one, which extends along the whole height of the storage, is a stainless steel corrugated coil heat exchanger for domestic hot water “production”. A third energy conversion device can directly interact in open circuit with the fluid stored in the tank. The tank is insulated with a layer of 100 mm thick polyurethane.

Figure 1.1 shows how the different components are connected each other. The MCHP thermally interacts with the lower internal heat exchanger (IHE1) of the TES. The IHE2 is not used. The IHE3 is used for DHW “production”. The heat transfer fluid (water) of the

space heating circuit directly interacts in open circuit with the fluid stored in the TES. If the water temperature at the outlet of the TES is lower than 50 °C, the peak boiler is turned on in order to keep the supply temperature, to the fan coils, in the range 50-55 °C.

1.2 Modelling approach

The analyzed system and its energy interaction with the end users is modelled by means TRNSYS (TRaNsient SYstem Simulation program) [42], a dynamic simulation software. It was developed by University of Wisconsin's Solar Energy Lab and the University of Colorado's Solar Energy Applications Lab in the 1970s. It is a transient simulation software widely used, in the field of energy, to simulate the interaction between buildings and energy conversion systems. It is used by engineers and researchers around the world to validate new energy concepts, from simple domestic hot water systems to the design and simulation of buildings and their equipment, including control strategies, occupant behavior, alternative energy systems (wind, solar, photovoltaic, hydrogen systems), etc.

TRNSYS has a modular structure and each component of the system is modelled by means of subroutines ("types") available in its library [42][43]. The components can be connected together to create complex systems. A graphical interface (Simulation Studio) allows to build the model by means the connection of the outputs one component to the inputs of another. Once the necessary links between components are made and values of each component parameters (time independent values) are assigned the Simulation Studio interface can build the TRNSYS input file. TRNSYS simulation engine (called the kernel) reads and processes the input file, iteratively solves the system, determines convergence, and plots and/or saves system variables.

TRNSYS software is able also to model the thermal behavior of a building by means the TRNBuild tool; it is an interface for creating and editing all enter inputs data for multizone buildings model. It allows the user to specify all the non-geometry information required by the TRNSYS building model, such as the building structure details (wall and layer material properties, windows optical properties), ventilation and infiltration profiles, internal gains caused by occupancy and use, heating and cooling

schedules, etc. The model is defined in TRNBuild tool and it is linked with Simulation Studio through the Type 56 component.

In order to model the transient thermal behavior of an energy system the weather data of different locations is often required. Therefore TRNSYS has different types able to read standard or user defined format weather files. In this way, simulations can be performed using available weather data based on weather stations measurements. Some weather data are distributed with TRNSYS; they are based on two data sources:

- US-TMY2 (Typical Meteorological Year) data sets from US National Renewable Energy Lab (NREL) and derived from the 1961-1990. The dataset includes 237 locations in the United State, and 2 files for Puerto-Rico and Guam.
- Selected worldwide stations from Meteonorm [44] (distributed under license from Meteotest), that includes more than 1000 locations, in about 150 countries. The weather data are available in "TMY2" output format.

In the following sub-sections the main models used in the simulations are described.

1.2.1 Micro-cogenerator model

The microcogeneration system was simulated through a dynamic model developed within IEA/ECBCS Annex 42 [45][46]. It is a combustion-based cogeneration device model which is able to accurately predict the thermal and electrical outputs of any combustion-based CHP systems.

The model operation requires the calibration of 103 coefficients; therefore the model needs to be calibrated by means of experimental data. The CHP performances are modelled using empirical data contained within a "performance map" and by knowledge of thermally massive elements of CHP in order to carry out its dynamic thermal performance.

The internal energy exchanges that occur in the CHP system are described with two empirical correlations that define the system's part-load electrical and thermal efficiencies.

The dynamic thermal characteristics of CHP are defined by means mass and energy balances on three control volumes (Figure 1.5):

- the energy conversion control volume includes the engine working fluid, combustion gases and engine alternator. This control volume uses the information from the performance map in order to evaluate the electricity production and the generated thermal energy input to the thermal model;
- the thermal mass control volume take in account the aggregated thermal capacitance of the engine block and most internal heat exchange equipment;
- the cooling water control volume take in account the thermal capacity of the cooling water flowing through the CHP and the part of heat exchanger in immediate thermal contact with the cooling water.

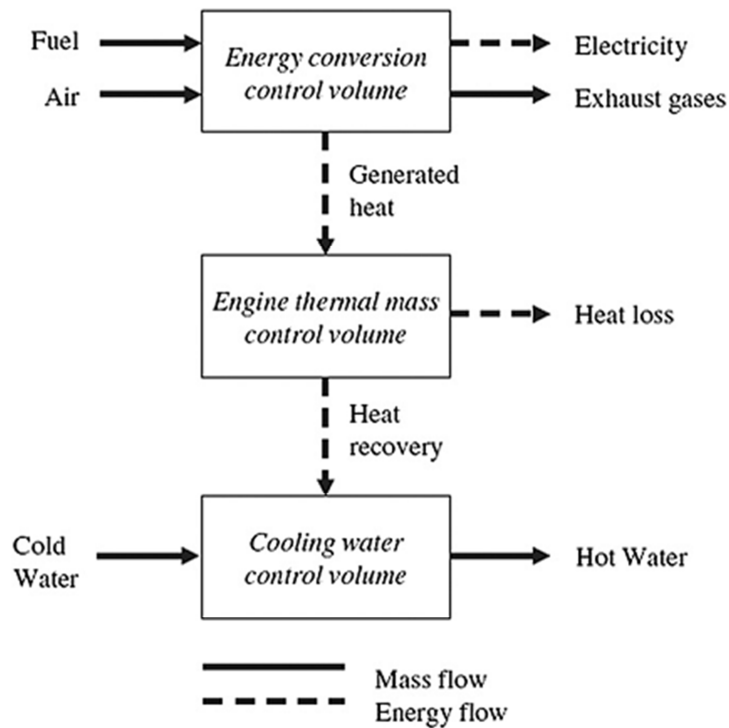


Figure 1.5. Cogeneration model control volumes.

The conversion of fuel chemical energy into thermal and electric energy under steady conditions is considered in the energy conversion control volume:

$$P_{\text{net,ss}} = \eta_{\text{el}} q_{\text{gross}} \quad (1.1)$$

$$q_{gen,ss} = \eta_{th} q_{gross} \quad (1.2)$$

$$q_{gross} = \dot{m}_{fuel} LHV_{fuel} \quad (1.3)$$

where $P_{net,ss}$ is the steady-state electrical output [W], $q_{gen,ss}$ is the steady-state rate of heat generation within the engine [W], q_{gross} is the gross heat input into the CHP system [W], η_{el} and η_{th} are, respectively, the thermal and electric steady-state efficiencies under part-load condition, \dot{m}_{fuel} and LHV_{fuel} are the fuel flow rate and its lower heating value respectively.

The steady-state conversion efficiencies are expressed as function of cooling water mass flow rate, \dot{m}_{cw} , cooling water inlet temperature, $T_{cw,i}$, and net electrical power output under steady-state condition, $P_{net,ss}$:

$$\eta_{el} = f(\dot{m}_{cw}; T_{cw,i}; P_{net,ss}) \quad (1.4)$$

$$\eta_{th} = f(\dot{m}_{cw}; T_{cw,i}; P_{net,ss}) \quad (1.5)$$

The efficiencies are represented by two above 2nd order truncated tri-variate polynomial functions. Each correlation has 27 empirically derived coefficients.

Due to the effects of heat losses and thermal mass of the engine, which store some of the “produced” heat, the heat recovered could differ from steady-state rate of heat “generated”. Therefore the thermal energy transferred from the engine to the cooling water, q_{HX} , could be expressed as follows:

$$q_{HX} = [UA]_{HX}(T_{eng} - T_{cw,o}) \quad (1.6)$$

where $[UA]_{HX}$ is the overall thermal conductance between the engine and the cooling water control volumes, T_{eng} is the average temperature of engine control volume and $T_{cw,o}$ is the cooling water temperature exiting the CHP device.

The heat losses are proportional to the temperature difference between the engine control volume and the surroundings:

$$q_{\text{loss}} = [UA]_{\text{loss}}(T_{\text{eng}} - T_{\text{room}}) \quad (1.7)$$

where $[UA]_{\text{loss}}$ represents the effective thermal conductance between the engine control volume and the surroundings.

The engine temperature and the cooling water temperature exiting the CHP can be obtained from an energy balance on the engine thermal mass and cooling water control volumes:

$$[MC]_{\text{eng}} \left(\frac{dT_{\text{eng}}}{dt} \right) = q_{\text{gen,ss}} - [UA]_{\text{HX}}(T_{\text{eng}} - T_{\text{cw,o}}) - [UA]_{\text{loss}}(T_{\text{eng}} - T_{\text{room}}) \quad (1.8)$$

$$[MC]_{\text{cw}} \left(\frac{dT_{\text{cw,o}}}{dt} \right) = [UA]_{\text{HX}}(T_{\text{eng}} - T_{\text{cw,o}}) + [\dot{m}c_p]_{\text{cw}}(T_{\text{cw,i}} - T_{\text{cw,o}}) \quad (1.9)$$

where $[MC]_{\text{eng}}$ and $[MC]_{\text{cw}}$ represent the thermal capacities of the corresponding control volumes; while $[\dot{m}c_p]_{\text{cw}}$ is the thermal capacity flow rate associated with the cooling water.

The maximum rate of variation allowed in the fuel flow is ensured by the following equations:

$$\frac{d\dot{m}_{\text{fuel}}}{dt} = \frac{|\dot{m}_{\text{fuel,demand}}^{t+\Delta t} - \dot{m}_{\text{fuel}}^t|}{\Delta t} \quad (1.10)$$

$$\dot{m}_{\text{fuel}}^{t+\Delta t} = \begin{cases} \dot{m}_{\text{fuel,demand}}^{t+\Delta t} & \text{if } \frac{d\dot{m}_{\text{fuel}}}{dt} \leq \left(\frac{d\dot{m}_{\text{fuel}}}{dt} \right)_{\text{max}} \\ \dot{m}_{\text{fuel}}^t \pm \left(\frac{d\dot{m}_{\text{fuel}}}{dt} \right)_{\text{max}} & \text{if } \frac{d\dot{m}_{\text{fuel}}}{dt} > \left(\frac{d\dot{m}_{\text{fuel}}}{dt} \right)_{\text{max}} \end{cases} \quad (1.11)$$

where $\dot{m}_{\text{fuel,demand}}^{t+\Delta t}$ is the system fuel flow rate requested by a high-level control (kg/s), t is time (s), and Δt is the duration of the simulation time step (s); $\left(\frac{d\dot{m}_{\text{fuel}}}{dt} \right)_{\text{max}}$ represents the maximum rate of change in the system fuel flow rate.

Likewise, the rate of variation in the CHP system's power output is compared to the maximum rate of change empirically derived:

$$\frac{dP_{\text{net}}}{dt} = \frac{|P_{\text{net}}^{t+\Delta t} - P_{\text{net}}^t|}{\Delta t} \quad (1.12)$$

$$P_{\text{net}}^{t+\Delta t} = \begin{cases} P_{\text{net,ss}}^{t+\Delta t} & \text{if } \frac{dP_{\text{net}}}{dt} \leq \left(\frac{dP_{\text{net}}}{dt}\right)_{\text{max}} \\ P_{\text{net}}^t \pm \left(\frac{dP_{\text{net}}}{dt}\right)_{\text{max}} & \text{if } \frac{dP_{\text{net}}}{dt} > \left(\frac{dP_{\text{net}}}{dt}\right)_{\text{max}} \end{cases} \quad (1.13)$$

where $\left(\frac{dP_{\text{net}}}{dt}\right)_{\text{max}}$ is the maximum variation rate in the CHP system's power output.

The previous equations describe the function of MCHP system in normal operation. However CHP system can operate in other three operation mode:

- Standby: when no electric or thermal energy is required. Therefore the CHP system does not consume fuel, but the operation of the control system requires electricity. The function in this operation mode is described by the following equations:

$$\begin{aligned} P_{\text{net}} &= P_{\text{net,standby}} \\ q_{\text{gen}} &= 0 \\ \dot{m}_{\text{fuel}} &= 0 \end{aligned} \quad (1.14)$$

where $P_{\text{net,standby}}$ is the electricity required in standby mode.

- Warm-up: it is the period during which there is a static time delay between activation of the unit and electrical power generation. This time delay is the warm up time, $t_{\text{warm-up}}$. The Annex model assumes that the warm-up characteristics of internal combustion engines do not depend to engine temperature. If t_0 is the time at which the CHP is started, the power "generated" is expressed by:

$$\begin{cases} P_{\text{net,warm-up}} = 0 & \text{if } (t - t_0) < t_{\text{warm-up}} \\ P_{\text{net,warm-up}} = P_{\text{demand}} & \text{if } (t - t_0) \geq t_{\text{warm-up}} \end{cases} \quad (1.15)$$

- Cool-down: in this operation mode the engine does not consume fuel, but it does not generate thermal energy. The electricity consumption is due to auxiliary electrical systems required to complete the shutdown. Therefore:

$$\begin{aligned}
P_{\text{net}} &= P_{\text{net,cool-down}} \\
q_{\text{gen}} &= 0 \\
\dot{m}_{\text{fuel}} &= 0
\end{aligned}
\tag{1.16}$$

The switching between the different operation modes depends on the activation and deactivation of the CHP system. The normal operation mode persists for indefinite periods of time, until the unit is deactivated. Likewise the standby persists until the unit is activated. Otherwise the warm-up and cool-down mode are intermediate operation mode that persist until the specified period lapses. So the warm-up mode occurs in the switching from stand-by to normal operation, while the cool-down occurs in the opposite transition (from normal mode to stand-by).

More detailed information about the analyzed MCHP model is available in reference [45]. The Annex MCHP model was calibrated and validated for the analyzed MCHP (AISIN SEIKI unit) in ref. [46]. In Table 1.2 the parameters used in the MCHP model are reported. All the information about the calibration and validation methodology and results can be find in ref. [46].

Table 1.2. MCHP model parameters.

Number	Parameter name	Description	Value	Unit
1	fPower_Out_max	System maximum power	5596.2	W
2	fPower_Out_min	System minimum power	300	W
3	fCW_Temp_max	Maximum cooling water outlet temperature	90	°C
4	iFuel_Type	Fluid type (liquid or gaseous)	2	-
5	fFuel_LHV	Liquid fuel lower heating value LHV	9.59	kWh/N m ³
6	fFuel_CO2_intensity	Liquid fuel CO ₂ factor	0.2	Kg/ Nm ³
7	fFuel_Comp(Hydrogen)	% hydrogen in fuel gas mixture	0	mol/mol
8	fFuel_Comp(Methane)	% methane in fuel gas mixture	0.99461	mol/mol
9	fFuel_Comp(Ethane)	% ethane in fuel gas mixture	0.00063	mol/mol
10	fFuel_Comp(Propane)	% propane in fuel gas mixture	0.00009	mol/mol
11	fFuel_Comp(Butane)	% butane in fuel gas mixture	0.00008	mol/mol
12	fFuel_Comp(Pentane)	% pentane in fuel gas mixture	0	mol/mol
13	fFuel_Comp(Hexane)	% hexane in fuel gas mixture	0.0001	mol/mol
14	fFuel_Comp(Methanol)	% methanol in fuel gas mixture	0	mol/mol
15	fFuel_Comp(Ethanol)	% ethanol in fuel gas mixture	0	mol/mol
16	fFuel_Comp(C_Monoxide)	% CO in fuel gas mixture	0	mol/mol
17	fFuel_Comp(C_Dioxide)	% CO ₂ in fuel gas mixture	0.0003	mol/mol
18	fFuel_Comp(Nitrogen)	% nitrogen in fuel gas mixture	0.00419	mol/mol
19	fFuel_Comp(Oxygen)	% oxygen in fuel gas mixture	0	mol/mol
20	fFuel_Flow_Change_max	Maximum rate of change in fuel flow	1000000	-
21	fGross_Power_Change_Max	Maximum rate of change in power output	760	-
22	fEffective_MC_Engine	Power system thermal mass	82845	J/K

23	fEffective_UA_HX	Effective heat recovery UA coefficient	3493	W/K
24	fEffective_UA_Loss	Effective heat loss UA coefficient	58	W/K
25	fEffective_MCHX	Heat exchanger thermal mass	7955	J/K
26	fPeriod_Dur_(OP_Startup)	Start-up (warm-up) period duration	129	s
27	fPeriod_Dur_(OP_Shutdown)	Cool-down period duration	331	s
28	iCooldown_Mode	Cool-down period mode	1	-
29	el_out_CD_Period	Electric output at cool-down	-190	W
30	el_out_standby	Net electrical output in standby mode	-90	W
31	fCorr_MIN_Power_Out	Power output correlation minimum bound	500	W
32	fCorr_Max_Power_Out	Power output correlation maximum bound	5630	W
33	fCorr_MIN_CW_temp	Cooling water temperature correlation minimum bound	15	°C
34	fCorr_MAX_CW_temp	Cooling water temperature correlation maximum bound	70	°C
35	fCorr_MIN_CW_Flow	Cooling water flow correlation minimum bound	0.18	kg/s
36	fCorr_MAX_CW_Flow	Cooling water flow correlation maximum bound	0.29	kg/s
37	fPM_elec_coeff	Coefficient	0.0361	-
38	fPM_elec_coeff	Coefficient	-4.389 10 ⁻⁹	-
39	fPM_elec_coeff	Coefficient	6.6907 10 ⁻⁵	-
40-63	fPM_elec_coeff	Coefficient	0	-
64	fPM_Therm_coeff	Coefficient	0.9368	-
65	fPM_Therm_coeff	Coefficient	4.4399 10 ⁻⁹	-
66	fPM_Therm_coeff	Coefficient	-6.9417 10 ⁻⁵	-
67-90	fPM_Therm_coeff	Coefficient	0	-
91	iCW_Loop_conf	Cooling water loop: pump configuration	2	-
92-100	PM_flow_coeff	Coefficient	0	-
101-103	PM_air_coeff	Coefficient	0	-

1.2.2 Thermal energy storage model

Thermal energy storage (TES) is attracting growing interest for different applications such as space heating and cooling and domestic hot water production. TES would appear to be the most appropriate method to reduce the mismatch that sometimes occurs between energy supply and demand.

There are three different categories of TES system:

- sensible heat storage, in which thermal energy is stored by raising the temperature of a solid or liquid without phase change in the temperature range of the storage process [47],[48];
- latent heat storage, based on heat absorption or release when a storage material undergoes a phase change from solid to liquid or liquid to gas or vice versa [48], [49] and [50];

- thermochemical energy storage, based on energy absorbed and released in breaking and rebuilding molecular bonds in a completely reversible chemical reaction [48].

The use of TES systems can bring about several benefits including [48]:

- Increased “generation” capacity. Thermal energy demand for heating and cooling is seldom constant over time. During low demand periods, therefore, the excess available “generation” can be used to charge a TES, thereby increasing the effective generation capacity during high-demand periods. This allows for the installation of a smaller production unit, increasing its utilization factor.
- to shift energy purchases to low-cost periods. This allows energy consumers subject to time-of-day pricing to shift energy purchases from high to low-cost periods.
- Increased system reliability. As a general rule, any form of energy storage increases system reliability.

On the other hand the introduction of TES does have some disadvantages, such as its cost and the energy losses towards the environment. Furthermore, it is important to note that correct TES sizing, with reference to both CHP (Combined Heating and Power) rated output and end-user characteristics, is essential to the energy performance of the building-integrated CHP system.

The diffusion of solar thermal systems and CHP [3],[10],[51] and CCHP (Combined Cooling, Heating and Power) [52],[53] systems in small size applications shows the importance of using TES systems, which are able to temporally decouple energy “production” from “use”.

In applications related to space heating, where operating temperatures are low (below 90°C), the most commonly-used TES systems are sensible ones that use water as a storage material. This is because water has relatively high specific heat and density; it is also non-toxic and low-cost.

The importance of TES in solar thermal system, due to the discontinuity and uncertainty of solar source, is obvious. Moreover TES are important also in other applications. Arteconi et al. [54] investigate the effect of demand-side management in a domestic

heating system, which consisted of a heat pump coupled with a TES unit, in Northern Ireland (UK) scenario. Using TES system allowed to switch off the heat pump during peak hours, therefore it was possible to achieve a reduction of the electricity bill if a “time of use” tariff structure was adopted.

Furthermore TES coupled with CHP and CCHP systems enables to store the surplus thermal energy, in order to increase operating hours and consequently obtain primary energy savings with respect to traditional systems based on separate “production”. Several studies confirmed that the introduction of TES in CCHP systems provides energy, environmental and economic benefits.

Haeseldonckx et al. [55] evaluated the impact of TES on the operating behavior of a micro cogeneration system for residential use. It was established that the introduction of TES led to longer operating hours and more continuous operation of the cogeneration system, resulting in a CO₂ reduction almost three times higher than without the TES.

Pagliarini et al. [56] analyzed a practical case study of a cogeneration system coupled with a TES system in buildings belonging to Parma University (Italy). The results of the energy and economic analysis confirmed the effectiveness of the TES-based solution, providing important guidelines in the choice of optimal size.

Smith et al. [57] investigated the benefits of a TES combined with a CHP system in eight different commercial building types. In each case, the CHP system reduced operating costs, primary energy consumption, and carbon dioxide emissions with respect to the reference case based on separate “production”. For six of the eight buildings, adding thermal storage provided further energy, environmental and economic improvements.

Fragaki et al. [58] analyzed the economics and optimum size of CHP, based on gas-fuelled engines and thermal storage in British market conditions. The authors stressed that thermal storage could improve the overall economics of CHP plants in UK applications.

Barbieri et al. [59] highlighted the influence of the size of TES on the energy and economic performance of a CHP system. The results showed that the effect of the size of the thermal energy storage was not linear and increased the more the thermal power delivered by the CHP system.

All these studies have shown the importance of including TES in a CHP plant, but in some of these the hot water tank is modeled as ideal. In some studies, the energy balance was based on only first law of thermodynamics, neglecting storage fluid temperature and the system (fan coil, radiator, etc.) used to satisfy the user's demand. The energy losses by the TES and thermal stratification were often neglected. Celador et al. [60] showed the effect of different hot water storage tank modeling approaches on the global simulation of residential CHP plants as well as their impact on economic feasibility. More specifically, the authors showed that the global energy and exergy efficiency of the plant for the three modelled cases were similar, while important differences were found in terms of economic results.

In some applications, such as solar thermal systems, neglecting the effect of thermal stratification can affect simulation results. Cristofari et al. [61] showed that, with a high degree of stratification, energy saving was greater (5.25% per annum) than with a fully mixed tank.

The importance of using appropriate mathematical models in TES simulation is therefore clear. It is today possible to model the behavior of a hot water tank with high accuracy, through the use of multidimensional models using computational fluid dynamics codes. The design of innovative storage concepts and the optimization of existing systems make them particularly attractive [62]. The use of multidimensional models of TES in long-term energy simulations (yearly based, for example) involves high computational costs. The possibility of using one-dimensional models is based on the consideration that the temperature gradient exists along the vertical direction only, while it is negligible along the radial direction. This assumption was confirmed by the experimental study reported in [63].

In this section an experimental analysis of a storage tank with a capacity of approximately 1,000 liters, was performed in order to calibrate and validate a 1-D model of the TES.

More specifically, the experimental data enabled to:

- evaluate the effective heat capacity;
- estimate the overall heat transfer coefficient for heat losses;

- estimate the overall heat transfer coefficient for heat losses of the bottom surface;
- calibrate a Nusselt–Rayleigh correlation in order to evaluate the natural convection heat transfer coefficient of the heat exchanger immersed in the water storage tank;
- validate the TES model.

Finally, different dynamic simulations of solar thermal heating systems are carried out in order to highlight the influence of the TES model and its calibration and validation on annual energy performance.

1.2.2.1 Mathematical model

A model that enables the simulation of the behavior of the tank installed at the test facility is related to the "type 60f", the most detailed model available in "TRNSYS" to simulate a stratified thermal storage [42][64][65]. It models a stratified fluid storage tank with optional internal heaters and heat exchangers.

In order to simulate thermal stratification, the tank can be modeled with N ($N < 100$) fully-mixed equal volume nodes, for each of which uniform temperature is assumed. If N is equal to 1, the storage tank is modeled as a fully-mixed tank and no stratification effects are possible. Options of unequal size nodes, temperature dead band on heater thermostats, incremental overall heat transfer coefficient for heat losses, non-circular tanks, horizontal tanks, and flue losses of a gas auxiliary heater are also available.

The energy balance for the generic node i , Figure 1.6, is expressed as (neglecting the terms related to auxiliary electric and gas heaters and assuming constant specific heat and incompressible fluid) [42][64][65]:

$$m_i c \frac{dT_i}{dt} = \left[\frac{(k + \Delta k) A_{c,i}}{\Delta x_{i+1 \rightarrow i}} \right] (T_{i+1} - T_i) + \left[\frac{(k + \Delta k) A_{c,i}}{\Delta x_{i-1 \rightarrow i}} \right] (T_{i-1} - T_i) + (U_{\text{tank}} + \Delta U_i) A_{s,i} (T_{\text{env}} - T_i) + \dot{m}_{\text{down}} c T_{i-1} - \dot{m}_{\text{up}} c T_i + \quad (1.17)$$

$$- \dot{m}_{\text{down}} c T_i + \dot{m}_{\text{up}} c T_{i+1} + U A_{\text{hx1}} \Delta T_{\text{in1}} + U A_{\text{hx2}} \Delta T_{\text{in2}} + U A_{\text{hx3}} \Delta T_{\text{in3}} + \dot{m}_{\text{in}} c T_{\text{in}} - \dot{m}_{\text{out}} c T_i + \dot{m}_{2\text{in}} c T_{2\text{in}} - \dot{m}_{2\text{out}} c T_i$$

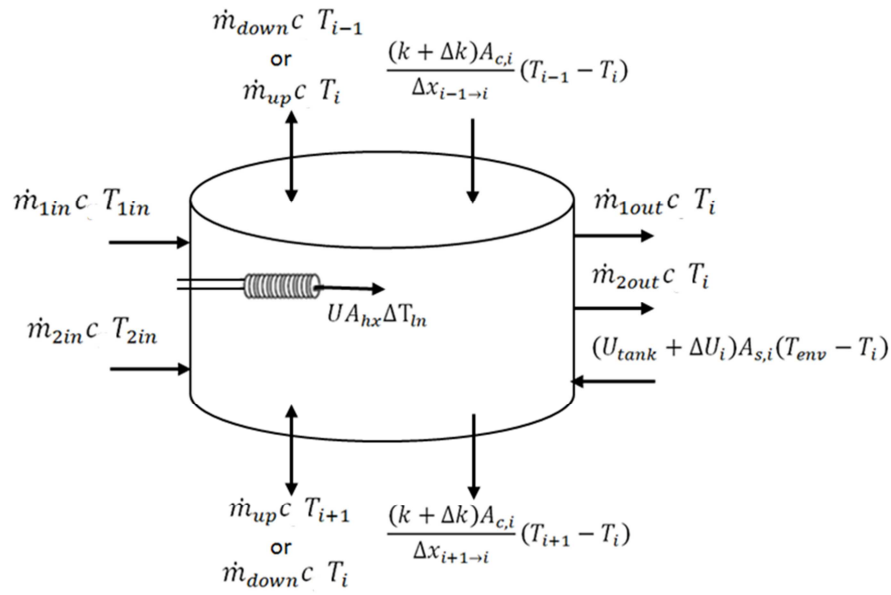


Figure 1.6. Energy balance for the generic node i.

The first term of the equation (1.17) represents the energy variation of node i of TES per infinitesimal unit time. The terms $[(k + \Delta k) A_{c,i} / \Delta x_{i+1 \rightarrow i}] (T_{i+1} - T_i)$ and $[(k + \Delta k) A_{c,i} / \Delta x_{i-1 \rightarrow i}] (T_{i-1} - T_i)$ show the thermal power exchanged by conduction between node i and those adjacent, by conduction. These terms take into account the de-stratification in the storage tank, which is mainly driven by thermal conduction within the fluid (k) and conduction along the tank wall (Δk). $(U_{tank} + \Delta U_i) A_{s,i} (T_{env} - T_i)$ represents the heat loss by node i of TES. Different overall heat transfer coefficients for heat losses can be considered for each node through an incremental coefficient (ΔU_i). The terms $\dot{m}_{down} c T_{i-1}$, $\dot{m}_{up} c T_i$, $\dot{m}_{down} c T$ and $\dot{m}_{up} c T_{i+1}$ represent the thermal power associated with the mass flow between adjacent nodes. The energy balance considers the possible heat flows associated with the presence of a heat exchanger in node i ($UA_{hx1} \Delta T_{ln1}$, $UA_{hx2} \Delta T_{ln2}$, and $UA_{hx3} \Delta T_{ln3}$). The heat transfer due to mass flows entering or exiting the TES represented by the last four terms on the right-hand side of the energy balance.

The next section gives a description of the terms included in Eq. 1.17.

1.2.2.2 Test facility

The test facility installed in the laboratory of Università degli Studi del Sannio (Italy) consists of (Figure 1.7):

- a thermal storage tank;
- a natural gas fired micro-cogeneration (MCHP, Micro Combined Heat and Power) system;
- a natural gas fired boiler;
- an air-to-water heat exchanger.

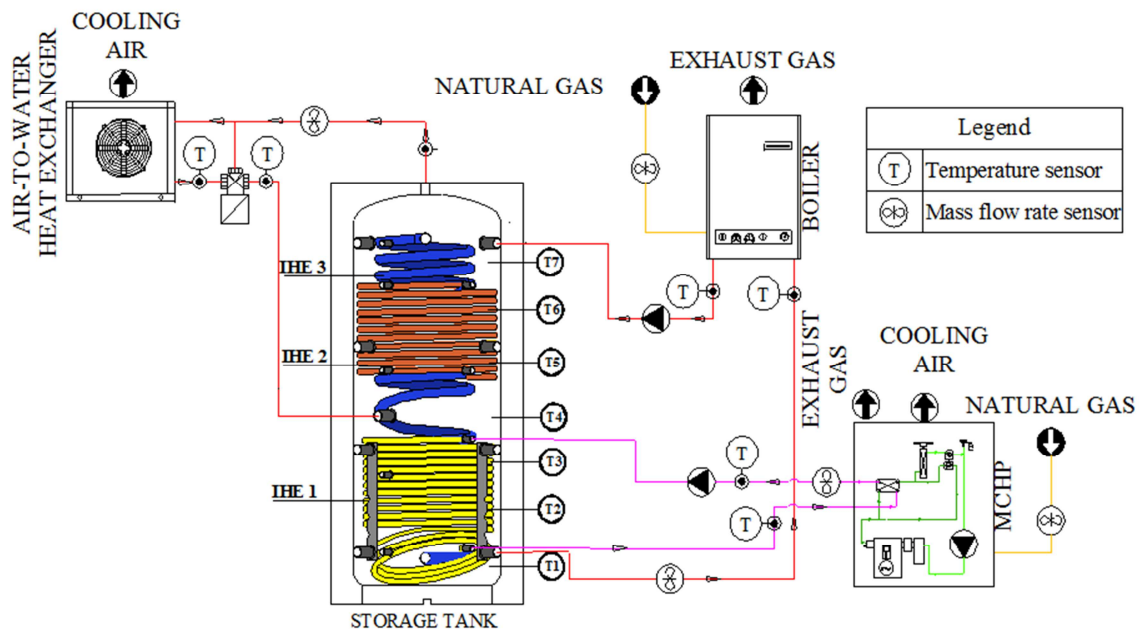


Figure 1.7. Diagram showing experimental plant installed in the laboratory of University of Sannio (Italy).

The main storage tank characteristics are described in the previous section 1.1. Figure 1.8 shows the connections between the TES and the other components as well as the detailed dimensional characteristics of the TES.

As shown in Figure 1.7, the lower heat exchanger of the storage tank is connected with the cogeneration system. The main characteristics of the installed MCHP system are reported in the previous section 1.1.

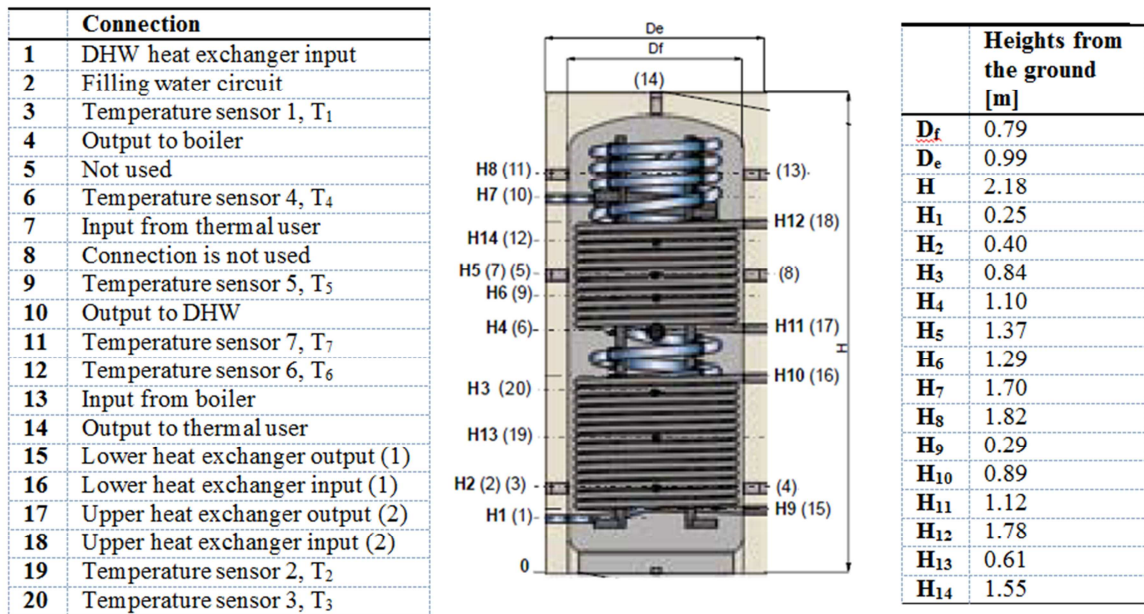


Figure 1.8. Connections and dimensional characteristics of TES [66].

The boiler interacts directly with the water in the tank. It is fuelled by natural gas and delivers a nominal heat output of 12.0 kW with a thermal efficiency of 90.2%.

The thermal energy requirements of the user are simulated by means of an air-to-water heat exchanger. A feedback control system, acting on the mass flow rate crossing the heat exchanger, enables the user's thermal load profile to be simulated.

The experimental plant is equipped with the following measuring sensors:

- ambient temperature;
- water temperature;
- water mass flow rate;
- natural gas mass flow rate.

Table 1.3 reports the characteristics of each measuring instrument installed in the laboratory.

The signals from the measuring instruments are acquired with field point system and sent to a PC where they are processed and recorded through a user interface that allows for the setting of the sampling period and monitoring of the test facility operation. It also enables to set the thermal load profile that the air-to-water heat exchanger must

follow, by means of the feedback control system. It uses a control signal to act on the three-way valve upstream of the air-to-water heat exchanger.

Table 1.3. Characteristics of measuring instruments installed in the laboratory.

Parameters	Unit	Instrument	Measuring Range	Accuracy
Water temperature	°C	Resistance thermometer Pt100	-10÷120 °C	±0.15 °C at 0°C
Mass flow rate of natural gas	Nm ³ /h	Thermal mass flow meter	0÷2.5 Nm ³ /h	±0.2% full scale
Volumetric flow rate of MCHP and boiler	L/min	Ultrasonic meter	flow 0.1÷50 L/min	≤0.01 % of full scale + 2% of measuring value
Volumetric flow rate of air-to-water HE	L/min	Ultrasonic meter	flow 1-200 L/min	≤0.01 % of full scale + 2% of measuring value
Ambient Temperature	°C	Resistance thermometer NTC	-40÷70 °C	±0.4 °C

1.2.2.3 Calibration and validation of the model

Experimental tests conducted in the test facility enabled the calibration and validation of the tank model.

The model parameters were set to take into account the three internal heat exchangers, as well as two inlets and two outlets of the stored fluid. A total of 50 nodes were considered to model thermal stratification. Table 1.4 reports a short description of the calibrated parameters; Table 1.5 gives the model input variables.

The parameters related to the heights of the storage inputs and outputs, as well as those of the heat exchangers, do not refer to the height above ground, rather tank base thickness (0.0375 m) has to be subtracted from overall height (Figure 1.8).

Table 1.4. Model parameters.

N°	Parameters	Value	Unit
1	Inlet position mode	2	-
2	Tank volume	986	L

3	Tank height	2.04	m
4	Tank perimeter	-1	m
5	Height of flow inlet 1	1.37	m
6	Height of flow outlet 1	2.04	m
7	Height of flow inlet 2	1.76	m
8	Height of flow outlet 2	0.36	m
9	Fluid specific heat	4187	J/kgK
10	Fluid density	985	kg/m ³
11	Tank loss coefficient	1.37	W/m ² K
12	Fluid thermal conductivity (water)	0.580	W/mK
13	Destratification conductivity	0.285	W/mK
14	Boiling temperature	127	°C
15	Auxiliary heater mode	-	-
16	Height of 1st auxiliary heater	-	m
17	Height of 1st thermostat	-	m
18	Set point temperature for element 1	-	°C
19	Deadband for heating element 1	-	°C
20	Maximum heating rate of element 1	-	kW
21	Height of heating element 2	-	m
22	Height of thermostat 2	-	m
23	Set point temperature for element 2	-	°C
24	Deadband for heating element 2	-	°C
25	Maximum heating rate of element 2	-	kW
26	Overall loss coefficient for gas flue	-	kW/K
27	Flue temperature	-	°C
28	Fraction of critical timestep	6	-
29	Gas heater	-	-
30	Number of internal heat exchangers	3	-
31	Node heights supplied	1	-
32	Additional loss coefficients supplied	1	-
33	Heat exchanger fluid indicator-1	1	-
34	Fraction of glycol-1	0	-
35	Heat exchanger inside diameter-1	0.029	m
36	Heat exchanger outside diameter-1	0.032	m
37	Heat exchanger fin diameter-1	0.032	m

38	Total surface area of heat exchanger-1	3.1	m ²
39	Fins per meter for heat exchanger-1	0	-
40	Heat exchanger length-1	30.85	m
41	Heat exchanger wall conductivity-1	45	W/mK
42	Heat exchanger material conductivity-1	45	W/mK
43	Height of heat exchanger inlet-1	0.85	m
44	Height of heat exchanger outlet-1	0.25	m
45	Heat exchanger fluid indicator-2	1	-
46	Fraction of glycol-2	0	-
47	Heat exchanger inside diameter-2	0.029	m
48	Heat exchanger outside diameter-2	0.032	m
49	Heat exchanger fin diameter-2	0.032	m
50	Total surface area of heat exchanger-2	2.5	m ²
51	Fins per meter for heat exchanger-2	0	-
52	Heat exchanger length-2	24.88	m
53	Heat exchanger wall conductivity-2	45	W/mK
54	Heat exchanger material conductivity-2	45	W/mK
55	Height of heat exchanger inlet-2	1.54	m
56	Height of heat exchanger outlet-2	1.08	m
57	Heat exchanger fluid indicator-3	1	-
58	Fraction of glycol-3	0	-
59	Heat exchanger inside diameter-3	0.0254	m
60	Heat exchanger outside diameter-3	0.0381	m
61	Heat exchanger fin diameter-3	0.0381	m
62	Total surface area of heat exchanger-3	7.8	m ²
63	Fins per meter for heat exchanger-3	0	-
64	Heat exchanger length-3	61	m
65	Heat exchanger wall conductivity-3	16.0	W/mK
66	Heat exchanger material conductivity-3	16.0	W/mK
67	Height of heat exchanger inlet-2	0.15	m
68	Height of heat exchanger outlet-3	1.6	m
69	Height of node -1	0.0408	m
70	Additional loss coefficient for node -1	0	W/m ² K
71-167	Node parameters	-	-
168	Additional loss coefficient for node -50	17.55	W/m ² K

Table 1.5. Input variables of the model.

N°	Input	Unit
1	Flow rate at inlet1, \dot{m}_{1in}	kg/s
2	Flow rate at outlet1, \dot{m}_{1out}	kg/s
3	Flow rate at inlet 2, \dot{m}_{2in}	kg/s
4	Flow rate at outlet 2, \dot{m}_{2out}	kg/s
5	Temperature at inlet 1, T_{1in}	°C
6	Temperature at inlet 2, T_{2in}	°C
7	Environment temperature, T_{env}	°C
8	Control signal for element 1	-
9	Control signal for element 2	-
10	Flow rate for heat exchanger -1	kg/s
11	Inlet temperature for heat exchanger-1	°C
12	Nusselt constant for heat exchanger-1	-
13	Nusselt exponent for heat exchanger-1	-
14-21	Parameters for heat exchanger 2 and 3	-

Parameter 1 represents the inlet position mode; there are two different inlet modes available. In mode 1, the flow stream enters the node that is closest to it in temperature. With sufficient nodes, this allows for a maximum degree of stratification. In mode 2, flow streams enter the tank at fixed, user-specified positions.

Parameters 2-8 show the geometric characteristics of the TES, while parameters 9, 10, 12 and 14 give the physical characteristic of the TES fluid (water). To model de-stratification due to mixing at node interfaces and conduction along the tank wall, the user may enter an additional conductivity parameter Δk (13). This term is added to the conductivity of the tank fluid and is applied to all nodes.

Parameters 15-27 and 29 represent auxiliary heater characteristics; these parameters are not taken into account because the TES analyzed has no auxiliary heater; therefore inputs 8 and 9 (Table 1.5) are set to zero.

Parameter 28 represents the fraction of the critical time step. In order to minimize errors, the "Type60" tank model uses its own internal time steps. This has the advantage of results being unaffected by the size of the TRNSYS time step [65].

Furthermore, in many circumstances, the tank may not be uniformly insulated. It is possible to take into account different insulation levels for certain nodes of stratified storage tanks by specifying the additional overall heat transfer coefficient for heat losses for node “i”. Parameters 31 and 32 are set to 1 in order to indicate different heights and heat loss coefficients for each node (parameters 69-168 if the number of nodes is set to 50).

Parameters 33-68 represent the geometric and physical characteristics of the heat exchanger. It has been assumed that the fluid in the heat exchangers is water. A more accurate description of the model parameters and inputs is reported in the component mathematical reference [42] and in [64], [65].

Overall heat transfer coefficient for heat losses.

Experimental tests were carried out in order to characterize the thermal energy loss of the storage tank. The TES was charged through thermal energy supplied by a boiler, after which a cool down test was performed. The temperature in different TES positions and the ambient temperature were acquired for a period of 60 hours with a sampling time of 10 seconds. The volume of the storage tank was divided into 7 nodes, one for each temperature sensor installed in the TES (see Figure 1.7). In each node a uniform temperature, equal to the temperature measured by the sensor, was considered (Figure 1.9). The sensor temperatures not shown in Figure 1.9 ranged between T2 and T7.

In order to evaluate the overall heat transfer coefficient for heat loss, an energy balance was performed in each node. For the generic node “i” this can be expressed as:

$$\frac{m_i c dT_i}{dt} = \left[\frac{(k + \Delta k) A_{c,i}}{\Delta x_{i+1 \rightarrow i}} \right] (T_{i+1} - T_i) + \left[\frac{(k + \Delta k) A_{c,i}}{\Delta x_{i-1 \rightarrow i}} \right] (T_{i-1} - T_i) + (U_{\text{tank}} + \Delta U_i) A_{s,i} (T_{\text{env}} - T_i)$$

(1.18)

multiplying by dt and integrating from initial time to final time, the following is obtained:

$$m_i c \int_{T_0}^{T_f} dT_i = \frac{(k + \Delta k) A_{c,i}}{\Delta x_{i+1 \rightarrow i}} \int_0^{T_f} (T_{i+1} - T_i) dt + \frac{(k + \Delta k) A_{c,i}}{\Delta x_{i-1 \rightarrow i}} \int_0^{T_f} (T_{i-1} - T_i) dt + (U_{\text{tank}} + \Delta U_i) A_{s,i} \int_0^{T_f} (T_{\text{env}} - T_i) dt \quad (1.19)$$

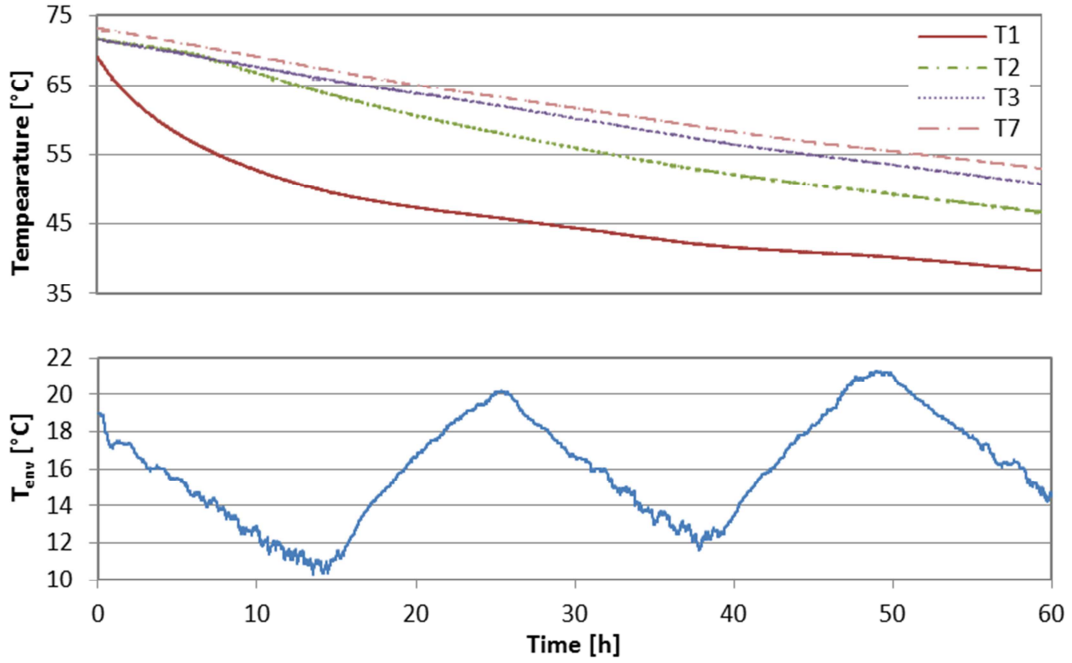


Figure 1.9. Temperature profile measured during cool-down test.

Calculating the overall heat transfer coefficient for heat losses, the following is obtained:

$$U_i = U_{\text{tank}} + \Delta U_i = \frac{m_i c \int_{T_0}^{T_f} dT_i - \frac{(k + \Delta k) A_{c,i}}{\Delta x_{i+1 \rightarrow i}} \int_0^{T_f} (T_{i+1} - T_i) dt + \frac{(k + \Delta k) A_{c,i}}{\Delta x_{i-1 \rightarrow i}} \int_0^{T_f} (T_{i-1} - T_i) dt}{A_{s,i} \int_0^{T_f} (T_{\text{env}} - T_i) dt} \quad (1.20)$$

where the integrals given in equation were solved numerically.

The de-stratification parameters in equation (1.20) were estimated as [42]:

$$k = k_{\text{tank wall}} \frac{A_{c,\text{tank wall}}}{A_c} \quad (1.21)$$

where $k_{\text{tank wall}}$ is the thermal conductivity of the tank wall (assumed equal to 45 W/mK, typical value of steel), A_c is the internal cross-sectional area of the TES and $A_{c, \text{ tank wall}}$ is the cross-sectional area of the tank wall (circular ring). This equation takes into account the conduction in the tank wall, which is usually made of metal and has a higher thermal conductivity than water (for more detail see [65]).

Table 1.6 shows the overall heat transfer coefficient for each node. The energy loss from the bottom of the tank (node 1) was much higher than that of the other nodes. This aspect is related to having neglected the convection current created by the thermal energy losses along the TES walls. In fact this aspect is not taken into account into the model. In order to consider this aspect an incremental heat transfer coefficient is considered for the bottom surface. Therefore, for the top and side walls of the tank, an average heat loss coefficient should be considered as equal to a weighted mean, where the weights are the corresponding surfaces of the nodes (Eq. 1.22). For the bottom wall an incremental heat loss coefficient must be used (Eq. 1.23). To take into account these effects, for the first node of the simulation model a heat loss coefficient equal to the weighted mean through the corresponding surfaces of the bottom and side walls was set (Eq. 1.24).

$$U_{\overline{27}} = \frac{\sum_2^7 U_i A_i}{\sum_2^7 A_i} \quad (1.22)$$

$$U_b = \frac{\sum_2^7 U_i A_i - U_{\overline{27}} (A_t - A_b)}{A_b} \quad (1.23)$$

$$U_{\text{bn}} = \frac{U_{\overline{27}} A_{\text{sl;bn}} + U_b A_b}{A_b + A_{\text{sl;bn}}} \quad (1.24)$$

Table 1.6. Overall heat transfer coefficient for heat losses for each node.

Node	Heat loss coefficient [W/m ² K]
7	1.05
6	1.56
5	1.71
4	1.39
3	1.35
2	1.49
1	3.01
2 – 7	1.30
bottom surface	7.90

Figure 1.10 shows the heat loss coefficient for each node, varying cool down test duration. For all nodes except the first the heat loss coefficient was almost constant with test duration. The first node shows a significant variation with test duration. This variation was even more evident for the bottom surface heat loss coefficient (Figure 1.11). This was due to the error committed considering that the temperature in the proximity of the base of the TES was equal to that measured by sensor 1.

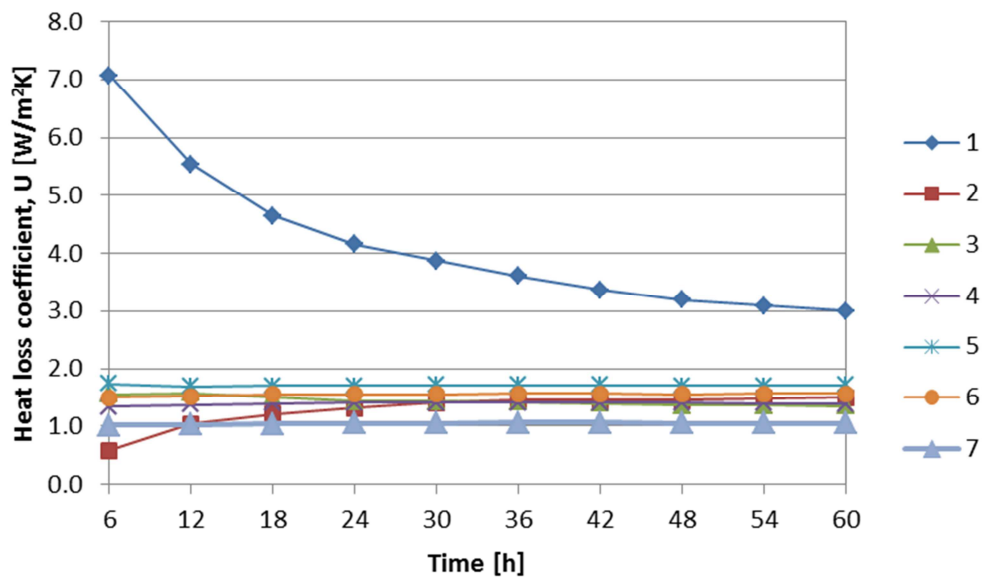


Figure 1.10. Heat loss coefficient for each node as a function of the cool down test duration.

Due to the high heat loss at the base of the TES (convection inside the TES), these two temperatures can instead differ significantly. Therefore, in order to reduce the error associated with this effect, the heat loss coefficient of the base of the TES was calculated considering only the first six hours of the cool down test.

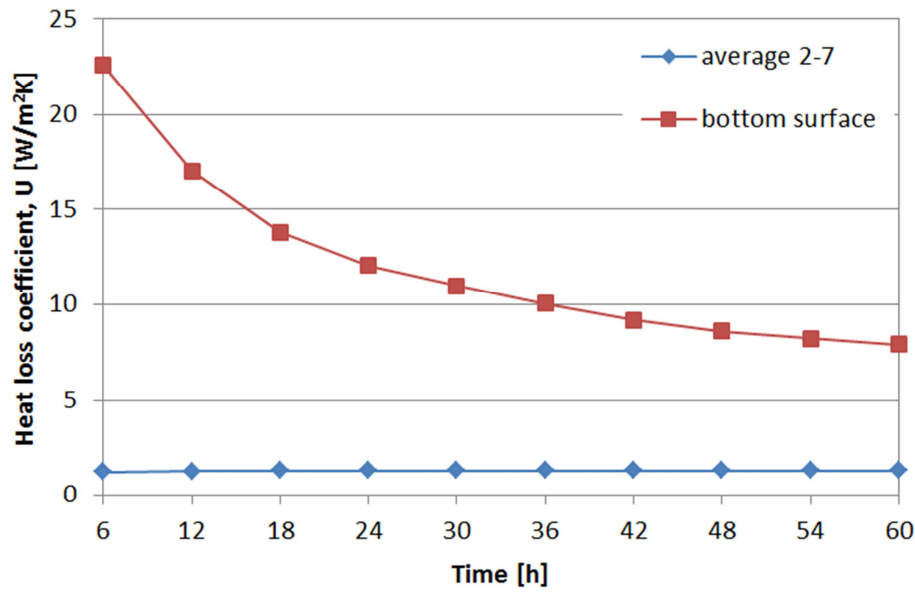


Figure 1.11. Heat loss coefficient of the node 2-7 and of bottom surface as a function of cool down test duration.

Therefore, assuming that the number of nodes for the simulation model is set to 50, the average heat loss coefficient of the first node (U_{bn}) is equal to $18.69 \text{ W/m}^2\text{K}$ and for the other node is $1.30 \text{ W/m}^2\text{K}$.

Thermal capacity of TES

After setting these parameters in TRNSYS, the simulated temperature behavior can be compared with the measured one for a charge test of the TES. In this test the boiler delivers thermal energy to the TES interacting directly with the water in the tank (see Figure 1.7 and Figure 1.8). The results for sensors 1 and 7 are shown in Figure 1.12. The comparison of the measured and simulated results shows the different thermal capacity

in the two cases. In fact, with the same heat supplied to the TES, the simulated temperatures increase more than the measured ones.

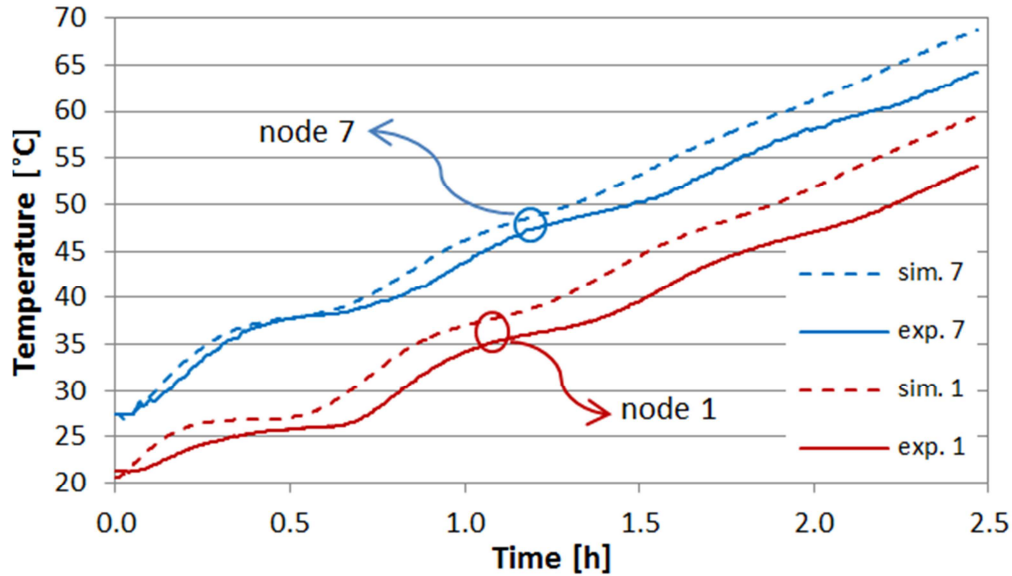


Figure 1.12. Comparison between measured and simulated temperature for a charge test of the TES.

In order to evaluate the actual thermal capacity of the system, an iterative approach was adopted. This approach used an optimization software [67] to identify the real value of the tank volume (which determines thermal capacity) through a coordinated search method. The software changes the value of the volume to minimize the following function:

$$E = \int_0^f |T_{\text{sim},1} - T_{\text{exp},1}| dt + \int_0^f |T_{\text{sim},3} - T_{\text{exp},3}| dt + \int_0^f |T_{\text{sim},5} - T_{\text{exp},5}| dt + \int_0^f |T_{\text{sim},7} - T_{\text{exp},7}| dt \quad (1.25)$$

where the integrals were solved numerically.

The value of volume that minimizes this function is 986 liters. Therefore, in recalculating the heat loss coefficients with the new volume, the results given in Table 1.7 were obtained.

Table 1.7. Heat loss coefficient with a volume of 986 L.

Node	7	6	5	4	3	2	1	$\overline{2-7}$	bottom surface
Heat loss coefficient [W/m ² K]	1.10	1.66	1.82	1.48	1.44	1.59	3.15	1.37	7.92

With this volume, the average heat loss coefficient of the first node is equal to 18.92 W/m²K (so the incremental heat loss coefficient is 17.55 W/m²K, parameter 168) while for the other nodes it is 1.37 W/m²K (parameter 11).

Figure 1.13 compares the simulated and measured data with the new values of the parameters for the same charge test of Figure 1.12. The greater coherence between the simulated and measured data is evident. In fact the comparison of the measured and simulated results (Figure 1.13) shows the same thermal capacity.

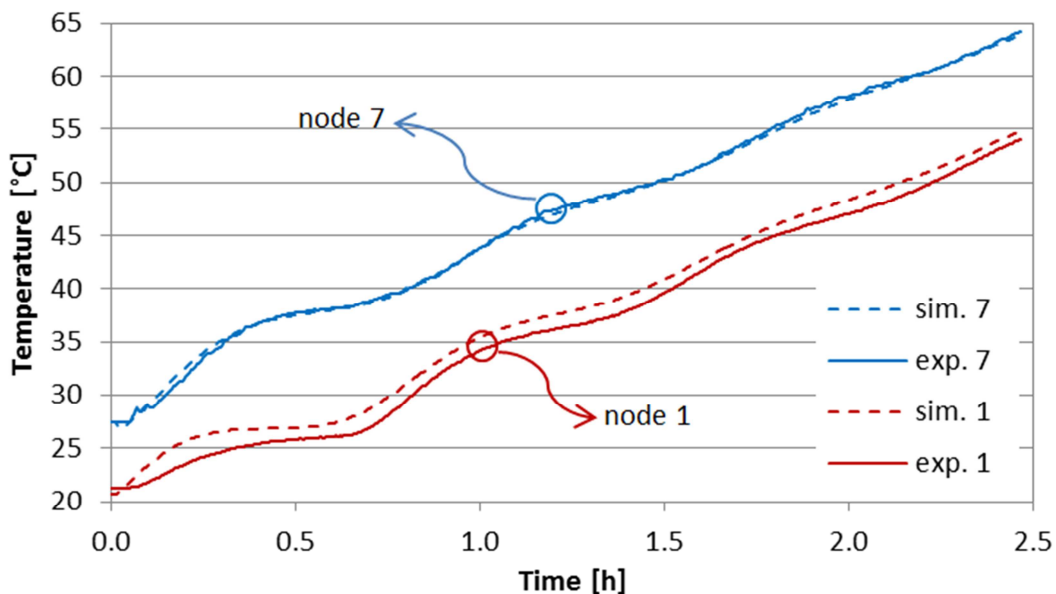


Figure 1.13. Comparison of measured and simulated temperature for a charge test of the TES after optimization.

In order to compare the results of the two simulations with the measured data, the following indices were defined:

- Error (ϵ), $\epsilon_i = T_{sim,i} - T_{exp,i}$

- Maximum Absolute Error (MAE), represents the maximum error between the measured and simulated data;
- Average Error (AE), $AE = \sum_{i=1}^N \varepsilon_i / N$;
- Average Absolute Error (ABE), $ABE = \sum_{i=1}^N |\varepsilon_i| / N$;
- Root Mean Square Error (RMSE), $ABE = \sqrt{\varepsilon_i^2 / N}$;

where:

- $T_{sim,i}$ is the predicted value of the temperature at time step i ;
- $T_{exp,i}$ is the measured value of the temperature at the time step i ;
- N is the number of the measurements.

Table 1.8 shows the statistical index for the temperatures of the nodes with respect to the two tank volume values. The reduction in errors is evident for all sensors.

Table 1.8. Statistical index for the two value of the volume of the storage.

	Volume 855 L				Volume 986 L			
	MAE [°C]	AE [°C]	ABE [°C]	RMSE [°C]	MAE [°C]	AE [°C]	ABE [°C]	RMSE [°C]
1	5.86	3.59	3.60	1.44	2.16	1.29	1.30	1.35
2	4.52	2.53	2.54	1.22	1.28	0.23	0.41	0.49
3	3.77	1.86	1.88	1.09	1.56	-0.43	0.65	0.76
4	4.57	2.24	2.24	2.51	1.18	-0.06	0.42	0.49
5	5.17	2.62	2.62	1.25	0.89	0.32	0.35	0.41
6	4.66	2.30	2.30	1.20	0.67	-0.02	0.25	0.31
7	4.70	2.21	2.22	1.36	0.90	-0.11	0.24	0.30

It is interesting to compare the average thermal loss coefficient obtained experimentally with the theoretical value obtained when ignoring the convective thermal exchanges with the environment. The theoretical value (equal to 0.34 W/m²K), calculated ignoring thermal resistance related to convective heat transfer is significantly lower than the

experimental value. This difference is due to the thermal bridges associated with pipe and sensor connections.

Heat exchanger

The free convection coefficient between the storage fluid and the internal heat exchanger wall is modeled with the following equation:

$$\bar{Nu} = C_1 \cdot Ra^n \quad (1.26)$$

the typical value for “ C_1 ” is about 0.5 and “ n ” is usually 0.25 [42],[68]. “ C_1 ” and “ n ” represent inputs 11 and 12 of the model (Table 1.5). In order to experimentally evaluate the value of these two input parameters, a charge test was performed. In this test the lower heat exchanger of the storage tank thermally interacts with the cogeneration system. Then the same measured values of water temperature and flow rate at the heat exchanger inlet were set as model inputs. Using the GenOpt software the “ C_1 ” value was changed to reduce the error between the measured and simulated temperatures at the heat exchanger outlet. A constant value of “ C_1 ” does not yield great correspondence of measured and simulated data. Thus, the input “ C_1 ” is calculated through the following equation:

$$C_1 = \alpha + \beta \cdot T_{33} \quad 20 \text{ }^\circ\text{C} < T_{33} < 70 \text{ }^\circ\text{C} \quad (1.27)$$

where:

- α and β are experimentally derived constants;
- T_{33} is the temperature of the water inside the TES near the heat exchanger in $^\circ\text{C}$

(in this case, the temperature of node 33).

The optimization software gives: $\alpha = 0.575$ and $\beta = -0.00256 \text{ } ^\circ\text{C}^{-1}$. In this mode, it is possible to obtain accurate behavior of the model as shown in Figure 1.14, where the measured and simulated thermal energy input to the heat exchanger are shown, as a result of further experimental testing.

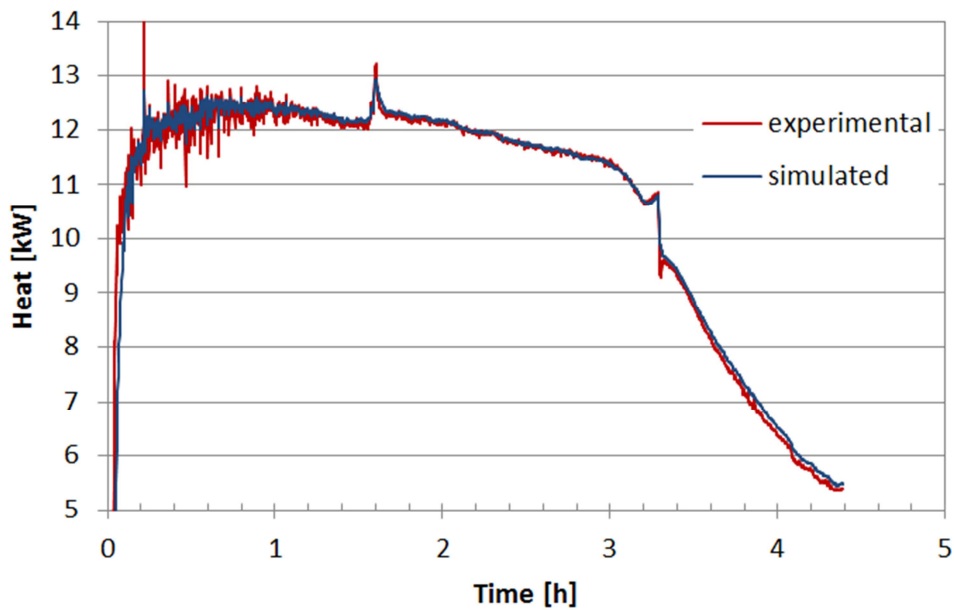


Figure 1.14. Measured and simulated heat transfer from the water to the heat exchanger.

Figure 1.15 shows the measured and simulated temperature in a charge test in which the water inside the tank is heated by the lower heat exchanger. When the charge of the TES is via the lower heat exchanger, the model does not provide a thermal stratification in the tank. The experimental data show a little stratification in the tank due to a temperature difference in the section where the heat exchanger is located. This aspect is not taken in account in the model.

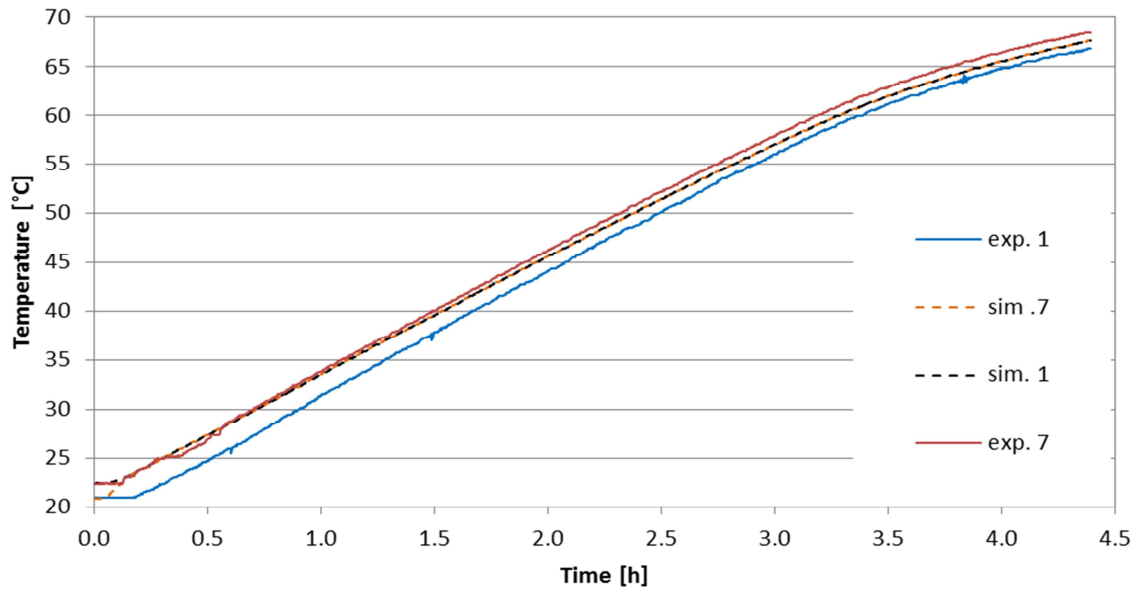


Figure 1.15. Measured and simulated temperature in a charge test with lower heat exchanger.

1.2.2.4 Simulation of solar thermal heating system

In order to investigate the impact of TES model type and accuracy and its calibration on simulation results, a dynamic model of a solar thermal heating system was developed. An illustrative scheme of the analyzed system is showed in Figure 1.16.

The solar field consists of two strings (10.19 m² per string) of evacuated tube solar collectors (SC in Figure 1.16). As seen in the previous section, the use of the lower heat exchanger provides only a very limited thermal gradient in the tank; therefore, in order to maximize the thermal stratification inside the TES, an external heat exchanger was introduced. It interacts with the solar collectors' fluid on the source side and with the fluid stored in the tank in open circuit (load side). The user is connected with the TES in open circuit (the tank has two inlets and two outlets). The user is a residential building with a total floor surface of 220 m². More details about the main characteristics of the building envelope are reported in [69]. A tempering valve and an auxiliary boiler (B in Figure 1.16) ensure the set-point temperature (50 °C) of the fluid sent to the in-room terminal systems.

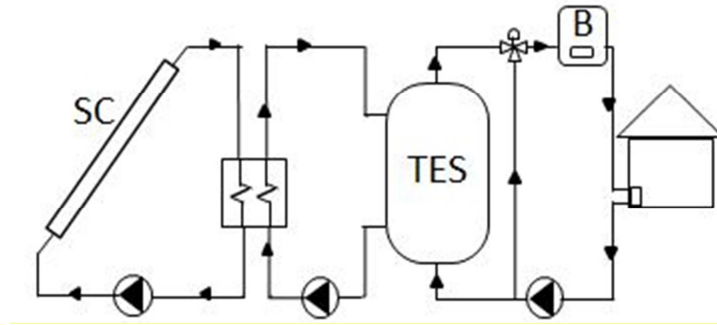


Figure 1.16. Illustrative scheme of the analyzed solar thermal system.

Table 1.9 summarizes the main components with the corresponding type of TRNSYS [42] model and the main parameters.

Table 1.9. Main component used in the TRNSYS model.

Component	Type	Parameters	Value
TES	60f	See section 1.1.2.4	
Heat exchanger	91	Effectiveness	0.60 [-]
		Specific heat of solar collector fluid	3.85 [kJ/kgK]
		Specific heat of TES fluid	4.19 [kJ/kgK]
Solar collector	71	Collectors area	20.48 [m ²]
		Intercept efficiency	0.676 [-]
		First order efficiency coefficient	1.15 [W/m ² K]
		Second order efficiency coefficient	0.004 [W/m ² K ²]
Building	56	Incidence Angle Modifiers (IAM)	See [70]
Boiler	751	See [69]	
		Rated capacity	20.0 [kW]

Five different simulations have been carried out, with different assumptions on TES model:

- case1, TES model calibrated and validated as in the previous paragraphs is considered;
- case 2, the same model of case1 is considered, but different values of some parameters are assumed: volume of the tank equal to the net volume (0.855 m³) and overall heat transfer coefficient for heat losses equal to the theoretical value (0.34 W/m²K);

- case 3, perfect mixing of storage fluid inside the tank is assumed (1 node). The volume of the tank and the overall heat transfer coefficient for heat losses are equal to the case 1;
- case 4, perfect mixing of storage fluid inside the tank is assumed (1 node). The volume of the tank and the overall heat transfer coefficient for heat losses are equal to the case 2;
- case 5, the same assumptions of case 4, except for the heat losses of the TES that are neglected.

Table 1.10 summarizes the simulation results on annual basis. In each case the energy required by the user is obviously the same, while the thermal energy provided by the solar collectors and by the boiler are different. Also the energy losses by the TES are different for each case.

Table 1.10. Simulation results on annual basis.

	Case 1	Case 2	Case 3	Case 4	Case 5
Thermal energy delivered by solar collectors [kWh]	4,867	4,810	3,290	3,195	3,166
Thermal energy delivered by boiler [kWh]	10,189	9,859	11,716	11,376	11,280
Thermal demand [kWh]	14,503	14,503	14,503	14,503	14,503
Energy losses by TES [kWh]	562	171	562	125	0

In order to compare the different simulations, the case 1, which uses the calibrated and validated TES model, is assumed as reference.

Table 1.11 reports the comparison between the reference case and the other ones. In case 2 the energy provided by solar collectors is less than the reference case because the temperature of the water at the inlet of solar collectors is higher than the reference case due to the lower TES losses. The lower TES losses bring about less thermal energy provided by the boiler. The comparison between the reference case and the case 3 is very interesting. These two cases differ only for the TES model used. In case 3 no stratification is assumed. This assumption causes a strong reduction of the thermal energy provided by solar collectors with a consequent increase of boiler integration. Also in cases 4 and 5 the energy results are very different with respect to the reference case due to the absence of stratification in the TES model.

Table 1.11. Comparison between the reference case and the other ones.

	Case 2	Case 3	Case 4	Case 5
Thermal energy delivered by solar collectors [%]	-1.2	-32.4	-34.4	-34.9
Thermal energy delivered by boiler [%]	-3.2	15.0	11.6	10.7
Energy losses by TES [%]	-69.6	0.0	-77.7	-100.0

In conclusion, in this section a 1-D model of thermal energy storage (TES) was experimentally validated and calibrated. A cool-down test showed overall heat transfer coefficient for heat losses ($1.37 \text{ W/m}^2\text{K}$) nearly four times greater than the theoretical value ($0.34 \text{ W/m}^2\text{K}$). This was due to the thermal bridges associated with the hydraulic and sensor connections. In order to consider the convective motions inside the TES an additional heat transfer coefficient for heat losses for the bottom surface was considered. A charge test revealed that the thermal capacity of the TES was greater than the value associated with the net tank volume. This was due to the presence of other materials (metal forming the walls of TES, heat exchangers, etc.) in the TES, which constitute an additional thermal capacity compared to the tank's water content. An optimization procedure identified a fictitious volume of 986 L (+15.3% with respect to the net value). This value is closer to the nominal value of the volume (1,000 L) than to the net value (855 L). This analysis showed that, in absence of experimental data, the use of nominal value (not the net one) of the volume is advisable to model the thermal energy storage.

A validation procedure showed good correspondence between the measured and predicted results. The RMSE in a charge test of 2.5 hours fell within the range $0.3\text{--}0.76 \text{ }^\circ\text{C}$ for all sensors except the one near the bottom surface, where the RMSE was $1.35 \text{ }^\circ\text{C}$. In order to simulate a heat exchanger immersed in the water storage tank, a Nusselt-Rayleigh correlation was experimentally calibrated. The experimental analysis showed a linear dependence of the pre-exponential coefficient with the water temperature of the storage tank. This correlation showed a good behavior of the model with respect to the experimental data.

To highlight the influence of the TES model accuracy and its calibration and validation process on the simulation results of a complete system, a solar thermal heating system was analyzed, considering five different cases, which differ for the type of model

(stratified or perfectly mixed), the tank volume and the overall heat transfer coefficient for heat losses. In the analyzed systems, the use of a model that does not take in account the stratification inside the TES bring about a reduction of the thermal energy provided by solar collectors (-32%) with a consequent increase of boiler integration (+15%). The design choice (solar collectors and TES interact trough an external heat exchanger) allows to maximize the stratification inside the TES. For this reason the model that does not take into account the stratification gives very different results. Moreover an accurate validation and calibration of the TES model allows to improve the model accuracy. However, these aspects have a less influence on the simulation results than the choice of a suitable model.

Simplified approaches (based on only first law of thermodynamics, neglecting storage fluid temperature, energy losses by the TES and thermal stratification) are often used in the literature. As showed in the simulation results, this approach could carry out very different energy results compared to the detailed model based on experimental tests. In conclusion, for a correct design of an energy system with TES, it is important to use a model that allows to simulate the correct behavior of the component.

1.2.3 Other components

In this section the main components used in order to model the analyzed MCHP system and its interaction with the users are described. The different components are modelled using TRNSYS subroutines ("types") [42], [43].

In some simulation the MCHP system meets the thermal load of different users. Therefore a thermal micro-grid is introduced in order to connect the users. It was simulated by the "type 31". This component models the thermal behavior of a fluid flow in a pipe or duct using variable size segments of fluid [42], [43].

The thermal micro-grid has been dimensioned starting from the knowledge of the maximum thermal power to be provided to users, the temperature difference between supply and return of the fluid and its flow rate. Knowing these data the pipe section was selected in order to keep the velocity value of the heat transfer fluid in the typical range $1\div 2.5$ m/s. A value of U (overall heat transfer coefficient) equal to 0.5 W/m²K has been

assumed. The selected overall heat transfer coefficient for the micro-grid represents the typical value for a pre-insulated pipe with an internal diameter of 2.5 cm [71]. The pipes thermally interact with the ground, whose temperature is simulated by means of the “type 77”.

The boilers are modelled through the “type 751”. It is based on an external performance map that provides the thermal efficiency as a function of the partial load ratio. More detailed information about “type 751” is available in ref. [43].

The heating system has fan coils as terminal units. They are modelled by means of “type 753” and “type 644” that interact each other. The “type 753” models a heating coil using a bypass approach in which the user specifies a fraction of the air stream that bypasses the coil, equal to 0.15 in the analyzed case. In order to take into account the electricity consumption of the fan, the “type 644” is used [43].

The buildings and the related thermal loads that represents the users were simulated using the interface "TRNBuild" of TRNSYS and its "type 56". The dimensional and the envelope characteristics, as well as the electric load and the internal gains are defined for each type of user in the following sections.

1.3 3-E analysis

In order to evaluate the performance of the analyzed system with respect to a traditional one an energy, environmental and economic analysis (3-E) [3] was implemented.

The energy performance was evaluated through the Primary Energy Saving (PES) which represents the primary energy (PE) saving of the proposed system (PS) with respect to a conventional one (CS, also indicated as Traditional System (TS)):

$$PES = \frac{PE_{CS} - PE_{PS}}{PE_{CS}} \quad (1.28)$$

In order to evaluate the primary energy consumption related to each user needs, in Table 1.12 the primary energy factors for natural gas and electricity are reported. In particular, the natural gas PE factor is used to evaluate the primary energy consumption related to the fuel input to the boiler and the MCHP system. The PE factor for the electricity drawn from the grid was assumed considering average Italian efficiency of the thermo-electric plants mix (44.8%) and the grid losses (6.23%), thereby obtaining an overall efficiency of 42% [72][73]. The PE factor for the electricity feed-in was determined assuming that electric energy from the MCHP is supplied to the low-voltage grid (3.4% losses [74]), thereby obtaining an overall efficiency of 43.5%.

Table 1.12. Primary energy and CO_{2eq} emission factors for natural gas and electricity.

	PE factors [kWh_PE/kWh]	CO_{2eq} factors [g/kWh]
Natural gas	1.0	207
Electricity grid mix	2.38	573
Electricity feed-in mix	2.30	550

The environmental performance of each case was evaluated through a simplified approach based on the evaluation of carbon dioxide equivalent emissions (CO_{2eq}). The comparison is based on the avoided CO_{2eq} emissions (ΔCO_{2eq}) of the PS with respect to CS:

$$\Delta\text{CO}_{2eq} = \frac{\text{CO}_{2eq,CS} - \text{CO}_{2eq,PS}}{\text{CO}_{2eq,CS}} \quad (1.29)$$

The CO_{2eq} emissions for each case are evaluated by means CO_{2eq} emission factors. In Table 1.12 the CO_{2eq} emission factors for natural gas and electricity are reported. The CO_{2eq} emission factor for the electricity drawn from the grid was based on the average Italian emissions of the thermo-electric plants mix (513.8 g/kWh) [75] and the grid losses (6.23% [74]), thereby obtaining an overall CO_{2eq} emission factor of 573 g/kWh. The CO_{2eq} emission factor for the electricity feed-in was determined assuming that electric energy

from the MCHP is supplied to the low-voltage grid (3.4% losses [74]), thereby obtaining an overall CO_{2eq} emission factor of 550 g/kWh.

The economic performances of the analysed system are evaluated by means a simplified approach. The Simple Pay Back (SPB) index is introduced:

$$SPB = \frac{\Delta IC}{OC_{CS} - OC_{PS}} \quad (1.30)$$

where ΔIC is the Investment Cost difference between the PS and the CS, while OC_{CS} and OC_{PS} represent the annual operational cost of the CS and PS respectively.

For the economic analysis, the natural gas tariff and the corresponding taxes for a civil user are reported in Table 1.13. In some Italian area a reduced national tax is applied; while the regional tax differs in each Italian Region. For reason of brevity it is reported only for two Regions (Campania and Piedmont). In addition to the tax reported in Table 1.13 a fixed tax of 95.8 € per year is considered. The natural gas cost is reported in euro per unit of volume expressed in Standard conditions (temperature of 15 °C and pressure of 101.325 kPa). For the natural gas that feeds the MCHP a different cost is considered (reduced tax) according to the Italian law for cogeneration [14], [76].

Table 1.13. Natural gas costs and tax in Italy.

Annual consumption [Sm ³ /year]	Cost [€/Sm ³]	National tax (reduced tax area) [c€/Sm ³]	National tax [c€/Sm ³]	Regional tax (Campania) [c€/Sm ³]	Regional tax (Piedmont) [c€/Sm ³]	Tax (VAT) (%)
0 - 120	0.413	3.80	4.40	1.90	2.20	10
121 - 480	0.597	13.50	17.50	3.10	2.58	10
481- 1,560	0.569	12.00	17.00	3.10	2.58	22
1,561 – 5,000	0.565	15.0	18.6	3.10	2.58	22
5,001 – 80,000	0.526	15.0	18.6	3.10	2.58	22
80,001 – 200,000	0.468	15.0	18.6	3.10	2.58	22
200,001 – 1,000,000	0.440	15.0	18.6	3.10	2.58	22
> 1,000,000	0.421	15.0	18.6	3.10	2.58	22

Table 1.14 reports the electricity cost and the corresponding taxes in function of time of use, for the residential and office users. The different time of use are defined in [77].

Table 1.14. Electricity costs for a residential and an office user.

	Residential users		No residential users			
	kWh/year:	Peak times	Off-peak times	Peak times	Mid-level times	Off-peak times
Electricity cost (€/kWh)	0 – 1,800	0.189	0.184	0.171	0.166	0.155
	1,801 – 2,640	0.206	0.201			
	2,641 – 4,440	0.245	0.240			
	> 4,440	0.287	0.283			
Fixed cost (€/year)		43.49		231.36		
Fixed cost (€/kW/year)		15.41		33.47		
Tax (VAT)		10%		22.0%		

The investment costs of the CS and PS are evaluated according to the following assumptions:

- MCHP investment cost equal to 18000 € [14];
- thermal micro-grid investment cost equal to 40 €/m [78];
- boilers investment cost is calculated according to ref. [79];
- the TES investment cost is equal to 3000 € [14].

1.4 Optimal thermo-economic control of the MCHP system with load sharing application

In this section the performances of the MCHP system described in section 1.1 were analyzed. The system provides thermal and electric energy to two end-users, the former is a tertiary building (office), where the generation system is located, and the latter is a residential building connected to the former through a district heating micro-grid. In order to analyze the influence of climatic conditions, two different geographical locations in Italy (Benevento and Milano) are considered, that are also characterized by different energy vectors tariffs. Particular attention is paid to the choice of the users, in

order to obtain more stable and continuous electric and thermal loads (load sharing approach) and to increase the operating hours per year of the MCHP unit.

The operation of the MCHP is governed by a control system, aimed to optimize a thermo-economic objective function. The models representing the components, the thermo-economic objective function and the buildings have been implemented in widely used commercial software for building simulations. The models are calibrated and validated through experimental and literature data, as explained in the previous sections. The results of the simulations highlight the potential benefits of the thermal load sharing approach. In particular, this study shows that an MCHP unit connected by means of a thermal micro-grid to different users in “load sharing mode” can obtain a high number of operating hours as well as significant energy (Primary Energy Saving) and environmental (avoided CO₂ equivalent emissions) benefits with respect to an appropriate reference system, even in Mediterranean areas, where the climatic conditions are not always suitable for cogeneration.

1.4.1. User description

In Figure 1.17 the analysed micro-cogeneration system is shown. The PS described in section 1.1 is installed in a tertiary building for office use (User #1). The thermal energy “produced” can also be transferred to a second residential user (User #2), connected to the MCHP system through a district heating micro-grid.

The analyzed boiler is fuelled by natural gas and delivers a nominal heat output of 24.1 kW with a thermal efficiency of 90.2%, requiring an electrical power equal to 0.125 kW.

The described system has been simulated in two different geographical locations (Benevento and Milano). The buildings and the related thermal loads have been properly sized to take into account the different climatic conditions of the two cities, as derived from the corresponding "Meteonorm" climate file, [44].

Table 1.15 shows the main dimensional characteristics and energy requirements of residential and office users for the two considered locations. In Table 1.16, the main characteristics of the buildings envelopes are reported.

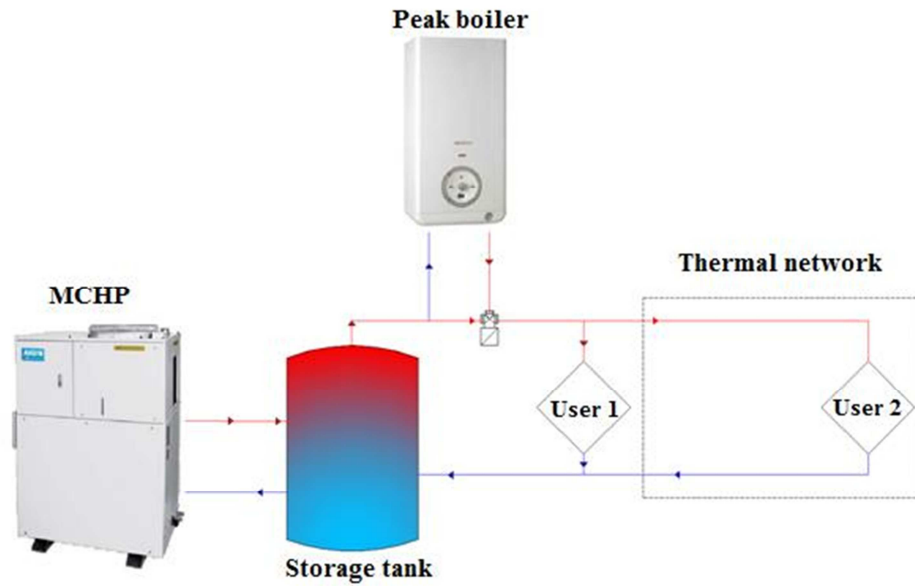


Figure 1.17. Micro-cogeneration system.

Table 1.15. Main characteristics of the considered building.

	Residential		Office	
	Benevento	Milano	Benevento	Milano
Floor surface [m ²]	220	110	524	377
Heated volume [m ³]	660	330	1004	723
Number of occupants [-]	7	4	9	6
Space heating thermal energy requirement [kWh/m ² /year]	59.7	146	28.3	62.5
Electric energy demand [kWh/m ² /year]	16.8	16.8	22.7	22.7

Table 1.16. Building envelope characteristics.

		Opaque building elements			Transparent building elements		
		Roof	External walls	Ground floor	North	South	West/East
Residential	U [W/m ² K]	2.30	1.11	0.297	2.83	2.83	2.83
	g [-]	-	-	-	0.755	0.755	0.755
Office	U [W/m ² K]	0.233	0.335-2.703	0.355	2.35	-	2.35
	g [-]	-	-	-	0.701	-	0.701

With regard to residential user located in Benevento, the following type day, for the characterization of the electrical load, were identified (Figure 1.18):

- Type day # 1: winter (January and February);
- Type day # 2: intermediate (16 September to 31 December and 1 March to 31 May);
- Type day # 3: summer (1 June to 15 September).

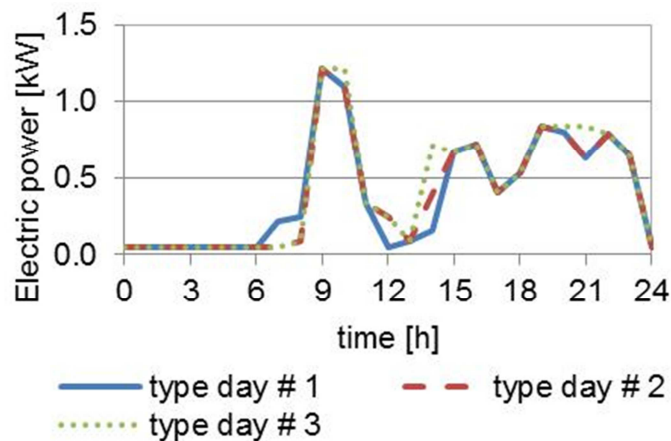


Figure 1.18. Electrical load profile for residential user (Benevento).

The similar electric load profile for the different type days is due to absence of electric consumption for space cooling.

Figure 1.19 shows the electric load for two different type days for the office user:

- Weekend day (Saturday, Sunday);
- Weekday (Monday, Tuesday, Wednesday, Thursday, Friday).

For the residential and office users located in Milano, the electric loads have been scaled from those of Figure 1.18 and Figure 1.19, considering the effects of the different floor area.

It was assumed that the system used to meet the energy demands of the users, consisting of MCHP, thermal storage tank and boiler, is physically placed at the office user. The installed boiler has a nominal heat output equal to 24.2 kW and nominal thermal efficiency of 90.2%, as rated values of the boiler actually installed in the

experimental laboratory. The thermal micro-grid also satisfies thermal energy requirement of residential user, which is assumed to be located at a distance of 50 m from the office.

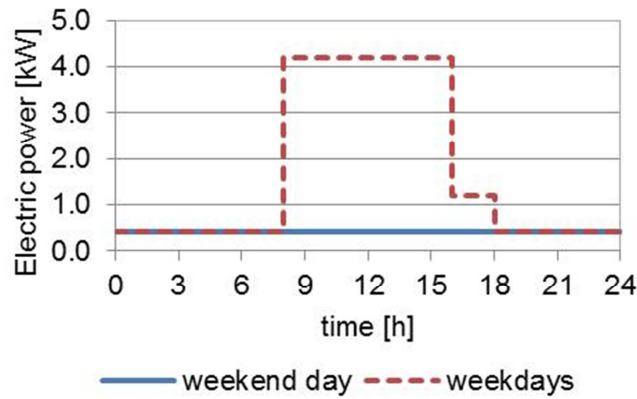


Figure 1.19. Electrical load profile for office user (Benevento).

For space heating in Benevento a maximum number of operating hours of the heating system equal to 10 hours/day during the period November 15 to March 31 was considered. For space heating in Milano 12 hours/day from October 15 to April 15 were considered.

1.4.2. Operating system optimization

Figure 1.20 shows the control scheme implemented in the simulation software. It is possible to define the input information to the Energy Management System (EMS) that has to operate the cogeneration system and the integration device through the control variables of the cogenerator (x_{CHP}) and the boiler (x_B), in the range: $0 \div 1$. The state "0" characterizes the condition of an inactive device, while the state "1" characterizes the operation at full load; intermediate values are associated with operating conditions at partial load. Thermal energy delivered by MCHP is supplied to the storage system, while the electrical power is used to cover the electricity demands of the users and/or sold to the electric grid. As regards the integration system (boiler), if the outlet temperature

from the storage tank is lower than the minimum required by the users, it provides thermal energy to heat-up the fluid to the required temperature.

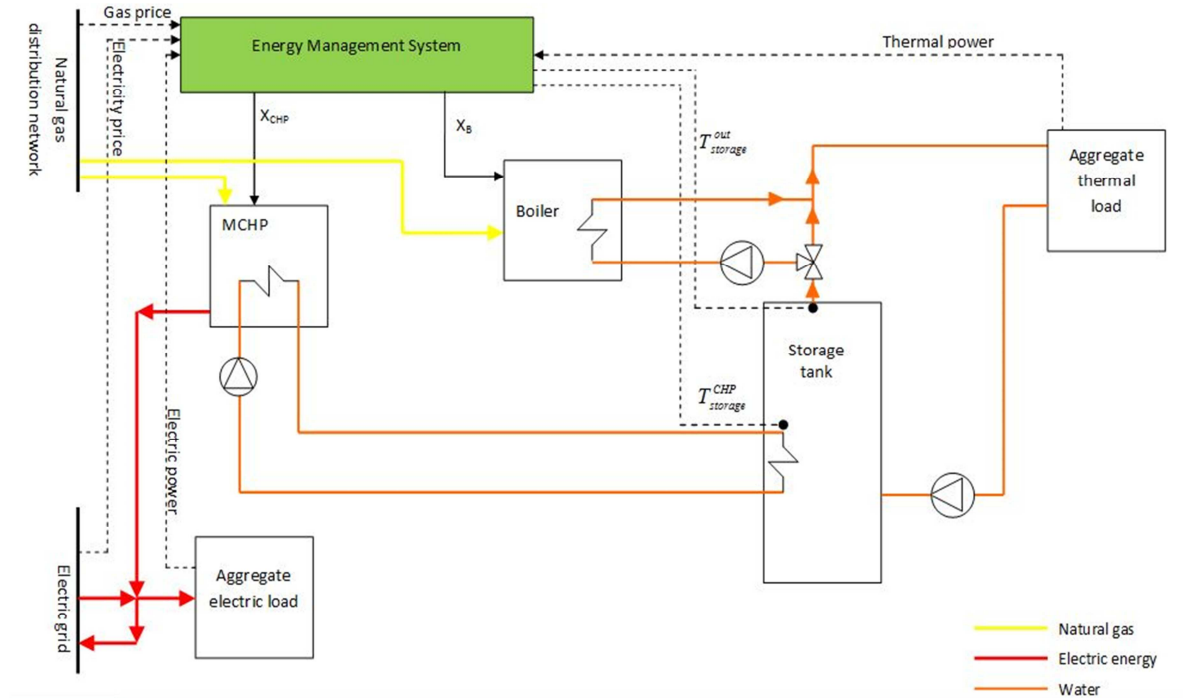


Figure 1.20. Control scheme of the experimental plant at the University of Sannio.

Figure 1.21 illustrates the energy flows for the proposed system and for the traditional one (consisting of boiler and electrical grid), in heating operation. The control system manages the operation of the plant according to a logic of thermo-economic optimization.

The first step of the optimization process is an initialization phase, in which the EMS initializes or assigns the values of the parameters and variables.

After the initialization process, the EMS estimates the electricity to buy or sell to the grid and calculates the operation costs of the conventional system (also called traditional system (TS)) and proposed system (PS). The operation cost of PS (OC_{PS}) is calculated as:

$$OC_{PS} = C_{ng}^{CHP} + C_{ng}^B + C_{maint}^{CHP} - C_{el}^{out} + C_{el}^{in} - C_{EEC} \quad (1.31)$$

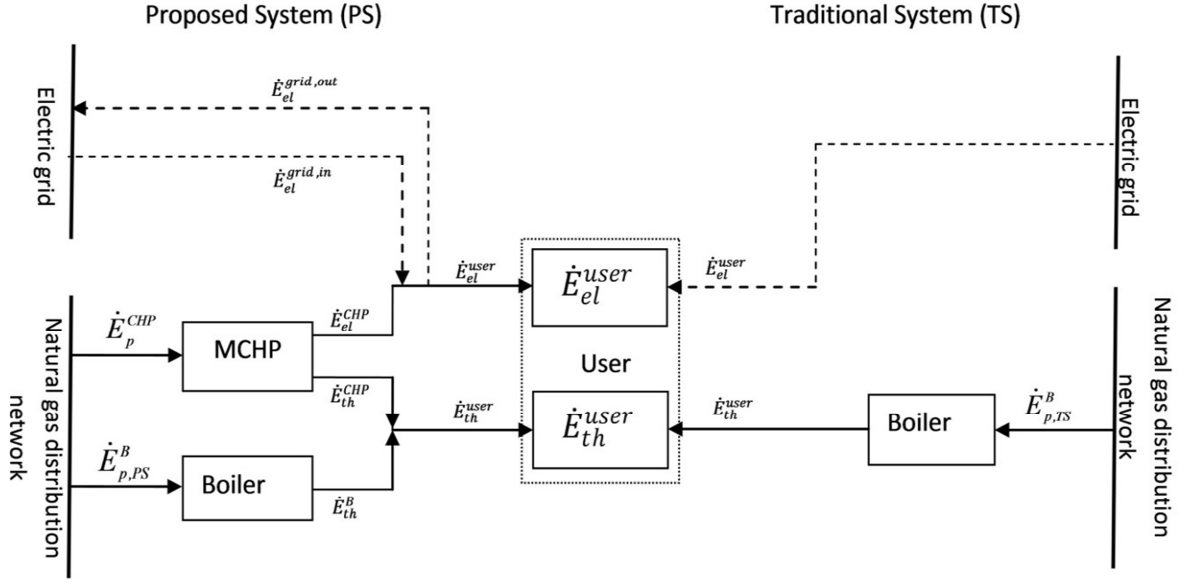


Figure 1.21. Comparison between the proposed system (PS) and the traditional system (TS).

where:

- C_{ng}^{CHP} is the cost associated with fuel for the cogenerator;
- C_{ng}^B is the cost associated with the fuel for the peak boiler;
- C_{maint}^{CHP} is the maintenance cost for the CHP;
- C_{el}^{out} represents the income from electricity sold to the grid;
- C_{el}^{in} represents the cost of purchasing electricity from the grid;
- C_{EEC} represents the revenue associated with the sale of Energy Efficiency Certificates.

The previous equation becomes:

$$OC_{PS} = (\dot{E}_{el}^{CHP} \cdot c_{ng}^{CHP} \cdot \Delta t) / (\eta_{el}^{CHP} \cdot LHV) + ((\dot{E}_{th}^{user} - \dot{E}_{th}^{CHP}) \cdot c_{ng}^B \cdot \Delta t) / (\eta^B \cdot LHV) + c_{maint} \cdot \Delta t + \\ - c_{el}^{out} \cdot \dot{E}_{el}^{grid,out} \cdot \Delta t + c_{el}^{in} \cdot \dot{E}_{el}^{grid,in} \cdot \Delta t - ((\dot{E}_{el}^{CHP} / \eta_{el}^{ref}) + (\dot{E}_{th}^{CHP} / \eta_{th}^{ref}) - \dot{E}_p^{CHP}) \cdot \Delta t \cdot f_c \cdot c_{EEC}^u \quad (1.32)$$

where:

- Δt is the simulation time step (set to 0.1 h);

- c_{maint} is specific maintenance cost of MCHP (set to 0.07 €/h);
- C_{EEC}^u is the specific value of Energy Efficiency Certificates (EEC, set to 100 € for each certificate);
- η_{th}^{ref} is the efficiency of conventional boiler, assumed equal to 0.9;
- η_{el}^{ref} is the average efficiency of Italian electric grid, assumed equal to 0.46;
- LHV is the lower heating value of natural gas, assumed equal to 9.52 kWh/Sm³;
- f_c is a conversion factor equal to $8.6 \cdot 10^{-5}$ toe/kWh;

It should be noted that the MCHP operates at full load and if a thermal power delivered by MCHP is greater than a thermal power required by the user the surplus is stored in the TES. In this case the thermal load of the user can be considered equal to the thermal power of MCHP because the stored thermal energy can be used in a later period. If the temperature of the water contained inside the storage is higher than the TES set point the MCHP is turned off and the TES meets the thermal load of the buildings. In this case the thermal load of the users is considered equal to zero in the eq. 1.32.

In the calculation of the operating costs of the proposed system energy benefits are indirectly considered through EEC.

Similarly, the operating cost of the traditional system (OC_{ST}) can be expressed as:

$$OC_{CS} = (\dot{E}_{th}^{user} \cdot c_{ng}^B \cdot \Delta t) / (\eta^B \cdot LHV) + c_{el}^{in} \cdot \dot{E}_{el}^{user} \cdot \Delta t \quad (1.33)$$

The EMS compares the operating costs of the PS and CS:

1. if $OC_{CS} < OC_{PS}$, the MCHP is turned off;
2. if $OC_{CS} > OC_{PS}$, the MCHP is turned on.

In the second case, to proceed with the activation of the MCHP, a control on the temperature of the heat transfer fluid in the thermal storage near the heat exchanger connected to the cogenerator ($T_{storage}^{CHP}$) must be performed.

In particular if the cogenerator was on, it will be turned off ($x_{CHP}=0$) when the following inequality occurs: $T_{storage}^{CHP} > T_{max}^{CHP}$, where $T_{max}^{CHP} = 55^{\circ}\text{C}$ is the maximum value set for $T_{storage}^{CHP}$. Otherwise the cogenerator remains on. Conversely, if the cogenerator was off, it will be turned on ($x_{CHP}=1$) when the following inequality occurs: $T_{storage}^{CHP} < T_{min}^{CHP}$, where $T_{min}^{CHP} = 50^{\circ}\text{C}$ is the minimum value set for $T_{storage}^{CHP}$.

The introduction of a switch-on (T_{min}^{CHP}) and a switch-off temperature (T_{max}^{CHP}) allows to reduce the number of starts and stops of the MCHP, allowing to preserve its durability.

Next step is to calculate the thermal power provided by the peak boiler. Afterwards, a new calculation of the control variables for the following time step is performed. The algorithm of MCHP system is explained in the flowchart shown in Figure 1.22.

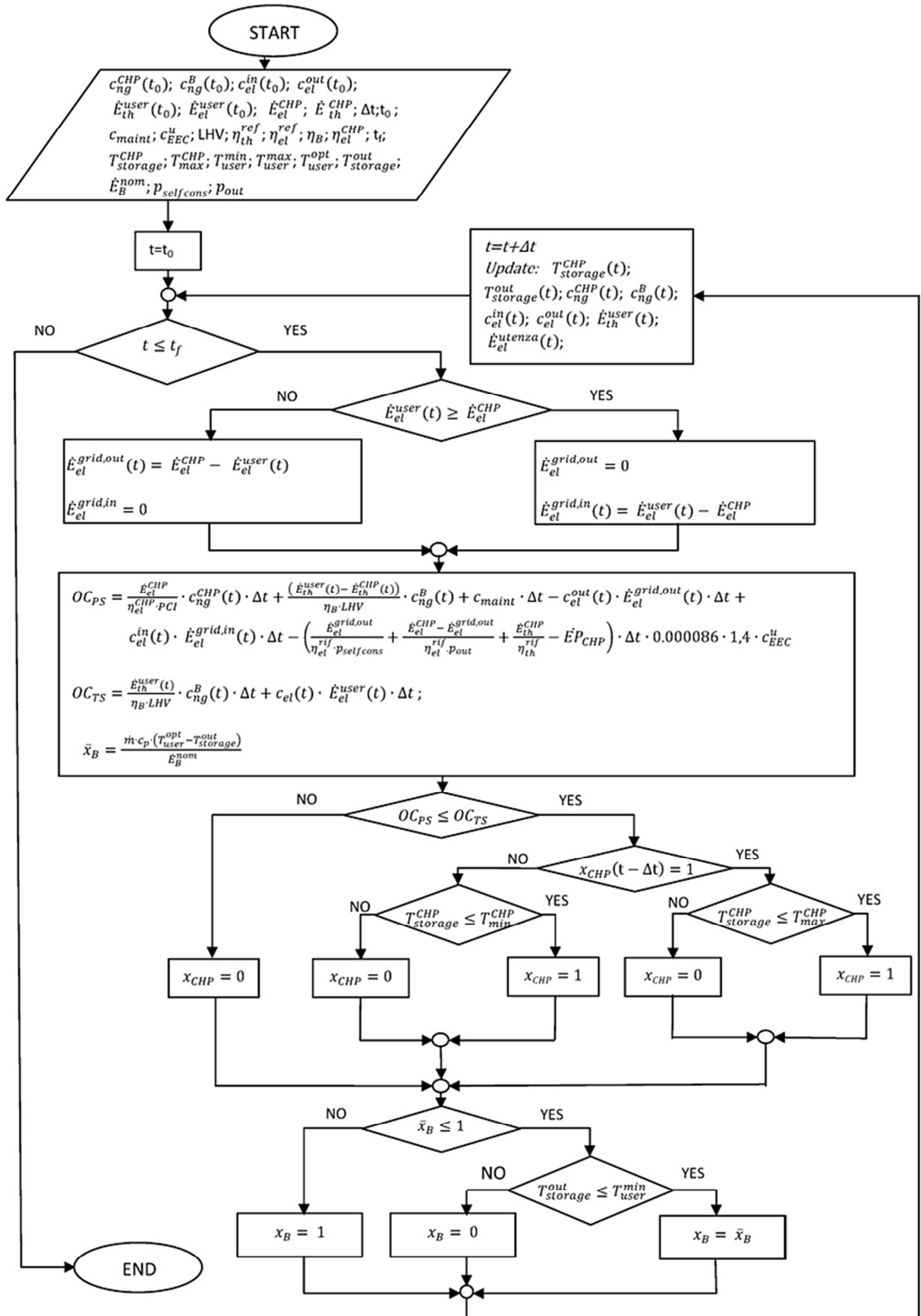


Figure 1.22. Control algorithm of micro-polygeneration system.

1.4.3. Discussion and results

Table 1.17 shows the main results obtained from the simulations in Benevento and Milano. Two different scenarios were analyzed. Firstly (Table 1.17) it was assumed that the unit costs of electricity and natural gas are equal for the traditional system and for the proposed one. The simulations were performed for the period of year during which the heating system is allowed to be used.

Table 1.17. Simulation results during the heating period.

	Benevento	Milano
Heating hours [h]	2154	3294
MCHP operation hours [h]	1906	2448
Total heating demand [kWh]	28807	38472
Thermal energy from MCHP [kWh]	21602	27698
Electrical energy produced by MCHP [kWh]	10571	13529
Thermal energy from boiler [kWh]	7205	10774
Thermal energy lost by TES [kWh]	865	1162
Thermal energy lost by thermal micro-grid [kWh]	443	583
Total electricity demand [kWh]	5821	7780
Electricity purchased from the grid [kWh]	1394	2538
Electricity sold to the grid [kWh]	6015	8104
PES [%]	18.5	16.9
ΔCO_2 [%]	25.9	23.9
MCHP Maintenance cost [€]	133	178
EEC [-]	1.28	1.78
Operational cost reduction [€]	542	703

The load sharing approach guarantees a high number of operation hours for the proposed system in Benevento (1906 h) and Milano (2448 h). The number of operation hours of the MCHP in Milano is about 28% higher than in Benevento, due to the higher number of heating hours during the day in Milano than in Benevento. For both geographic locations, the thermos-economic optimization always allows the operation of the cogeneration system. This is due to the lower natural gas tariff for the cogeneration system. In Milano, the higher number of operating hours leads to a greater electric and thermal energy "production" by the MCHP, as well as a greater primary energy demand to meet the total heating requirements.

As the MCHP has been sized with respect to the thermal load of users, it results to be oversized compared to the users electric demands. Therefore the electricity “produced” is greater than the required one, hence a share of the “produced” electricity is sold to the grid. The electricity demand is also partially covered by the electric grid, indeed electric energy is taken from the grid when there is a corresponding request, but the MCHP is off.

A small amount of thermal energy produced (4.5%) is lost in the TES and in the thermal micro-grid.

The primary energy saving (*PES*) is higher in Benevento (18.5%) than in Milano (16.9%). Besides the primary energy savings, the proposed system allows to obtain a reduction of CO₂ emissions (Δ CO₂) of 25.9% and 23.9% respectively for Benevento and Milano (Figure 1.23). As regards the economic analysis, the reduction of operating cost of PS with respect to CS is 542 € for Benevento and 703 for Milano.

The analysis showed that the use of MCHP involves energy and environmental advantages. The reduction of operation cost is good but not high enough to ensure an adequate payback period. Indeed considering an additional investment cost of the PS with respect to the CS equal to 22000 €, the SPB reach high values (Figure 1.23).

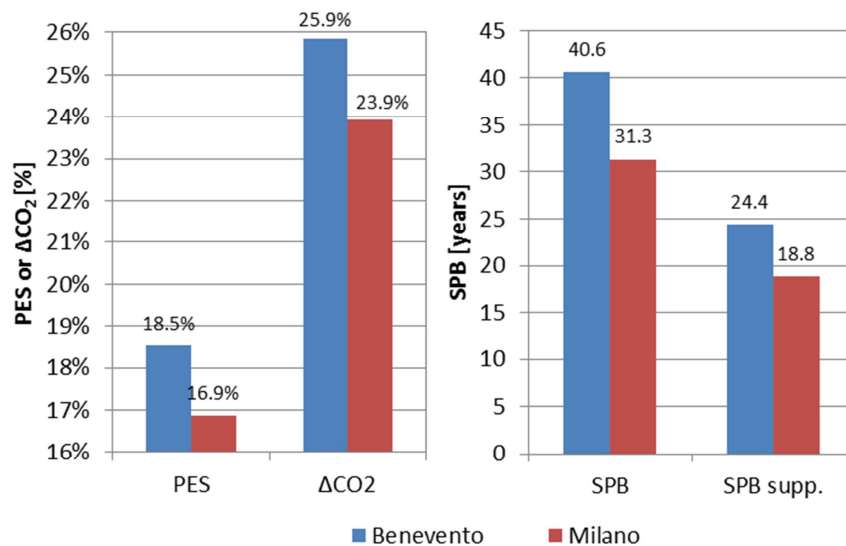


Figure 1.23. Energy, environmental and economic analysis for the analyzed system.

In some case there are economic support mechanisms which can provide up to the 40% of the investment cost. Nevertheless, the SPB still has high values (SPB supp. in Figure 1.23).

As described in the introduction chapter, the introduction of an Energy Service Company (ESCO) could help to solve the economic problem. In fact, an ESCo, managing a large number of distributed systems, could obtain a purchase price of natural gas and electricity lower than that applied to individual customers. For this reason in the second scenario it has been assumed that the prices of energy vectors for the proposed system were 20% lower than the prices for the traditional system.

For both locations, the energy and environmental results are the same of the previous case, while the improvements of economics results are evident. The reduction of annual operation cost is 1394 € and 1880 €, respectively for Benevento and Milano. In this case the SPB could reach interesting value especially in presence of support mechanisms (Figure 1.24).

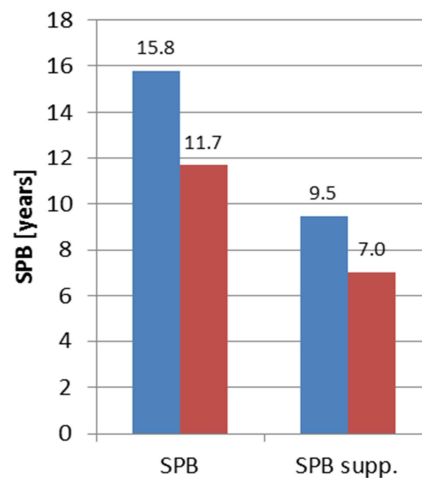


Figure 1.24 SPB in case of reduced purchasing costs of energy vectors

Finally, the results show that the analyzed system allows obtaining a high number of operating hours of the micro-cogenerator, also in Mediterranean areas where the climate conditions are not favorable to diffusion of this technology. It should be noted that the needs of domestic hot water and thermal energy for space cooling requirements (by means of thermally activated equipment) were not taken into account. The proposed system showed good energy (*PES* in the range 16.9%-18.5%) and

environmental (ΔCO_2 in the range 23.9%÷25.9%) results. The economic analysis highlights the need of appropriate support mechanisms to promote the diffusion of this interesting technology. Moreover the introduction of an Energy Management System that controls the MCHP operation according to a thermo-economic objective function could be an interesting solution in order to minimize the operational cost of the whole system. However with current energy vectors costs the MCHP system has lower operating cost with respect to the CS, in every time of the day.

1.5 Microcogeneration in buildings with low energy demand in load sharing application

In this section the introduction of the MCHP system that is described in section 1.1 in buildings with higher level of thermal insulation with respect to the current building stock is investigated. A load sharing approach between a multifamily residential building and an office one is taken in account. Dynamic simulations are carried out in order to evaluate the thermo-economic performance of the analyzed system. Particular attention is given to the estimation of the electric load of the different users as the economic profitability of an MCHP system is strongly influenced by the amount of self-consumed electricity. In order to analyze the influence of climatic conditions, two different geographical locations in Italy (Napoli and Torino) are considered. From this point of view, the weather data referred to these two Italian cities, are characterized by 1034 (Napoli) and 2617 (Torino) heating degree days. The results of this study indicate that the installation of MCHP systems based on reciprocating internal combustion engine, in insulated buildings allows increasing the percentage of self-consumed electricity reducing the bidirectional electricity flow between the users and the external grid, reducing the impact on the grid itself due to the large diffusion of distributed generation systems. Finally, a sensitivity analysis with respect to the share of self-consumed electricity is carried out to investigate on the influence of this parameter on the economic performance of the MCHP system.

1.5.1. Users description

The users analyzed in this work are referred to two separate buildings with different uses. The first building is a typical multifamily house with six apartments, while the second one is an office building. The main characteristics of the two buildings are described in the following subsections. Different characteristics of the buildings envelope are defined for Napoli and Torino, taking into account the different climates. Both buildings are equipped with low temperature heating devices (fan coils) according to the supply temperature of the heating system.

1.5.1.1 Residential user

The residential user is an Italian multifamily house, which consists of six different apartments. Each apartment has a floor surface equal to 100 m² with a heated volume of 300 m³. The apartments are placed on 3 floors (2 apartments for each floor), Figure 1.25. The building has a south-oriented sloped roof. The characteristics of the building envelope are reported in Table 1.18.

Table 1.18. Main characteristics of building envelope.

	Transmittance [W/m ² K]		Thermal mass [kg/m ²]		g-value [-]	
	Napoli	Torino	Napoli	Torino	Napoli	Torino
External wall	0.40	0.34	373	373	-	-
Roof	0.38	0.30	322	322	-	-
Ground	0.42	0.33	689	689	-	-
Window	2.60	2.20	-	-	0.60	0.48

The transmittance of each component is chosen according to the Italian law [80]. The thermal mass for the buildings located in Torino and Napoli is the same, because the two envelopes differ only for the thickness of insulation, whose contribution to the thermal mass is negligible due to the very low density. The transmittance of windows refers to an average value that takes into account the transmittance of both the window frame and of the glass, assuming a ratio between the frame and the total surface of the window

(glass and frame) equal to about 20%. Moreover the windows represent about 20% of the external walls surface. Table 1.18 reports the g-value (solar gain) of the transparent surface. In order to reduce the solar gain in summer period, a horizontal shading device is installed above each window.

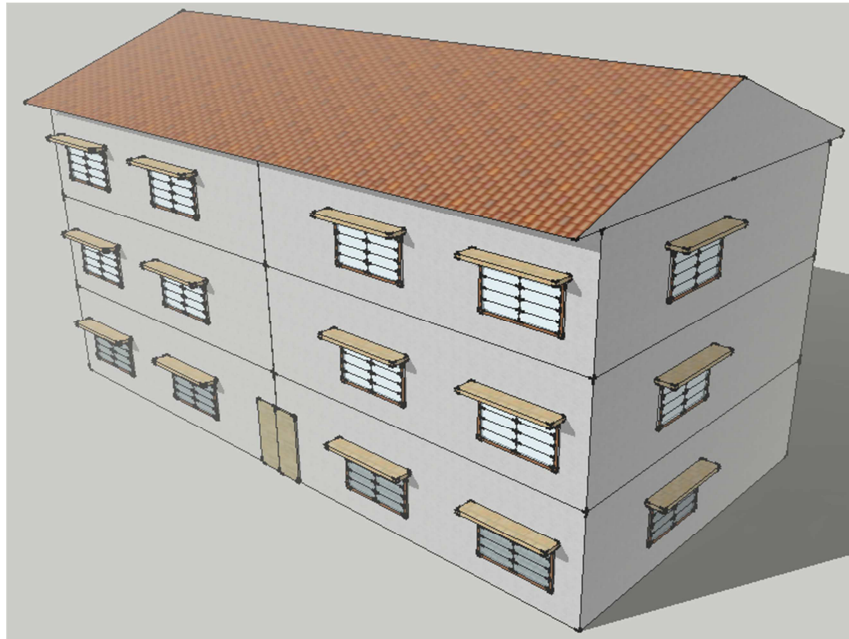


Figure 1.25. Residential building.

A careful analysis about the electric demand of each building is carried out. The electric loads of each flat are based on a high-resolution (1 minute) model of domestic electricity use. The model is based on a pattern of active occupancy, a list of installed appliances and daily activity profiles that characterize how people spend their time performing certain activities. A detailed description of the used model is reported in ref. [81]. Different typical residential users are defined:

- #1 is composed by four occupants (two employed adults and two young students) with an average annual electricity demand of 3100 kWh/year;
- #2 is composed by four occupants (two employed adults, one young student and one retired person) with an average annual electricity demand of 3250 kWh/year;

- #3 is composed by two occupants (two employed adults), with an average annual electricity demand of 1350 kWh/year;
- #4 is composed by two occupants (two retired persons) with an average annual electricity demand of 1400 kWh/year.

Figure 1.26 reports the number of active occupants (when people are at home and awake) for each residential user and for two type days, week day (wd) and week end day (we). These occupancy profiles are defined based on the different behavior of the people that live in the flats.

Based on active occupants profiles, on typical appliances installed in an Italian house and on annual electric demand of each typical user, the model is able to estimate the electric load (Figure 1.27).

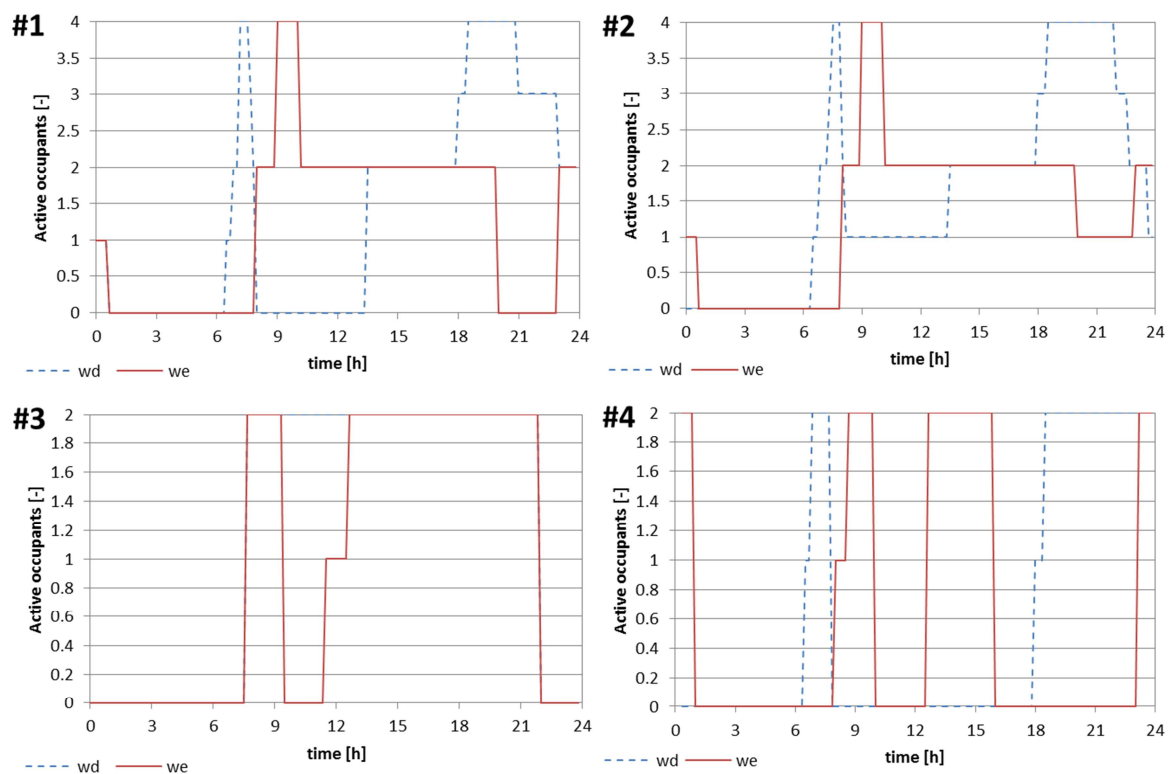


Figure 1.26. Daily profile of active occupants for each type of residential user.

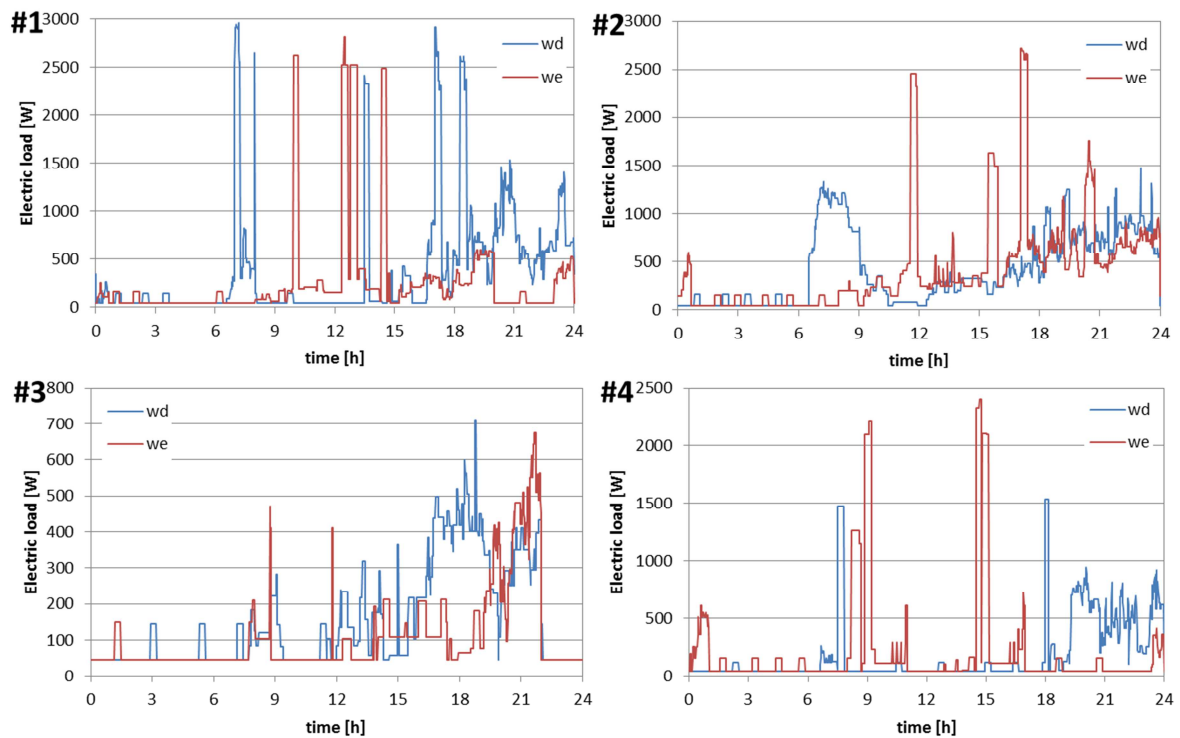


Figure 1.27. Daily electric demand for each type of residential user.

As the residential building is composed by six flats, it was assumed that there are two users of type #1, two of type #2, one of type #3 and one of type #4.

The residential domestic hot water draw profile was developed by means of a software [82] developed within the scope of the Solar Heating and Cooling Program of the International Energy Agency (IEA SHC) Task 26. In order to take into account fairly realistic DHW (Domestic Hot Water) demands for a period of one year a time step of 6 minutes was chosen. The average daily demand was assumed equal to 150 l/day for each flat [83]. The hot water profile for the residential user (cumulative hot water demand for the six flats) is reported, only for the first week of the simulated year (for clarity reasons), in Figure 1.28.

The heating period was assumed from November 15th to March 31st for Napoli and from October 15th to April 15th for Torino. The daily operational hours of the heating system must respect a maximum limit according to Italian law [84]. This limit depends on the climatic zone of the user and it is 10 hours/day in Napoli and 14 hours/day in Torino. Therefore, the heating system is turned on according to the following time schedule:

- 6:00-9:00 and 17:00-22:00 for the buildings located in Napoli;
- 5:00-10:00 and 16-24:00 for the buildings located in Torino.

When the heating system is turned on the set-point of room thermostats is set to $20\pm 0.5^{\circ}\text{C}$. Therefore the fan coils are turned on when the temperature is less than 19.5°C and turned-off when it is higher than 20.5°C .

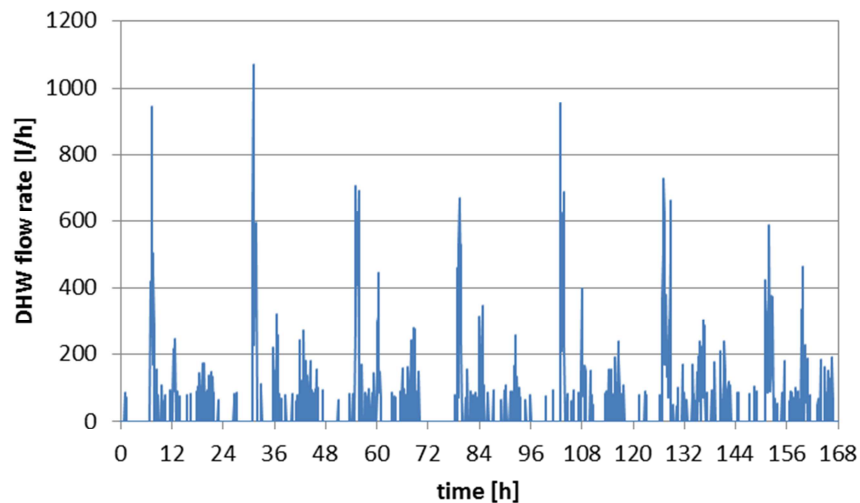


Figure 1.28. Hot water demand profile for residential user in the first week of year.

The buildings are modelled by means TRNSYS [42] simulation software.

Figure 1.29 reports the duration diagram of the space heating load for the residential building located in Napoli and Torino. The figure shows the influence of the climate on the operation of the heating system. The operational hours of the heating system located in Napoli are about the half of the same system located in Torino. The peak value of the thermal load for the residential user located in Torino is higher than the user located in Torino due to different climate conditions.

The annual thermal energy demand for space heating purposes is $27 \text{ kWh/m}^2/\text{year}$ for Napoli and $55 \text{ kWh/m}^2/\text{year}$ for Torino.

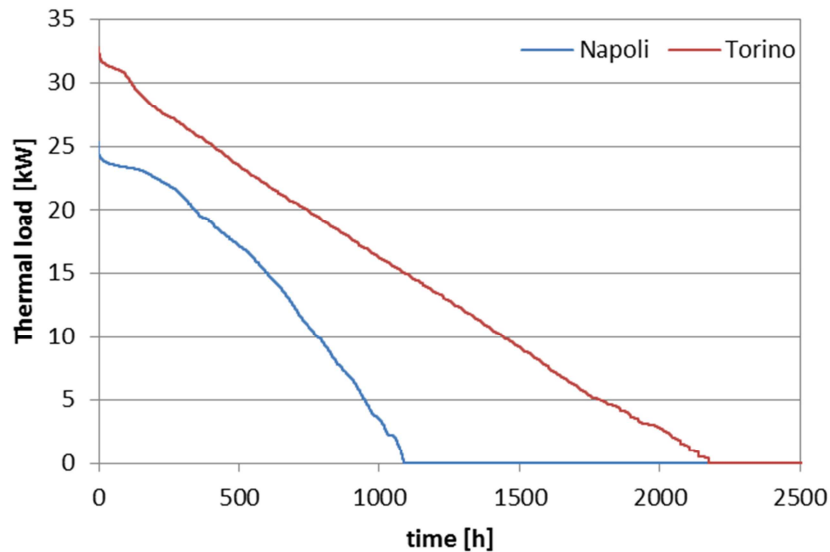


Figure 1.29. Duration diagram of the space heating load for residential buildings.

1.5.1.2 Office user

The office building has the same envelope characteristics and the same size of the residential one. The main differences between the two buildings are the following:

- the office building has a larger transparent surface (the windows represent about the 25% of the surface of the external walls);
- the office building has a flat roof.

The electric annual demand of the office building is defined according to the target value indicate in EL-TERTIARY study for office buildings [85]. This study monitored the electricity consumption in the tertiary sector. For this work, the annual consumption is assumed equal to 52 kWh/m²/year. The electric load profile is defined according to ref.[86]. Figure 1.30 reports the electric load profile for two type days (wd and we), while Figure 1.31 shows the number of occupants for the office building in a work day. In a weekend day there are no occupants in the office. The hot water demand for the office user is not taken in account because it is negligible with respect to the heating load.

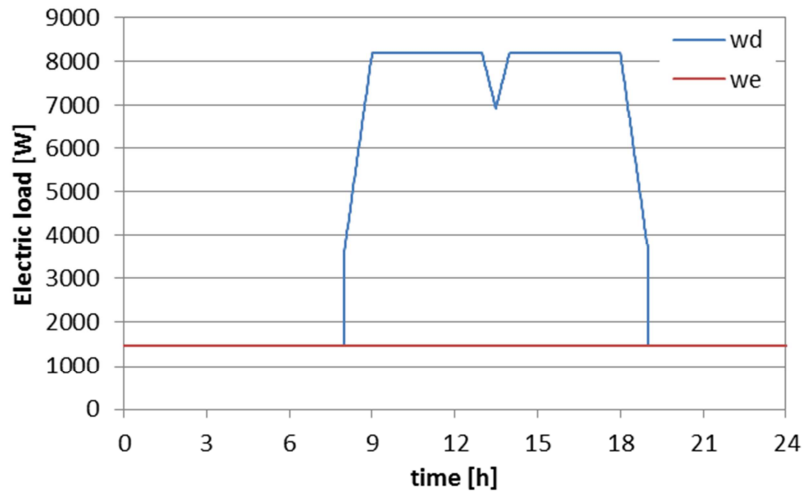


Figure 1.30. Electric load profile for office user.

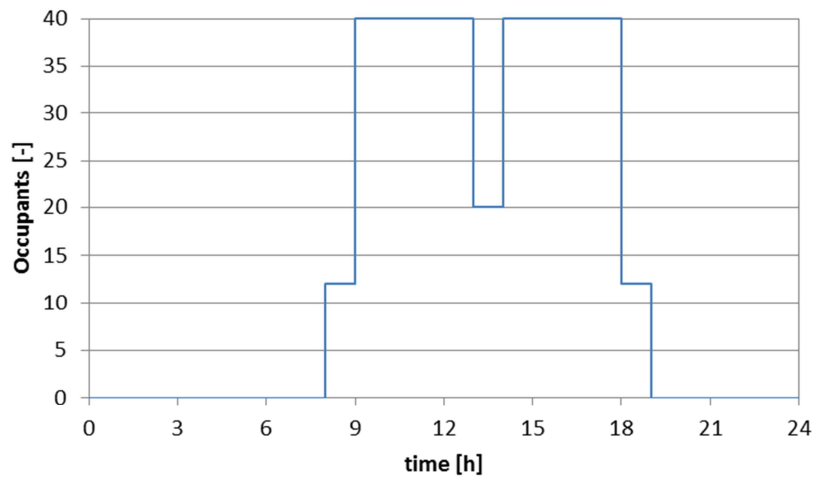


Figure 1.31. Number of occupants for the office building in a work day.

The heating period and the set-point of room thermostats are the same of the residential building; the operation time of the heating systems is assumed between 8:00 to 18:00, in a work day, for the building located in Napoli. For the office user located in Torino the heating system is turned on between 7:30 to 18:00. Moreover in Torino on Monday the heating system is turned on at 6:00 because the building requires a longer warm-up time. In weekend the heating systems is turned off in both cities. The building is simulated by means of the TRNSYS software. The duration diagram of the space heating load for the office building is reported, for the two geographic locations, in Figure 1.32.

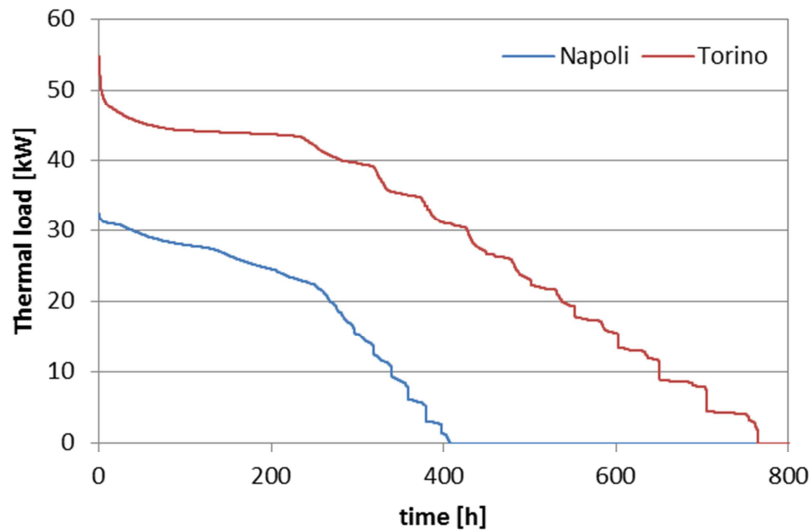


Figure 1.32. Duration diagram of the space heating load for the office building.

Even for the office user the peak value of the thermal load and the operational hours of the heating system are different for the two locations.

The annual thermal energy demand for space heating purposes is equal to 14 kWh/m²/year for Napoli and 38 kWh/m²/year for Torino. The lower heating demand of the office building with respect to the residential one is due to a different operation time of the heating system; in fact in the office building the heating system is turned on only during the work time. Moreover the different internal gains of the two users (occupants and electric appliances) concur to provide different heating demands.

1.5.1.3. Load sharing

The duration diagrams of the space heating load for the office and residential buildings, reported in Figure 1.29 and Figure 1.32, highlight the few operation hours of the heating system, especially in mild climate condition such as in Napoli. The introduction of an MCHP systems in these two buildings could lead energy and environmental advantages, but the few operation hours of the system could lead to bad economic performance, such as a long payback period. In order to increase the operation hours of the MCHP systems it is possible to share the users' loads by means of a thermal and electric micro-grid. This solution leads, as an example, to a duration diagram of the space heating load

for the two buildings (residential and office users), in load sharing approach, as that one showed in Figure 1.33.

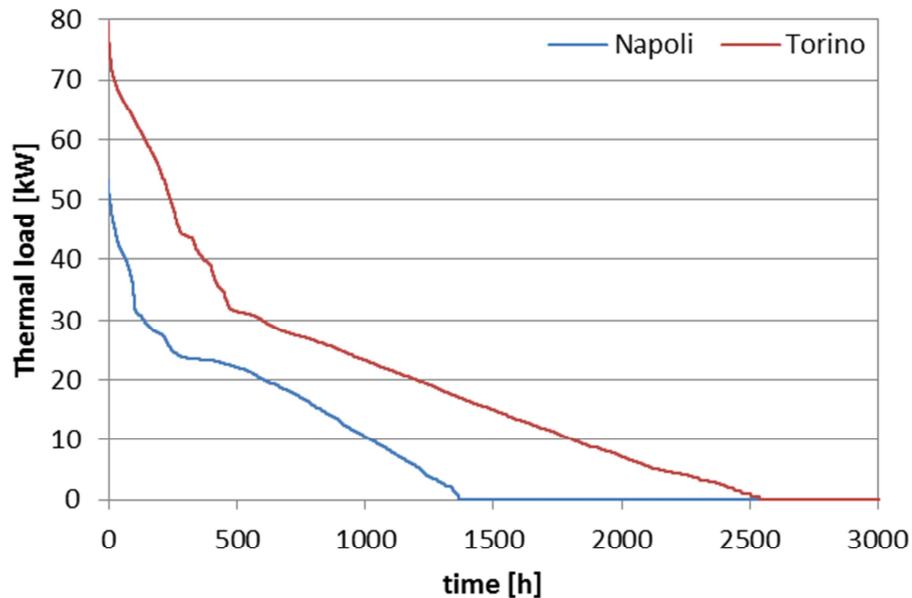


Figure 1.33. Duration diagram of the space heating load for the two buildings in load sharing approach.

The configuration of the MCHP system is described in the previous section 1.1. The MCHP plant is installed in the residential building and the thermal energy is transferred to the office building by means of a thermal micro-grid with a length of 50 m (Figure 1.34). An electric connection between the MCHP plant and the office is created in order to use the electricity “produced” by the MCHP also in the office building.

The peak boiler delivers a nominal heat output of 35 kW for the user located in Napoli and 60 kW in Torino. The nominal thermal efficiency is equal to 92.6% and to 93.6% for the user located in Napoli and Torino, respectively. The thermal efficiency of boiler is reported as a function of partial load ratio for different boilers size in ref. [87].

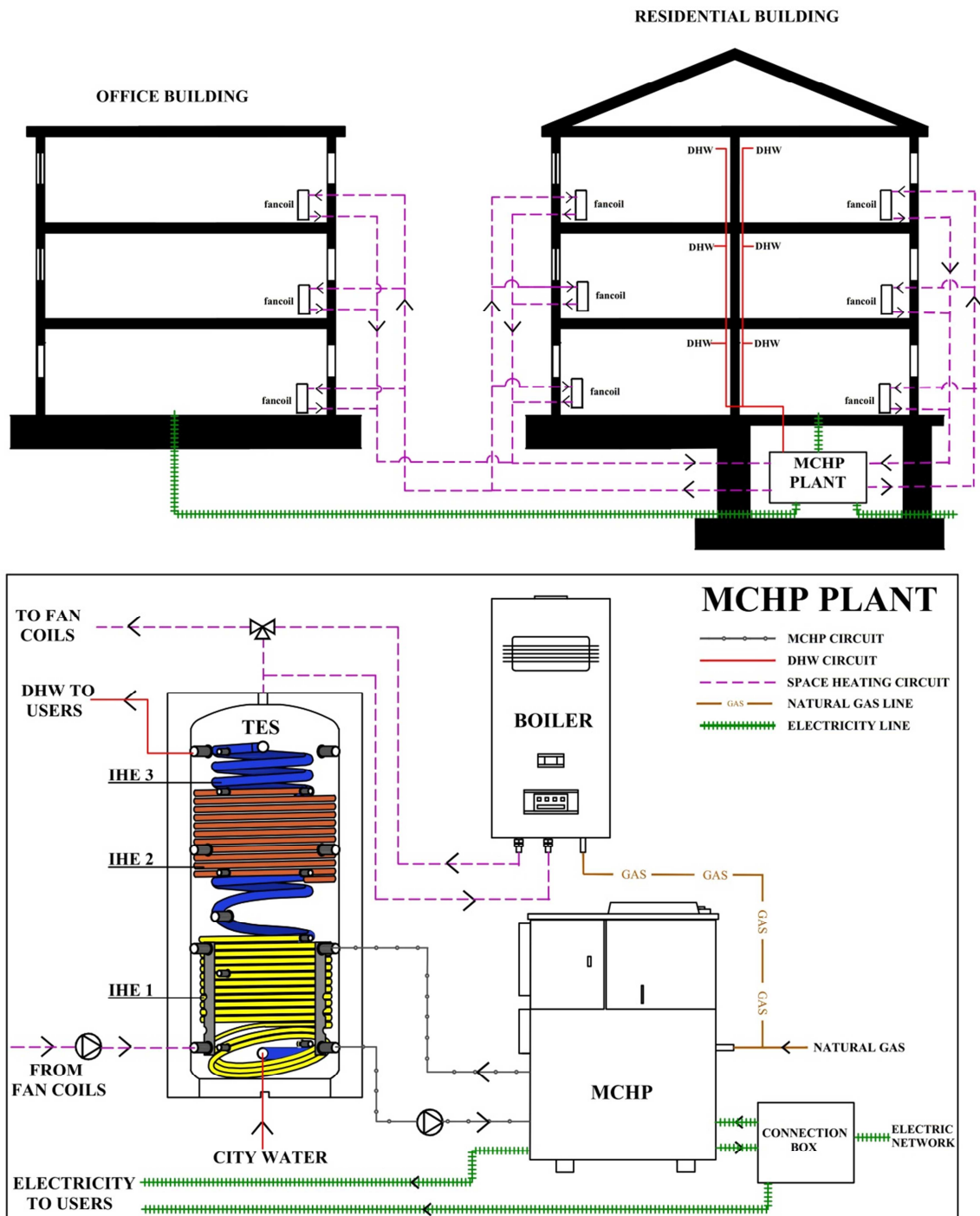


Figure 1.34. System configuration.

The performances of the MCHP plant (Proposed System, PS) are compared with those of a conventional system (CS) that consists of:

- two separate boilers for residential and office buildings. In the residential user, the boiler has a nominal thermal capacity of 25 kW for Napoli climate and 35 kW for Torino climate, with a nominal efficiency of 92.1% and 92.6%, respectively;

while in the office user, the boiler has a nominal thermal capacity of 35 kW for Napoli and 50 kW for Torino, with a nominal efficiency of 92.6% and 93.1% respectively;

- a TES is installed in the residential building in order to meet the DHW demand without oversizing the boiler. The installed TES has the same characteristics of that one installed in the MCHP plant.

1.5.2. Discussion and results

Figure 1.35 reports the simulation results for the users located in Napoli in a typical winter day. In particular the diagram on the top-left side reports the thermal power provided by the fan coils to the office (P_{th} office) and to the residential user (P_{th} house) and that one provided by the MCHP (P_{th} MCHP) in a week day. The energy demands of the two users occur in a different time of the day and the profiles are quite complementary. The thermal power provided to the residential building has less variation than the office one, as the residential building is divided in six thermal zone (one for each flat) and the activation of the fan coils for each zone is not contemporary. The office building is modelled as one thermal zone so the activation of all fan coils occurs in the same time. For this reason in some hours of the day the switching on and off of the fan coils can determine a huge variation of thermal power required by the office user. The presence of the TES allows the MCHP system to work continuously with few on-off cycles. The diagram on the top-right of Figure 1.35 reports the electric load profiles of the combined users (P_{el} user) and the electricity purchased from (P_{el} purchased) and sold to (P_{el} sold) the external grid in a week day. In addition the electricity provided by the MCHP (P_{el} MCHP) is reported. Only in the evening (between 21:00 and 22:00) there is a small quantity of electricity (less than 1% of the “production”) sold to the grid.

The diagram on the bottom-left of Figure 1.35 reports the thermal power provided by the fan coils to the two users and provided by the MCHP in a weekend day. The load profile of the residential user is the same of the previous case while the heating system is turned off in the office building. In a weekend day the electricity demand is lower than in the week day due to the lower energy demand of the office user (bottom-right

diagram). In a typical winter weekend day, the amount of electricity sold to the grid is about 35% of the “production”.

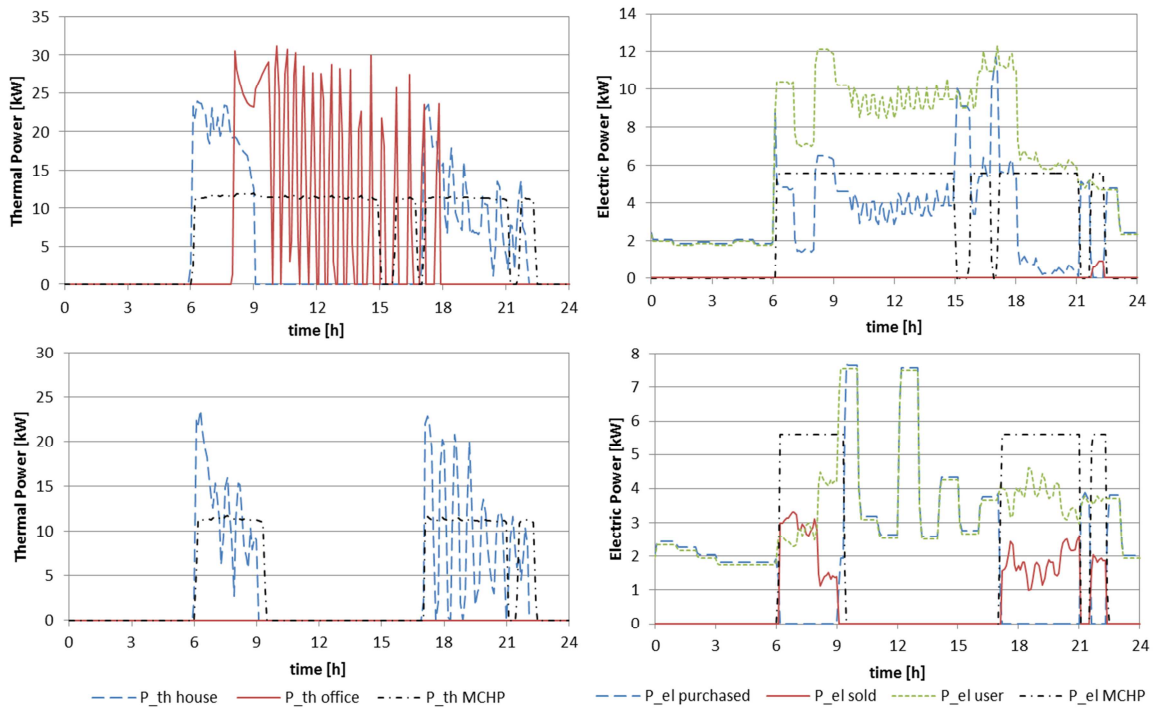


Figure 1.35. Simulation results for the users located in Napoli in a typical winter day.

Similarly, Figure 1.36 reports the simulation results for the users located in Torino in a typical winter day. In this case the thermal power peak in the office and residential building located in Torino are greater than that one located in Napoli due to different climate. In a typical winter day, the MCHP system meets the base thermal load and it operates at full load for the most part of the day thanks to the presence of the TES. The electricity produced is largely self-consumed (about 93% of the “production” is self-consumed) in a week day while it is partially sold to the grid in weekend day (about 35% of the “production”). In a no-heating period, the MCHP operation is due only to the DHW demand. Even in this case the presence of TES allows the MCHP to operate continuously at full load.

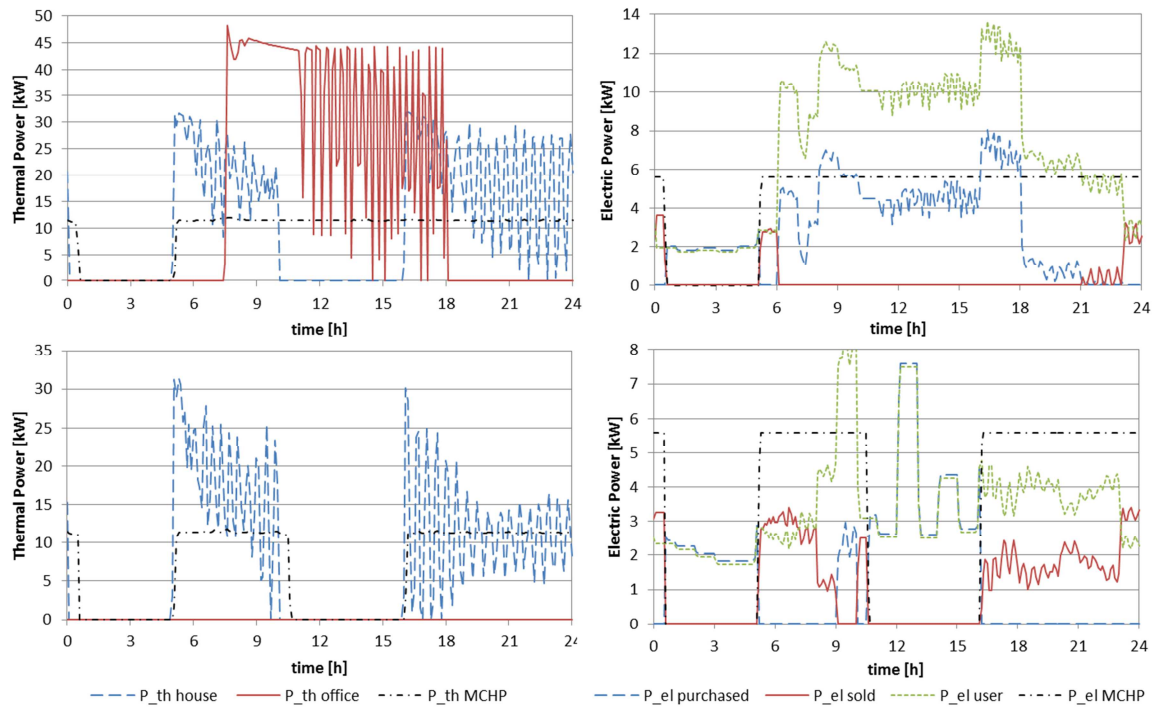


Figure 1.36. Simulation results for the users located in Torino in a typical winter day.

Table 1.19 provides the results obtained from the annual simulations for buildings located in Napoli and in Torino. In particular the table summarizes:

- the energy demands of the users in terms of heating, electricity and DHW;
- the thermal energy losses of the TES and of thermal micro-grid and the auxiliary consumptions of fans and pumps of the heating system (both PS and CS);
- the thermal energy provided by MCHP and boilers (both PS and CS);
- the electricity provided by MCHP and the percentage of self-consumed electricity in PS;
- the Primary Energy (PE) required by the MCHP and boilers (both PS and CS).

The heating demand for the buildings located in Torino is more than two times the heating demand of the buildings located in Napoli. Electricity and DHW demands are about the same for the two cities. The MCHP meets a large percentage of the heating and DHW demand for both locations (70% for Napoli and 56% for Torino). A very important result emerging from the data is that a large percentage of the “produced” electricity is self-consumed by the users; in both locations this percentage is greater than 85%. The introduction of an MCHP system based on reciprocating internal

combustion engine in a building with a well-insulated envelope leads to high value of self-consumed electricity. This is due to the different ratio between thermal and electric loads with respect to a building with a lower insulation level. In fact the thermal load of a building strongly depends on the insulation level of the envelope, while the electric load is not related to the building envelope characteristics.

Table 1.19. Energy simulations results on annual basis.

			Napoli	Torino
Energy demand [kWh]		Heating demand of residential user	16,270	33,233
		Heating demand of office user	8,560	22,702
		Total heating demand	24,830	55,935
		Electricity demand of residential user	15,438	15,438
		Electricity demand of office user	31,485	31,485
		Total electricity demand	46,923	46,923
		DHW demand of residential user	9,694	9,694
Thermal energy losses and auxiliary consumption [kWh]		Thermal energy lost by thermal micro-grid	293	401
	PS	Thermal energy lost by TES	1,833	1,851
		Auxiliary consumption (fans + pumps)	975	2,040
	CS	Thermal energy lost by TES	1,694	1,791
		Auxiliary consumption (fans + pumps)	900	2,385
Thermal energy "production" [kWh]	PS	Thermal energy from MCHP	24,984	37,248
		Thermal energy from boiler	11,659	30,629
	CS	Thermal energy from the office boiler	8,582	22,385
		Thermal energy from the residential boiler	27,573	44,690
PE [kWh]	PS	Primary energy input of boiler	12,547	31,769
		Primary energy input of MCHP	43,690	65,398
	CS	Primary energy input of office boiler	9,318	24,039
		Primary energy input of residential boiler	29,964	48,002
Electricity [kWh] or [%]	PS	Electrical energy produced by MCHP	11,203	17,228
		Self-consumed electricity	89.6%	85.2%

For this reason if the MCHP is sized on the basis of the thermal load, the percentage of self-consumed electricity is high for an insulated building. This aspect leads to different advantages:

- the economic revenue associated to the self-consumed electricity is generally higher than that associated with the electricity sold to the external grid. This is due to the different prices between the electricity sold to the grid and that purchased from the grid. In Italy the revenue associated to the electricity sold to the grid, for an MCHP system, is about the 70% of the purchase price. Therefore the high value of self-consumed electricity leads to economic advantages.
- the wide diffusion of distributed generation systems leads to management issues on the electric grid. If a high level of self-consumption is achieved, the impact of the MCHP on the grid is reduced. In addition the introduction of an electric micro-grid that connects the two buildings (load sharing) concurs to reduce the bidirectional electricity exchange with the external grid.

In order to compare the performance of a microcogeneration plant in a load sharing scenario (PS) with respect to a reference one (CS), a thermo-economic analysis [3] has been implemented according to the index and the tariffs defined in the section 1.3.

According to the tariffs defined in section 1.3, the natural gas cost results equal to 0.90 €/Sm³ and 0.86 €/Sm³ for Torino and Napoli, respectively. For the natural gas that feeds the MCHP a different cost is considered (reduced tax) according to the Italian law for cogeneration (0.79 €/Sm³ for both the locations). The electricity cost is assumed equal to 0.21 €/kWh for both the locations.

Figure 1.37 compares the energy, environmental and economic results for the buildings located in Napoli and Torino. The energy, environmental and economic performances of the users located in Torino are better than those of the users located in Napoli. This result can be explained by the different operational hours of the MCHP system. In fact in Torino the MCHP operates for about 3200 hours with respect to 2150 hours in Napoli. The PES is equal to 6.2% and 8.8%, respectively, for Napoli and Torino. Moreover the PS allows to obtain a reduction of carbon dioxide equivalent emissions equal to 6.7% in Napoli and to 8.3% in Torino.

The economic results are not so good for both locations. In fact the SPB is equal to 18.4 and 11.6 years respectively for Napoli and Torino. However in some case there are economic support mechanisms which can provide up to the 40% of the investment cost. If these incentives are taken into account, the SPB could reach interesting values, especially in Torino.

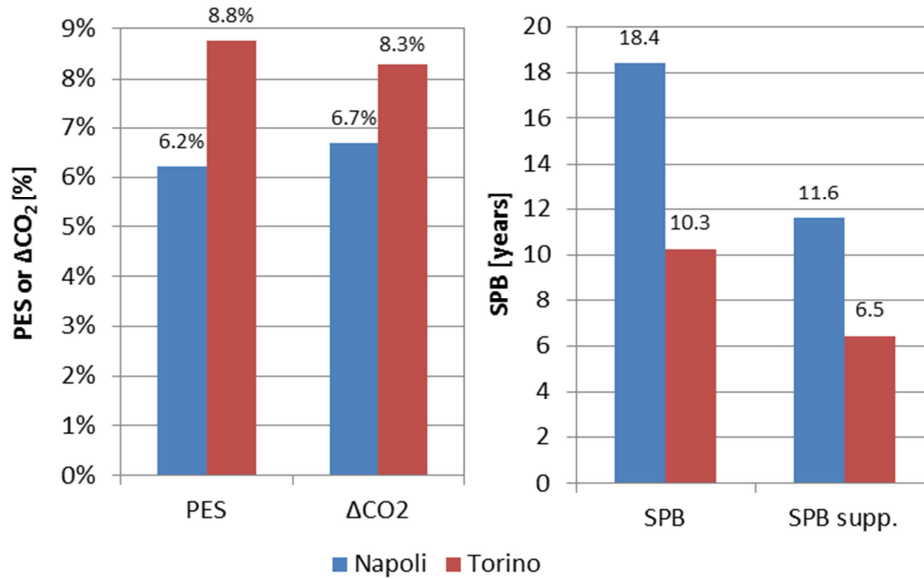


Figure 1.37. Energy, environmental and economic analysis.

In order to highlight the influence of the self-consumed electricity share on economic results, a sensitivity analysis with respect to this parameter is carried out, Figure 1.38. As can be seen from Figure 1.38 the payback period strongly depends on the percentage of self-consumed electricity. For both the locations the SPB period reaches interesting value for high share of self-consumed electricity. If the user sells all the “produced” electricity to the external grid, the economic sustainability of the MCHP system is difficult to achieve also in presence of economic incentives (dashed line).

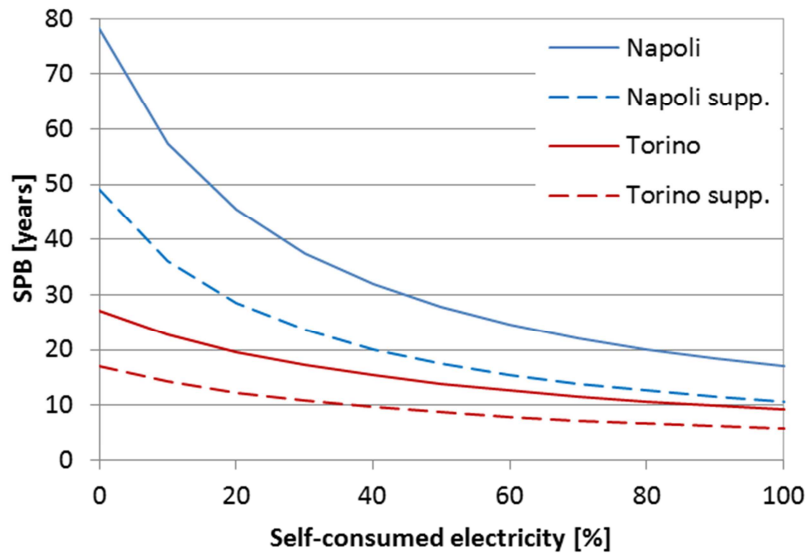


Figure 1.38. SPB as function of the percentage of self-consumed electricity.

Therefore, this section has investigated the introduction of MCHP systems in buildings with low energy demand. In order to increase the operational hours of the MCHP system a load sharing between two different users was proposed. Moreover the simulations were performed considering two different Italian cities to analyze the correlation between the energy, environmental and economic performance with the climatic conditions. The following conclusion can be drawn from the present study:

- the installation of MCHP systems in insulated buildings allows to increase the percentage of self-consumed electricity reducing the bidirectional electricity flow between the local users and the external grid. This aspect allows to reduce the impacts of the large diffusion of distributed generation systems on the grid. Moreover the high value of self-consumed electricity leads to economic advantages.
- The sensitivity analysis with respect to the share of self-consumed electricity highlights the influence of this parameter on the economic results. Generally an MCHP system is sized on the base of the thermal load. This analysis shows that a careful assessment of the economic performance of an MCHP system may not go beyond by knowledge of user electric load.
- In order to obtain energy, environmental and economic benefits, it is essential to install the MCHP system where there is a suitable heating demand. The results of

this study indicate that, in well-insulated building, the introduction of a micro-grid between different users can help to have thermal and electric load profiles suitable for the MCHP application.

- The load sharing approach between users with different load profiles allows to increase the operational hours of an MCHP systems. This aspect leads to better energy, environmental and economic results with respect to a conventional system.
- The climatic conditions play an important role on the MCHP operational hours and hence on the thermo-economic performance of the system. Mainly, the MCHP operational hours have a strong influence on the SPB period. In mild climatic condition (Napoli), the increase of the MCHP operational hours due to the load sharing approach is not enough to obtain interesting value of the SPB without economic incentives. In this case, the introduction of a trigeneration system, able to meet also the cooling demand of the buildings in summer period, can improve the energy, environmental and economic performance of the system.
- Well-insulated buildings, having lower demand-side heat-to-power ratios (in the range 2.5-3 in the investigated paper) with respect to the average existing stock, perfectly match with the quite low values of the plant-side heat-to-power ratio of MCHPs based on internal combustion engines (about 2 in the investigated case). Other technologies are less suitable for this application, either because they have higher heat-to-power ratios (such as about 4-7 for Stirling engines, suitable for standard buildings with lower insulation levels) or higher investment costs (such as fuel cells).

These findings suggest that the installation of an MCHP system in residential or tertiary buildings with low energy demand is suitable if more users are coupled together by means of a thermal and electric micro-grid (load sharing approach).

1.6 Integration between electric vehicle charging and a micro-cogeneration system

In the near future the diffusion of plug-in electric vehicles (EVs) could play an important role in the reduction of emissions and oil dependency associated with the transport sector. However this technology could have a big impact on the electric network because EVs require a considerable amount of electricity. In order to meet the growing load due to the diffusion of EVs, the construction of new infrastructures will be required. The introduction of micro-cogeneration systems could represent a key factor in the reduction of the negative effects on the electric network related to EVs charging. The EVs are often driven during the day and recharged during the night; so the overnight charge of the EVs allows to reduce the amount of electricity exported to the grid. In this way the economic benefits associated with the introduction of micro-cogenerator system (Micro Combined Heat and Power, MCHP), that depend on the economic value of the “produced” electricity, can be improved. At the same time the impact of EVs charge on the electric network can be reduced when electricity is provided by MCHP.

In this section, the interaction among the MCHP system, which is described in section 1.1, the EV charging and typical semidetached house is investigated by means of dynamic simulations. The analysis is carried out in two different locations (Torino and Napoli) in order to evaluate the effects of climatic conditions on the system performance. A parametric analysis with respect to the daily driving distance of the EV is carried out in order to highlight the effect of this parameter on the simulation results. Moreover, this section analyzes the effects that the EV charging strategy could have on the energy, environmental and economic results of the analyzed system. Two different EV charging strategies are taken in account: a normal charging strategy and an optimized one. In the first one, charging occurs when the EV is parked at home until the full charge is reached, while in the optimized strategy, charging is related to the MCHP operations in order to maximize the amount of self-consumed electricity and reduce the impact of EVs charging on the electric grid. The simulation results are strongly influenced by the daily driving distance of the EV, therefore a sensitivity analysis with respect to this parameter is carried out. Due to the different energy demand of scenarios with different EV daily driving distance, the thermo-economic analysis is performed as both absolute and relative comparison.

1.6.1. User description

The user is a residential semidetached house with a total floor surface of 324 m², equally divided on two adjacent apartments. Each apartment is arranged on two floors connected by an indoor staircase. Combining the electric and thermal load of several apartments, it is possible to increase the capacity of the MCHP system, so the specific investment cost (€/kW_{el}) and the energy performance are positively affected (size effect). Generally, the more the number of apartments, the more this size effect is important. Nevertheless, as a cautionary assumption, the minimum number of separate apartments (two) has been considered in this work. The results are expected to improve with a higher number of apartments. The analysis is performed in two different geographical locations in Italy, Napoli (NA) and Torino (TO), characterized by 1,034 (NA) and 2,617 (TO) heating degree days, respectively. Different buildings envelope characteristics are defined for Napoli and Torino in order to represent a typical semidetached house for each analyzed area. The envelope characteristics of the building located in Napoli are defined according to a study on the current building stock reported in a draft of Energy Plan of Campania Region [88]. The characteristics of the building located in Torino are chosen according to a reference building for Piemonte Regional building stock reported in the European project “*Tabula*” [89]. Table 1.20 reports the main thermo-physical features of building envelope for the two locations. The reference building in Torino has better envelope characteristics (more thermally insulated) with respect to the building located in Napoli due to the colder climatic conditions. In both locations, the windows represent about the 20% of the external walls surface. The ratio between the frame and the total surface of the window (glass and frame) is equal to 20% too.

Table 1.20. Main characteristics of building envelope [88] [89].

	Transmittance [W/m ² K]		Thermal mass [kg/m ²]		g-value [-]	
	NA	TO	NA	TO	NA	TO
External wall	0.957	0.755	372	292	-	-
Roof	1.00	1.00	360	360	-	-
Ground	1.44	0.98	746	714	-	-
Window	2.95	2.83	-	-	0.77	0.75

The electric loads of the two apartments are based on a high-resolution (1 minute) model of domestic electricity use. The model estimates the electric load according to: a list of installed appliances, a pattern of active occupancy, and daily activity profiles that characterize how people spend their time performing certain activities. An exhaustive description of the used model is reported in [81]. The loads are defined considering four occupants for each apartment. In particular apartment #1 is inhabited by two employed adults and two young students with an average annual electricity demand of 3,100 kWh/year, apartment #2 is inhabited by two employed adults, one young student and one retired person with an average annual electricity demand of 3,250 kWh/year. The definition of the kind of occupants is essential in order to define the active occupants profile and consequently the electric load.

Figure 1.39 shows the active occupants (when people are at home and awake) for the two apartments and for two type days, week day (wd) and week end day (we). The occupancy profiles are defined according to the different behavior of the people that live in the house.

The model is able to estimate the electric load of the users according to active occupant profile, typical appliances installed in an Italian user and annual electric demand of each apartment (Figure 1.40). An average annual electric profile has been considered.

The residential domestic hot water (DHW) draw profile was obtained by means of a software [82] developed within the “*Solar Heating and Cooling Program (IEA SHC, Task 26)*” of the International Energy Agency. The DHW demand is defined for a period of one year with a time step of 6 minute. The average daily demand was assumed equal to 190 l/day for each apartment [83], equivalent to 5.52 kWh/day (2015 kWh/year), assuming an average supply temperature of the DHW demand equal to 40°C and an average city water temperature of 15°C. Figure 1.41 shows the hot water profile for the two users, only for the first week of the simulated year (for reasons of brevity).

The heating period was assumed different for the two locations: from November 15th to March 31st for Napoli and from October 15th to April 15th for Torino. The daily operation hours of the heating system follows the maximum limit according to Italian law [84]. This limit depends on the climatic zone and it is equal to 10 hours/day in Napoli and 14 hours/day in Torino. According to this limit, the heating system is turned on according to the following schedule:

- 6:00-10:00 and 17:00-23:00 in Napoli;
- 5:00-11:00 and 16-24:00 in Torino.

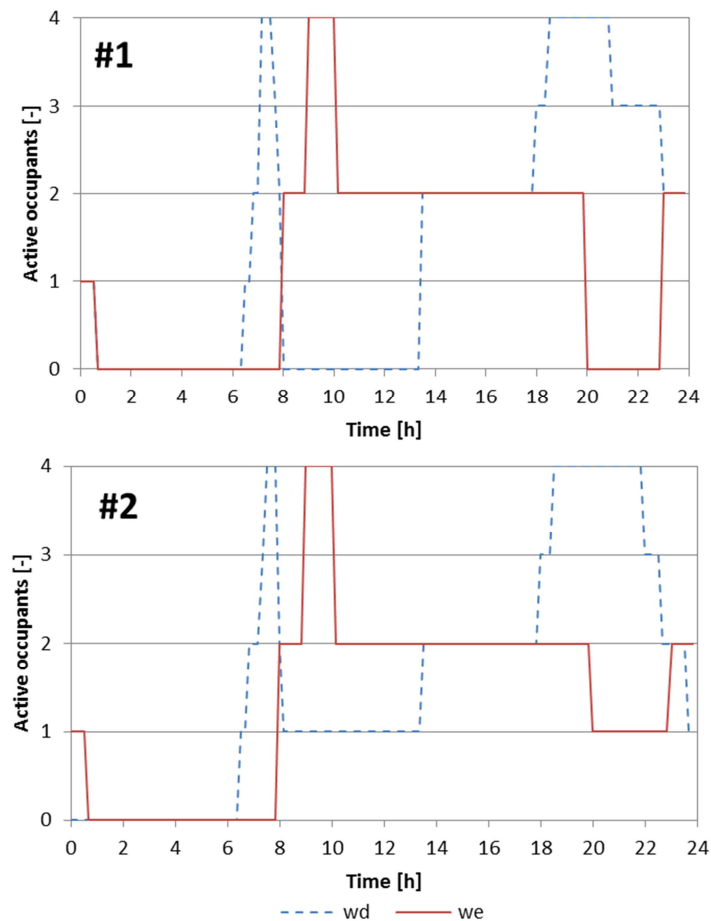


Figure 1.39. Daily profile of active occupants.

The building is modelled, using a simulation software [42], assuming four thermal zone. Each apartment is divided in two thermal zones (one for each floor). When the heating system is turned on the zone thermostats set-point is assumed equal to $20 \pm 0.5^\circ\text{C}$. Therefore the heating devices are turned-on when the inside temperature is less than 19.5°C and they are turned-off when it is higher than 20.5°C . The building is equipped with low temperature heating devices (e.g. fan coils, radiant systems) according to the supply temperature of the MCHP.

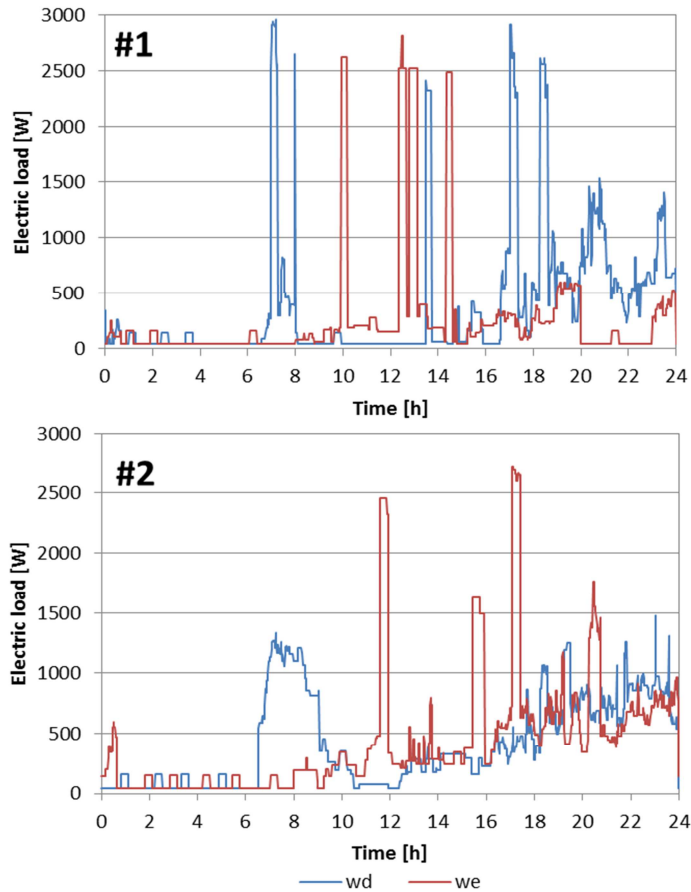


Figure 1.40. Daily electric demand.

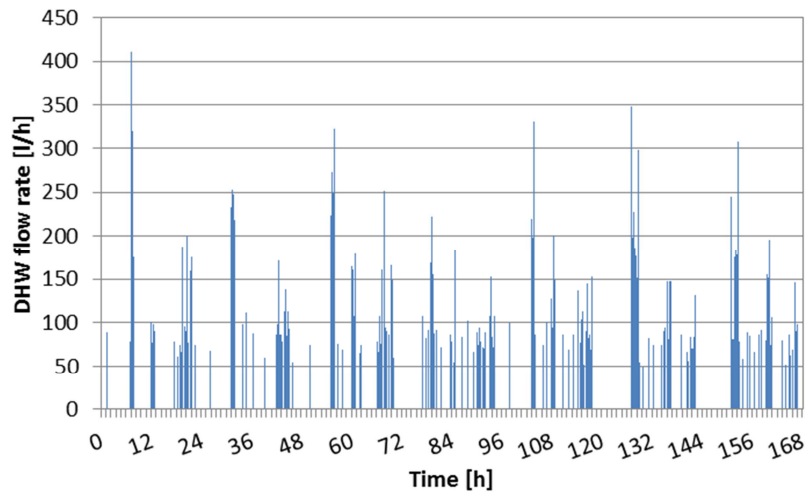


Figure 1.41. Hot water demand profile for the semidetached house in the first week of year.

The duration diagram of the space heating load, for the analyzed semidetached house, is reported in Figure 1.42. The figure highlights the influence of the climate on the duration diagram of the space heating load and hence on the operation hours of the heating

system. The building located in Torino has a higher peak (33.0 kW) of thermal power demand with respect to the one located in Napoli (22.5 kW), due to the different climate conditions. The operation hours of the heating system located in Napoli (1360 h) are less than the operation hours of the same system located in Torino (2300 h), due to the longer heating period of the latter as allowed by the law.

The annual space heating demand of the building is equal to 49 kWh/m²/year for Napoli and 83 kWh/m²/year for Torino.

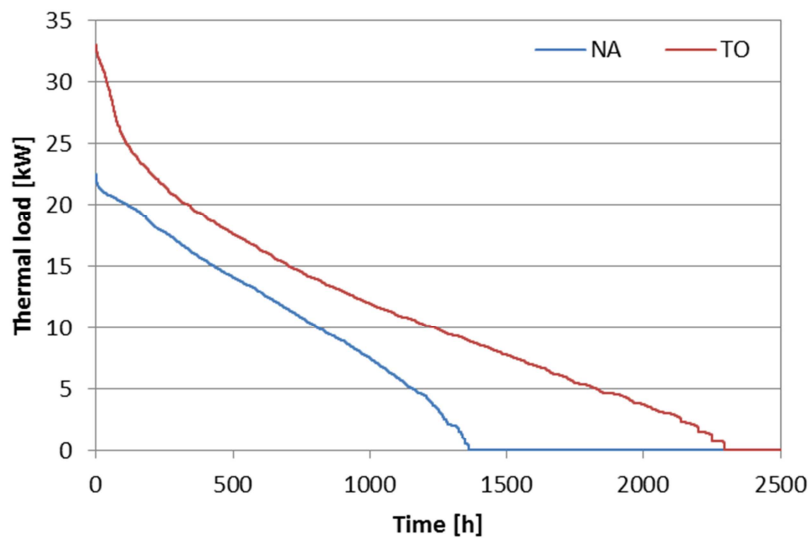


Figure 1.42. Duration diagram of the space heating load for the semidetached house.

As regards the energy demand for mobility purposes, the presence of one electric vehicle for the semidetached house was considered. The choice to consider the presence of only one EV for two families is a cautionary assumption, related to a partial penetration of the electric mobility. In fact, if an EV for each family is considered, the advantages related to the interaction between EV charging and MCHP system will be greater, as it will be described later. The analysis was conducted considering different daily driving distances, so the mobility need is considered as a parameter that varies between 0 and 120 kilometers per day.

Figure 1.43 shows the configuration of the Proposed System, PS. The MCHP system configuration is described in the previous section 1.1. The natural gas boiler delivers a nominal heat output of 25 kW, with a thermal efficiency equal to 92.1%.

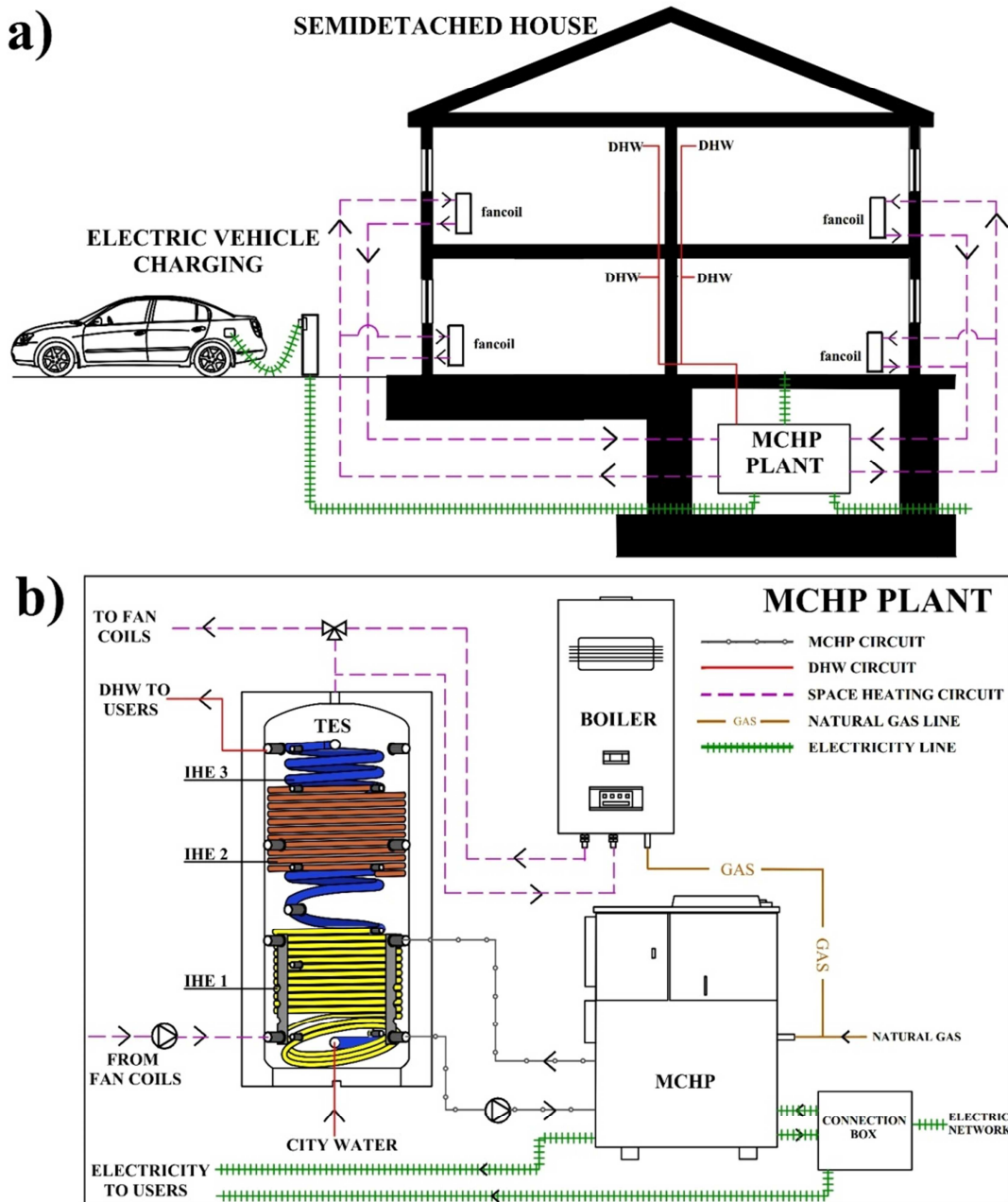


Figure 1.43. a) Interactions between building and MCHP plant; b) MCHP plant.

An electric vehicle charging station is installed in the premises of the building. The charging station has a charging power of 3.3 kW and an efficiency equal to 86% [90]. In this case the efficiency is the ratio between the power output and input to the charging station. The EV average performance is assumed equal to 0.173 kWh/km [91]. In order to evaluate the electric load associate to the EV charging for different daily driving distances two, different charging strategies are defined. In the first one (normal charging) the charging starts when the EV is parked at home (18:30) and stops when the

full charge is reached. The second strategy (optimized charging) allows to maximize the amount of self-consumed electricity supplied by MCHP. In fact, the charging occurs if the EV is parked at home and the MCHP is activated. Moreover a charging control system ensures that EV is fully charged at 7:30 am. The charging control system evaluate, in each simulation time-step, what is the time required for the fully recharge of the battery; if this time is less than the available one (that is, the time remaining time until 7:30 am) the EV charging is forced, from the electric grid, even if the MCHP is turned-off. The performances of the MCHP plant are compared with those of a conventional system (CS), that consists of a boiler for each apartment. Therefore two boilers of 25 kW in Napoli and two of 30 kW in Torino are installed. In the CS the electricity needs are met by the electric grid.

1.6.2. Discussion and results

The analyzed system is simulated in the heating period for the two locations. Figure 1.44 shows the thermal power provided to the building by the fan coils and that one provided by MCHP and boiler in a typical winter day. Thermal power required by the user has strong fluctuations due to the switching on and off of the fan coils (the building is divided in four thermal zones). The presence of the TES allows the MCHP to continuously operate, with few on-off cycles. The boiler operation (green line) is needed in order to ensure the supply temperature to the fan coils and it occurs in periods of high user thermal energy demand (morning and afternoon start-up phase).

The electric load of the user depends on the EV daily driving distance and on the adopted charging strategy. In Table 1.21 the electricity demand for EV charging for different daily driving distance is reported. The table reports also the charging time required to fully charge the EV battery. It linearly increases with the daily driving distance.

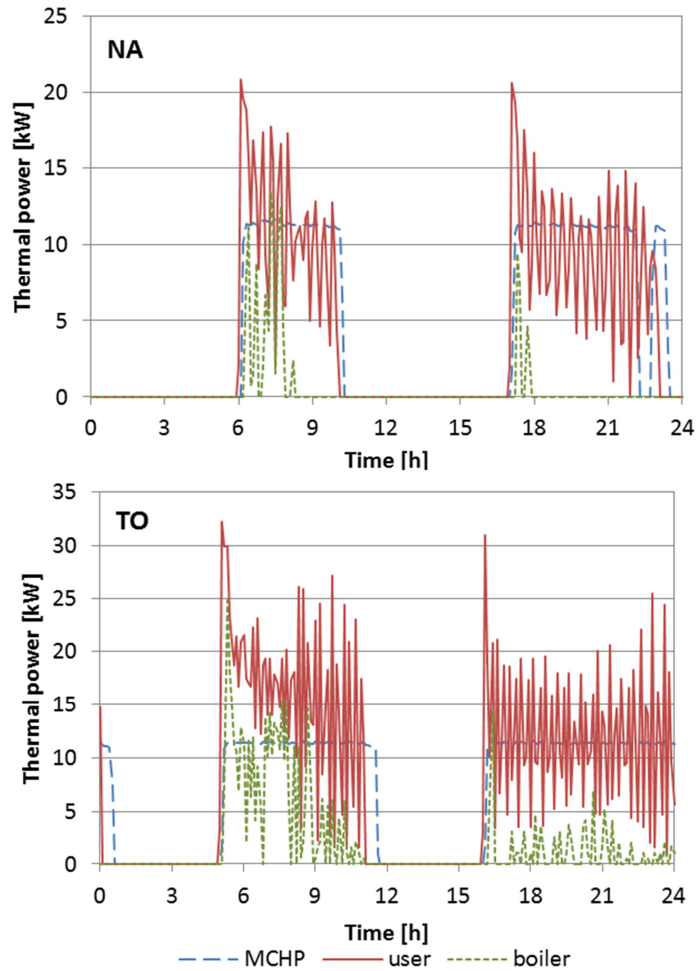


Figure 1.44. Thermal load of the semidetached house and thermal power provided by boiler and MCHP for the user located in Napoli (left) and Torino (right) in a typical winter day.

Table 1.21. Electricity demand for EV charging as function of EV daily driving distance.

Distance [km]	20	40	60	80	100	120
Output DC electricity [kWh]	3.46	6.92	10.38	13.84	17.3	20.76
Input AC electricity [kWh]	4.04	8.07	12.11	16.15	20.19	24.22
Charging time [h]	1.22	2.45	3.67	4.89	6.12	7.34

Figure 1.45 shows the electric power required by the semidetached house for some of the investigated daily driving distances with normal charging strategy in Napoli. Moreover the figure reports the electricity purchased from and sold to the electric grid. The pink areas indicate that the EV is in charging. It must be pointed out that when the MCHP is turned off, the purchased electricity is slightly higher than the user's demand,

due to the MCHP standby electric consumption (90 W). The EV charging starts at 18:30 and ends when the EV is fully charged. For a daily driving distance of 40 kilometers, the EV charging occurs when the MCHP is turned on, so the amount of self-consumed electricity is increased.

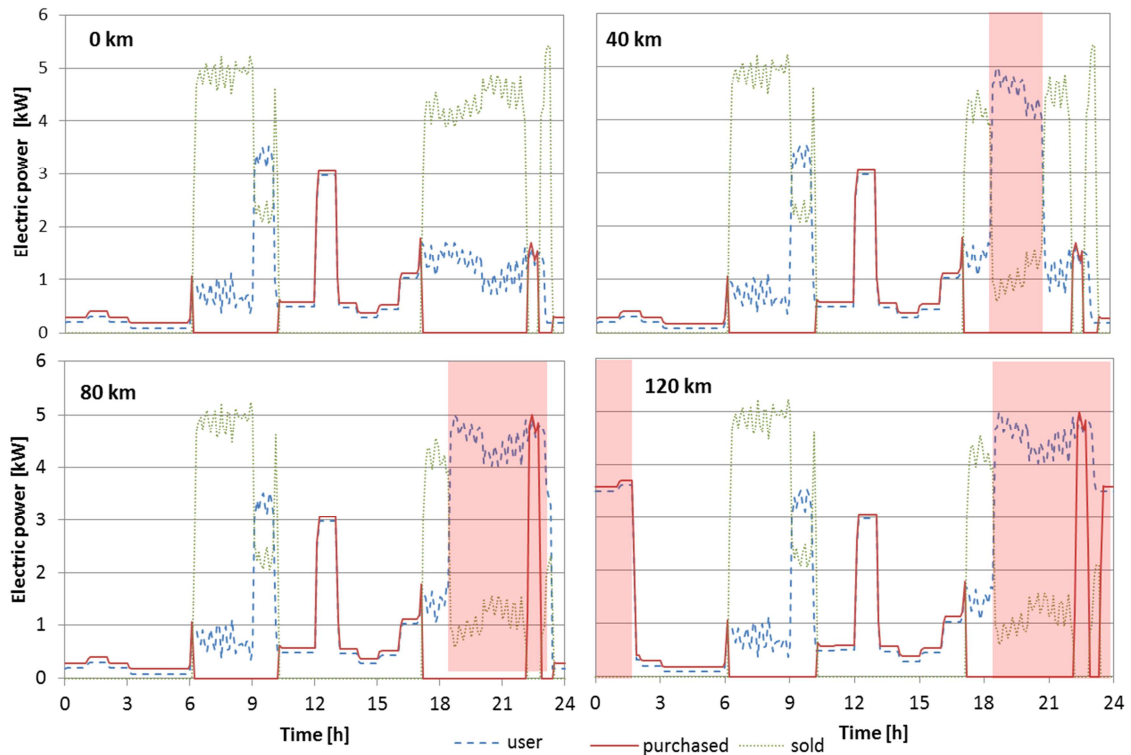


Figure 1.45. Electric power required by the user, sold to and purchased from the electric grid for different daily driving distances with normal charging strategy in Napoli.

Moreover the integration of EV charge with an MCHP system allows to reduce the electricity drawn by the electric grid. For a daily driving distance of 80 kilometers, in some periods (around 22:00), the charging occurs when the MCHP is turned off. In this case there is a high peak of electricity purchased from the grid, but it has short duration with respect to the case of absence of MCHP, and it occurs when the electric demand on the “national grid” is relatively low (off-peak hours). The same occurs for a driving daily distance of 120 kilometers.

Figure 1.46 reports the same information of Figure 1.45 but it is referred to the optimized charging strategy in Napoli. In this case the EV charging is related to the MCHP operation. In fact, as can be seen from the case of daily driving distance of 80 kilometers, the charging of EV is interrupted when the MCHP is turned off. This allows to maximize

the amount of self-consumed cogenerated electricity and to reduce the electricity peak on the electric grid. For a high daily driving distance (120 kilometers), in order to ensure that the EV is fully charged at 7:30, the EV charging occurs also in a period when the MCHP is turned off (between 4:30 and 6:00). Also in this case the peak of purchased electricity is shifted in off-peak hours. In addition to that, it is possible to self-consume part of the “produced” electricity due to the MCHP operation in the morning (when the heating system is activated).

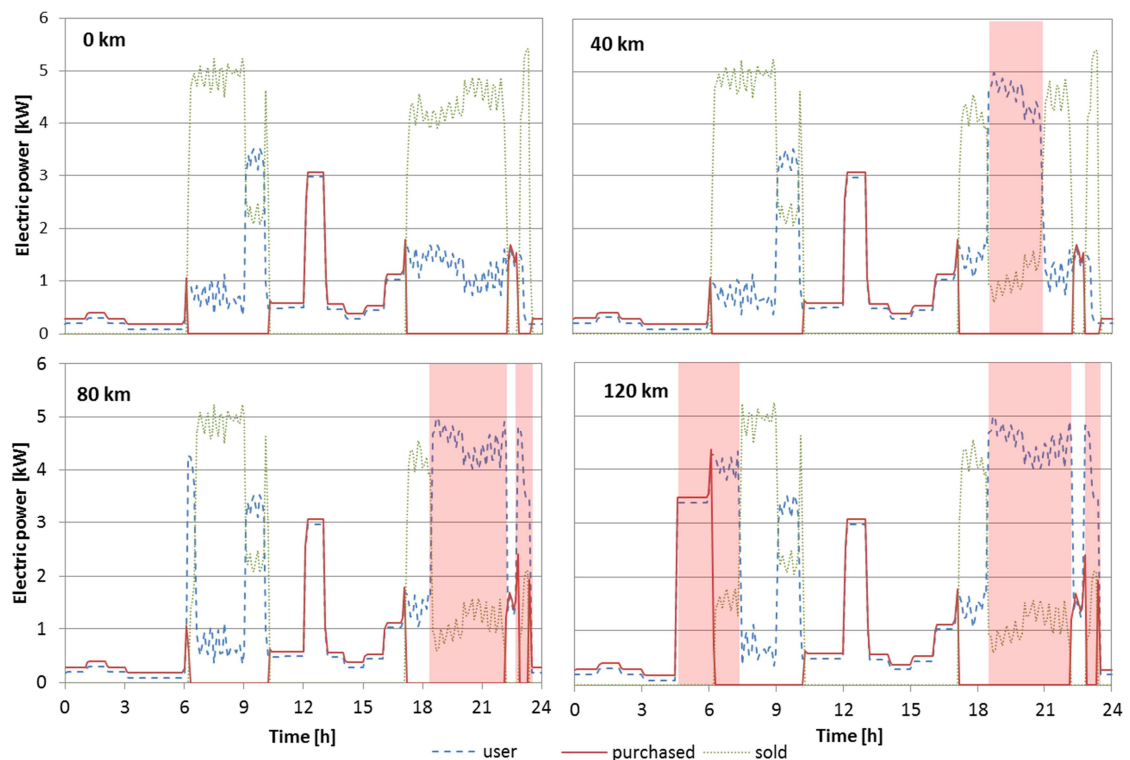


Figure 1.46. Electric power required by the user, sold to and purchased from the electric grid for different daily driving distance with optimized charging strategy in Napoli.

Figure 1.47 shows the same information of Figure 1.45, but it is referred to the building located in Torino. The amount of electricity purchased from the grid is lower than the previous case (Napoli) due to the higher daily operation hours of the heating system, and so of the MCHP system, in Torino. The optimized charging strategy allows to increase the amount of self-consumed electricity also for Torino (Figure 1.48). In this case also for a daily driving distance of 120 kilometers, the EV can be totally charged with the electricity produced by the MCHP.

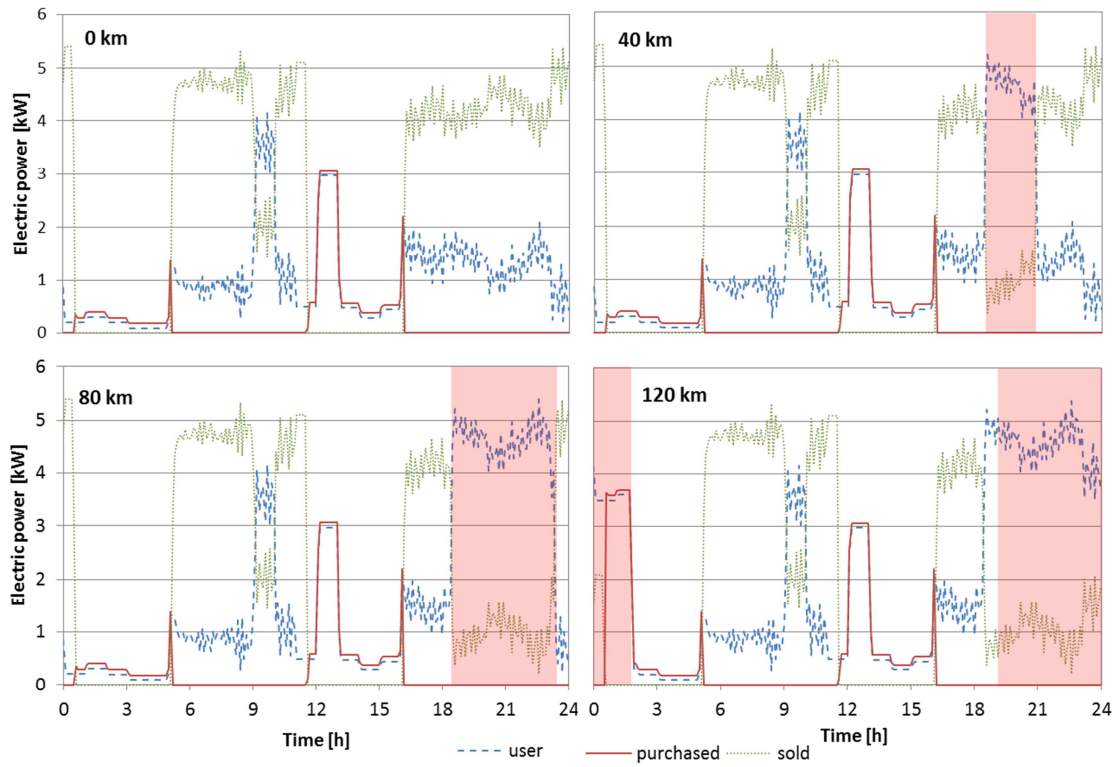


Figure 1.47. Electric power required by the user, sold to and purchased from the electric grid for different daily driving distances with normal charging strategy in Torino.

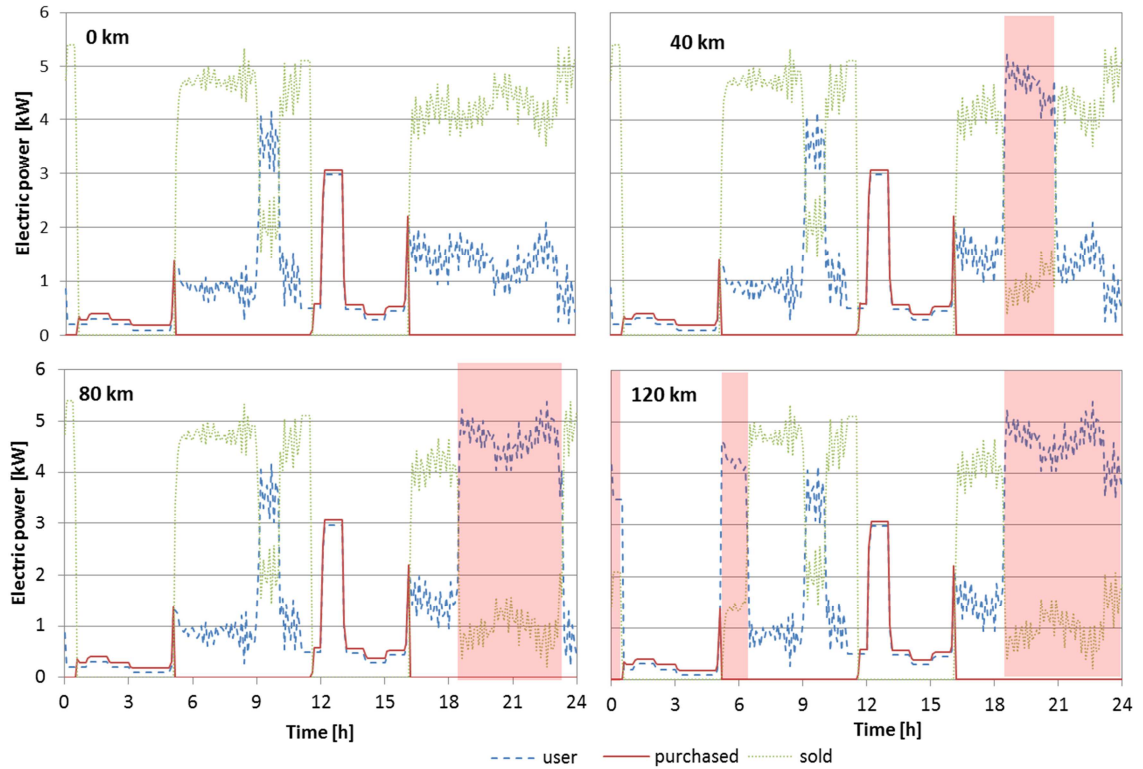


Figure 1.48. Electric power required by the user, sold to and purchased from the electric grid for different daily driving distances with optimized charging strategy in Torino.

Table 1.22 summarizes energy simulation results for the two locations in the heating period. As mentioned above, the operation of the MCHP is not influenced by the presence of EV charging because the MCHP operates in “heat” led mode. As expected, the heating demand in Torino is greater than in Napoli due to the different climatic conditions. The annual electricity demand (without the EV electricity demand) of the two building is the same, but the values reported in Table 1.22 are different because these values refer to the heating period only, that is different for the two locations. The same goes for the DHW demand.

Table 1.23 reports the electricity demand for the EV charging and the total electricity demand of the user as a function of the daily driving distance with normal and optimized charging strategy in both locations. The data are referred to the heating period. Moreover the table shows the self-consumed electricity and that one exchanged between the building and the electric grid.

Table 1.22. Energy simulations results for heating period in Napoli and Torino.

		NA	TO	
Energy demand [kWh]		Heating demand	15,841	26,995
		Electricity demand	2,340	3,152
		DHW demand	1,645	2,161
Thermal energy loss and auxiliary consumption [kWh]	PS	Thermal energy lost by TES	760	1,021
		Auxiliary consumption (fans + pumps)	725	1,149
	CS	Auxiliary consumption (fans + pumps)	671	1,060
Thermal energy “production” [kWh]	PS	Thermal energy from MCHP	14,701	24,436
		Thermal energy from boiler	3,525	5,539
	CS	Thermal energy from boilers (heating and DHW)	17,537	29,230
PE [kWh]	PS	Primary energy input of boiler	3,681	5,845
		Primary energy input of MCHP	26,737	44,426
	CS	Primary energy input of boilers (heating and DHW)	20,225	30,550
Electricity “production” [kWh]	PS	Electrical energy produced by MCHP	7,071	11,835

Table 1.23. Electricity user demand and electricity exchange between building and electric grid as a function of daily driving distance with normal and optimized charging strategy in Napoli and Torino.

		EV distance	0	20	40	60	80	100	120	
		[km/day]								
N A P O L I	Electricity user demand	EV charging [kWh]	0	545	1090	1635	2180	2724	3269	
		Total demand [kWh]	3065	3610	4155	4700	5245	5788	6333	
	Normal charging	Purchased [kWh]	1005	1060	1140	1211	1330	1833	2375	
		Sold [kWh]	5011	4525	4064	3594	3172	3133	3128	
		Self-consumed [%]	29%	36%	43%	49%	55%	56%	56%	
	Optimized charging	Purchased [kWh]	1005	1015	1033	1076	1212	1543	2052	
		Sold [kWh]	5011	4476	3949	3447	3038	2825	2790	
		Self-consumed [%]	29%	37%	44%	51%	57%	60%	61%	
	T O R I N O	Electricity user demand	Charging EV [kWh]	0	730	1462	2192	2923	3654	4385
			Total demand [kWh]	4301	5031	5762	6493	7224	7955	8686
Normal charging		Purchased [kWh]	1280	1464	1650	1800	1983	2212	2937	
		Sold [kWh]	8814	8268	7722	7142	6594	6093	6086	
		Self-consumed [%]	26%	30%	35%	40%	44%	49%	49%	
Optimized charging		Purchased [kWh]	1280	1304	1352	1434	1569	1789	2133	
		Sold [kWh]	8814	8106	7420	6768	6173	5662	5274	
		Self-consumed [%]	26%	32%	37%	43%	48%	52%	55%	

The introduction of EV charging allows to increase the amount of self-consumed electricity, that has a gradual increase with the daily driving distance. In addition, the introduction of the optimized charging strategy allows to increase the self-consumed electricity with respect to the normal charging strategy with the same daily driving distance. For example, for a daily driving distance of 120 km, in Napoli, the amount of self-consumed electricity is equal to 56.0% for the normal charging strategy and 61.0% for the optimized one. In Torino, the share of self-consumed electricity, expressed as a percentage of the electricity “production”, is lower than in Napoli. This is due to the higher electric and thermal load contemporaneity in the latter.

The evaluation of the performance of the PS with respect to the CS is carried out through energy, environmental and economic analysis (section 1.3) [3].

The energy performance of the analyzed systems was evaluated by means of the Primary Energy Saving (PES), while the environmental performance was evaluated through a simplified approach based on the evaluation of carbon dioxide equivalent emissions. The economic analysis was carried out to evaluate the influence of the

introduction of EV charging on operation cost (OC) of both PS and CS. So the operation cost reduction (ΔOC) of the PS with respect to the CS is evaluated for each case. For the evaluation of the operating costs, the natural gas and electricity tariffs and the corresponding taxes are considered for an Italian user (section 1.3). A tariffs analysis led to an electricity cost equal to 0.20 €/kWh for the purchased one and equal to 0.13 €/kWh for the sold one. The natural gas cost is 0.90 €/Nm³ and 0.86 €/Nm³ for Torino and Napoli, respectively. For the natural gas that feeds the MCHP a different cost is considered (reduced tax) according to the Italian law for cogeneration (0.79 €/Nm³ for Napoli and 0.80 €/Nm³ for Torino). The energy and environmental results obtained from this investigation are reported in Figure 1.49.

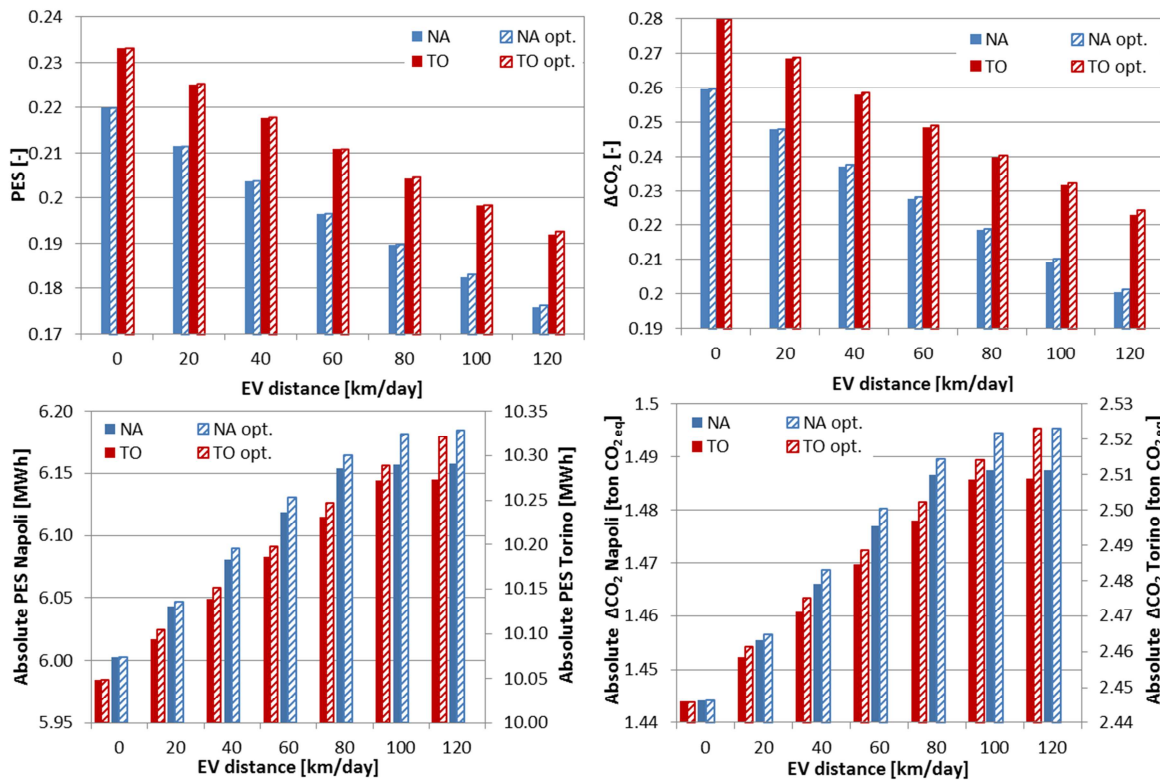


Figure 1.49. PES and ΔCO_{2eq} (percentage and absolute values) as a function of EV daily driving distance for the two charging strategies and for the two locations.

In the top left diagram of Figure 1.49 the PES is reported for the two locations and for the two charging strategies adopted. The PES is almost the same for the two charging strategies and it is in the range 17.6 ÷ 22.0% in Napoli and 19.2 ÷ 23.3% in Torino. It seems that the performance of the PS are better without the EV charging (PES is higher

when the EV daily driving distance is equal to zero), but these results should be carefully analyzed, as scenarios with different energy demands (different daily driving distance) are considered. The MCHP system has the same energy performance in all the scenarios, but the percentage values of the PES decrease due to the increasing primary energy consumptions of the reference system. If the absolute values of the PES (diagram on the bottom-left side of Figure 1.49) are analyzed, the primary energy saving increases with the EV daily driving distance. Also the optimized charging strategy allows to increase the absolute value of PES. These findings are due to the increasing value of the self-consumed electricity that allows to avoid the electricity losses on the low voltage grid.

Similar considerations can be made for the $\Delta\text{CO}_{2\text{eq}}$ reported in the top-right diagram of Figure 1.49. The $\Delta\text{CO}_{2\text{eq}}$ is in the range 20.0 ÷ 26.0% in Napoli and 22.3 ÷ 28.0% in Torino. Also in this case, the percentage value of the $\Delta\text{CO}_{2\text{eq}}$ decreases with the daily driving distance, while the absolute value increases. These findings have the same explanation of the previous case (PES).

Figure 1.50 shows the reduction of the operation cost of the PS with respect to the CS.

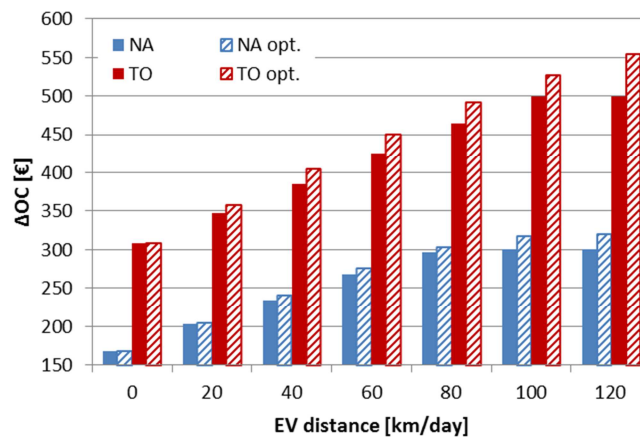


Figure 1.50. Operation cost reduction of the PS with respect to CS in the two different locations and for different charging strategy.

The MCHP system installed in the building located in Torino ensures higher ΔOC with respect to case of Napoli. This result is due to the colder climatic conditions of Torino that ensure higher operation hours of the MCHP system with respect to Napoli. The introduction of EV charging allows a marked reduction of operation costs especially with high EV daily driving distance. In fact for a daily driving distance of 120 kilometers, the

increase of ΔOC is equal to 61.9% for Torino and 78.3% for Napoli with respect to the base case (without EV) and considering a normal charging strategy. The introduction of an optimized charging strategy allows to increase the ΔOC , that becomes greater than 79.8% in Torino and 90.4% in Napoli with respect to the base case. Generally, the increase of ΔOC with the optimized charging strategy with respect to the normal strategy is in the range 1÷11%.

In conclusion, this section has investigated on the integration between an MCHP system and the energy demands of an electric vehicle and of a typical semidetached house. The analysis was carried out by means of dynamic simulations in two different geographical locations in Italy. Different daily driving distances of the EV were investigated in order to highlight the effect of this parameter on the simulation results. A normal charging strategy and an optimized charging strategy were implemented to analyze its influences on the performance of the proposed system. In the normal one, charging occurs when the EV is parked at home until the full charge is reached. In the optimized strategy, charging is related to the MCHP operations in order to maximize the amount of self-consumed electricity.

The more significant findings emerging from this study are:

- the integration of EV charging with an MCHP allows to reduce the impact of large diffusion of EVs on the electric network. With the overnight charging of EVs, the electricity “produced” by the MCHP to charge the EV batteries can be used. The peaks of electricity purchased from the grid presents can be lowered with thanks to the MCHP, and generally these peaks are shifted in periods of low electricity demands on the electric grid.
- Coupling EV charging with an MCHP system allows to reduce the amount of “produced” electricity exported to the grid. In this way the economic benefits associated with the introduction of an MCHP system, that depend on the economic value of the “produced” electricity, can be improved. In fact, the EV charge increases the amount of self-consumed electricity, as a result it allows to improve the economic feasibility of an MCHP system. The economic advantages are clear for both geographic locations (Napoli and Torino).
- Increasing the average daily driving distance of the EV, the amount of self-consumed electricity can be increased, and consequently the operation costs

decrease. This result could be achieved also increasing the number of EVs and considering a particular charging strategy that avoids the simultaneous charging of the EVs.

- The optimized charging strategy increases the share of self-consumed electricity with respect to the normal one. The reduction of operation cost due to this strategy is in the range 1÷11% .
- The energy and environmental results show a rise of the absolute savings in terms of both primary energy, MWh, and avoided CO_{2eq} emissions, kg of CO_{2eq}. This result is due to the reduction of exported electricity, that allows to reduce the electricity grid losses.

Even if good reductions of operating costs related to the integration between the EV charging and MCHP system can be achieved, the high investment cost of the MCHP equipment (18000 €, that can be reduced to 10800 €, considering public subsidies up to 40%) leads to quite high value of the investment payback period. However, it should be pointed out that this section takes into account only the system operation in the heating period, therefore the economic performance can be positively affected by the introduction of a thermally activated system (absorption chiller, desiccant cooling) to meet the cooling requirements of the building in summer period and to increase annual operating hours of the micro-trigeneration system.

On the other side, the integration between the MCHP system and an electric heat pump can concur to increase the amount of self-consumed electricity in the heating period. Nevertheless, the installation of an electric heat pump or a thermally activated cooling system would determine a further increase of the installation cost, therefore its introduction should be accurately evaluated by means of a detailed economic analysis.

Further strategies can be adopted to improve the economic feasibility, such as the introduction of MCHP system in multifamily house with more than two apartments, that can lead to a greater size of the micro-cogenerator with consequently lower investment specific cost (€/kWel). At last, a load sharing approach between residential and office building, as described in previous sections, can increase the operating hours of the MCHP system and improve the economic performance. Therefore, further analyses focused on these aspects are required.

This study is carried out for a 6 kW_{el} MCHP system serving a semidetached house with two apartments located in two different Italian climates, but it could be extended to other types of multifamily buildings (in terms of apartments number) and climatic zones, considering a different size of the MCHP system. In Italy, residential buildings are more than 12 million of which about 61% are multifamily houses [92], eligible for this technology. Therefore the integration of MCHP and EV in residential sector has an enormous number of possible applications, and it could be an interesting solution in order to overcome certain restrictions that hinder their diffusion.

Finally, this study suggests that the diffusion of distributed generation systems based on cogeneration can play an important role in the reduction of the negative effects that a wide diffusion of EVs could have on the electric network. The charging of EV battery with the electricity “produced” by an MCHP has positive effects not only on the electric network but also on the economic feasibility of the system.

CHAPTER 2: Dynamic simulations of hybrid energy systems in load sharing application

This chapter analyzes the energy, environmental and economic performance of different system configurations serving a residential and office buildings in load sharing approach, under Napoli (South Italy) weather conditions. The load sharing approach is investigated using dynamic simulations in comparison to a base case with separate conventional systems. In order to meet the energy requirements of the buildings five system configurations (cases) are defined:

- conventional case with one boiler and one chiller for each building;
- conventional case with a common boiler and chiller in load sharing approach;
- Ground Source Heat Pump (GSHP) systems in load sharing;
- Hybrid system with GSHP and micro-cogenerator based on FC in load sharing;
- Hybrid system with GSHP and Photovoltaic Thermal (PVT) collectors in load sharing.

Once the advantage of load sharing approach was demonstrated, the performances of two different hybrid systems in load sharing scenario were analyzed. The first hybrid system is based on FC and GSHP is not a hybrid renewable energy system because both the energy conversion device (FC and GSHP) are fed by traditional energy vectors (natural gas and electricity). Instead the second analyzed hybrid system is based on PVT collectors, which represent a renewable cogeneration system, and a GSHP. The performances of these two systems were also compared to a stand-alone GSHP system in order to analyze the advantages of hybrid systems to a single GSHP system.

2.1 System configuration

In order to investigate the performance of hybrid micro-cogeneration technologies, serving several users in load sharing approach, different cases were developed and analyzed:

- Case 1 utilizes stand-alone conventional boilers and chillers for each building in order to meet the heating and cooling load of the end users (Figure 2.1).

Domestic Hot Water (DHW) needs are met by means of a Thermal Energy Storage (TES) heated by a boiler.

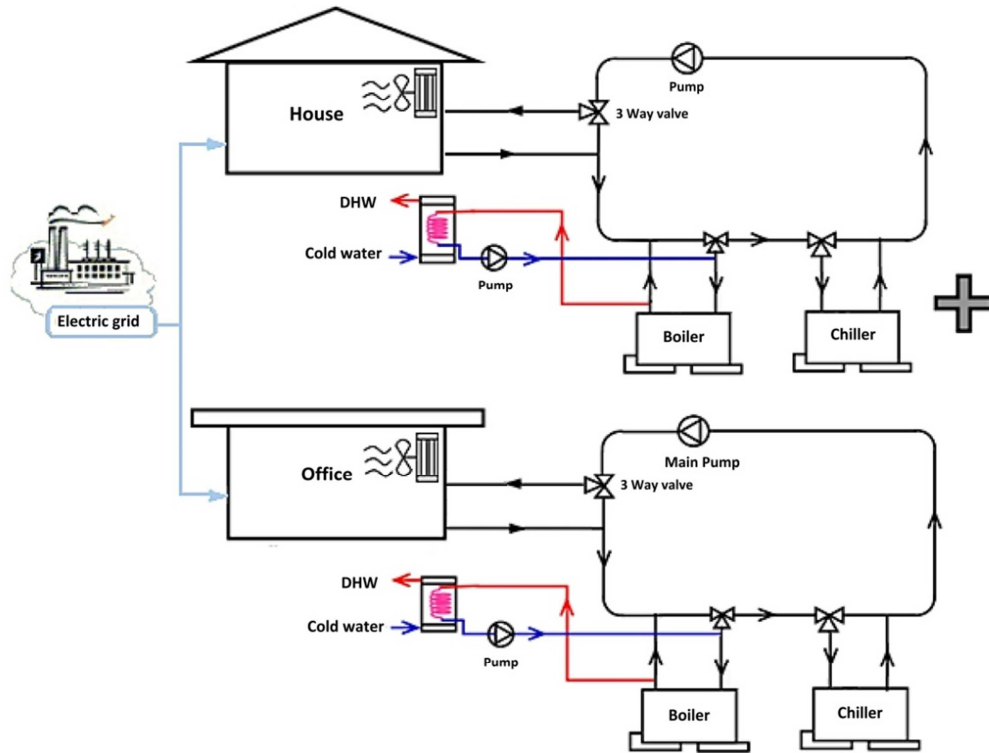


Figure 2.1. System configuration of case 1.

- Case 2 is a load sharing setup featuring single conventional boiler and chiller used to meet the combined load of the house and office (Figure 2.2). A centralized storage tank is used to store hot water for DHW demand.

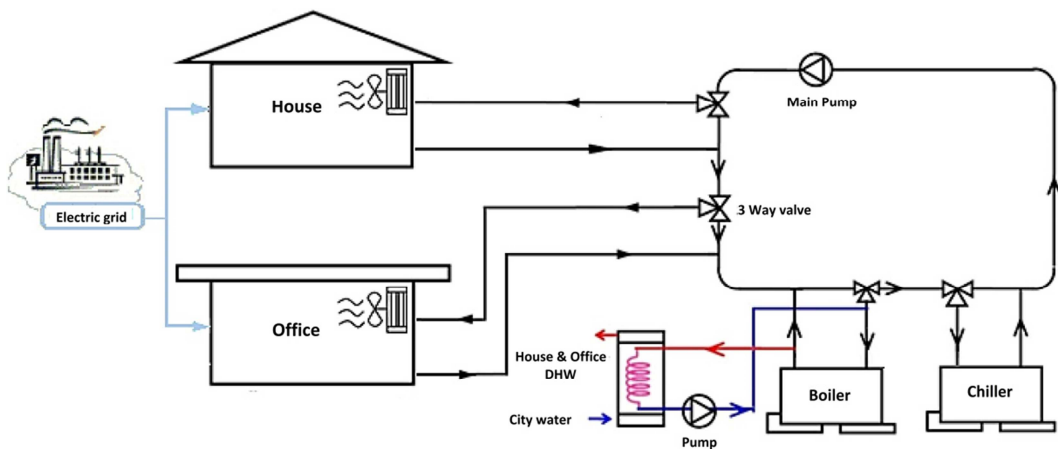


Figure 2.2. System configuration of case 2.

- Case 3 utilize a GSHP in order to provide heating and cooling demand of the combined users (Figure 2.3). The GSHP thermally interacts with the ground by means of a ground heat exchanger (GHX). A hot water tank, integrated with a peak/back up gas burner, is considered in order to provide the supplementary heat whenever the GSHP is not able to provide the required thermal energy or for the DHW in cooling period. A cold water storage tank is used in the cooling period. The DHW demand is met by means of an immersed heat exchanger in the hot water tank.

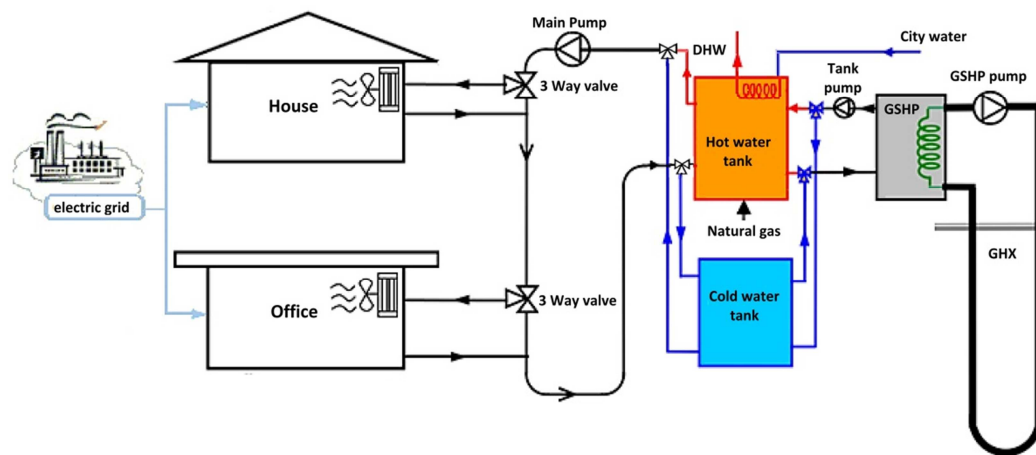


Figure 2.3. System configuration of case 3.

- Case 4 is a hybrid micro-cogeneration system, that consists of a GSHP and a micro-cogenerator based on FC. It is utilized to meet the combined load of the users (Figure 2.4). The system configuration is similar to case 3 except the presence of a micro-cogenerator. The electricity provided by the MCHP is used to meet the electric load of the users or it is sold to the grid. Moreover the thermal energy recovered by the cooling circuit of the FC is used to heat the hot water storage tank.

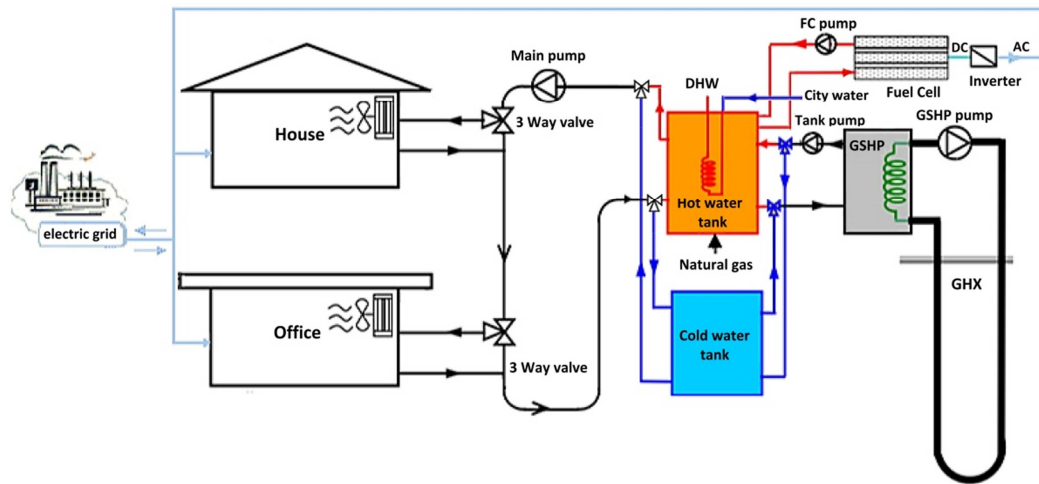


Figure 2.4. System configuration of case 4.

- Case 5 is a load sharing scenario where a hybrid micro-cogeneration system, which consists of a GSHP and PVT, is utilized to meet the combined load (Figure 2.5). The PVT panel generates electric and thermal energy. The electricity can be used in order to meet the electric load of the users or it can be sold to the grid. The thermal energy is provided by an immersed heat exchanger to a hot water tank. The other components are the same of the previous case.

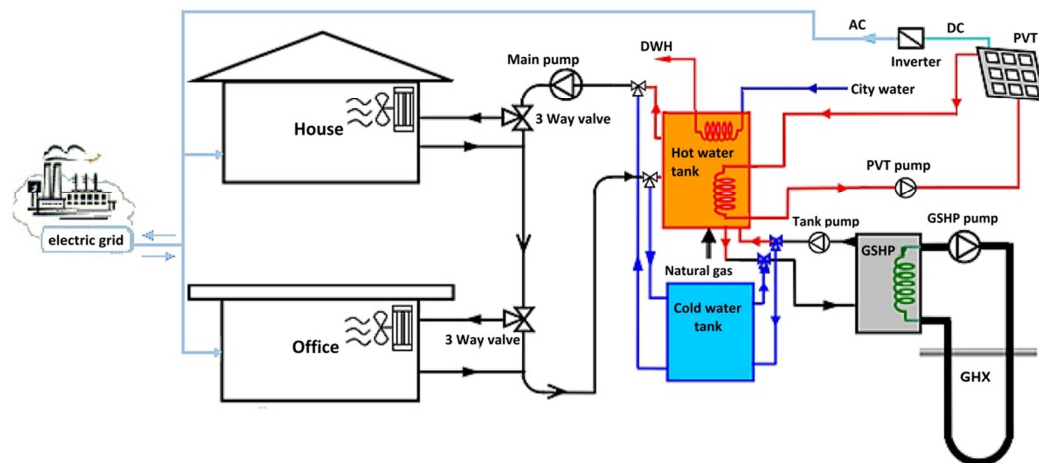


Figure 2.5. System configuration of case 5.

In each cases the residential and office users are equipped with low temperature heating devices (fan coils) according to the supply temperature of the heating systems. Moreover this choice allows to use the fan coils also in the cooling period.

2.2. Model description

The systems described in the previous section were modelled and implemented in TRNSYS software platform [42]. As described in previous section 1.2, it is a transient simulation software widely used, in the field of energy, to simulate the interaction between a building and energy systems. TRNSYS has a modular structure and each component of the system is modelled by means of subroutines (“types”) available in TRNSYS library [42][43]. The components can be connected together to form complex systems.

A TES is modelled through a “multi-node approach” (type 534) [43]. The consistence of this approach is shown in the previous section 1.2.2.

In load sharing scenarios the thermal micro-grid was simulated by "type 31" [42]. The thermal micro-grid has been dimensioned starting from the knowledge of the maximum thermal/cooling power to be provided to the remote user (office user), the temperature difference between supply and return of the fluid and its flow rate, in order to keep the velocity of the fluid in the typical range 1-2.5 m/s. The diameter of the pipe was therefore set to 2.5 cm. Finally, it was assumed a value of U (overall heat transfer coefficient) equal to $0.5 \text{ W/m}^2\text{K}$. The overall heat transfer coefficient selected for the network represents the typical value for a pre-insulated pipe with an internal diameter of 2.5 cm [71]. The thermal micro-grid thermally interacts with the ground, whose temperature is simulated by means the “type 77” [42].

“Type 557” is used in order to model a vertical heat exchanger (single U-tube) that interacts thermally with the ground. The design of ground heat exchanger (GHX) is based on German guideline for ground source heat pumps (VDI 4640 [93]), while the presence of rocky subsoil characterized by an average thermal conductivity of 1.5 W/(mK) is assumed. In order to take into account the thermally interaction between the different boreholes, the total length of the GHX is increased of 20%. The percentage increase of GHX length was evaluated by means dynamic simulation in order obtaining good value of the average seasonal coefficient of performance (around 4). According to this assumption the GHX consists of 8 boreholes up to a depth of 60 m. The water-to-water heat pump is modelled through “type 668”. This model is based on external data files containing catalog data readily available from heat pump manufacturers [95].

In case 5, “type 563” is used to model PVT panels. This model relies on linear factors relating the efficiency of the PV cells to both the cell temperature and the incident solar radiation. In addition, it is assumed that the cells are operating at their maximum power point condition. The thermal model of PVT collector relies on algorithms presented in Chapter 6 of reference [94] and the calibration of this model is based on “PVtwin” module tests [96].

In case 4 the micro-cogenerator system is based on FC. For small scale cogeneration application the FC technologies commonly used are proton exchange membrane fuel cell (PEMFC) and solid oxide fuel cell (SOFC) based systems [3]. These FC technologies guarantee the advantage of high overall efficiency, reduced environmental impact, and a good match with the residential thermal to power ratio [3]. PEM fuel cell operate at temperatures of up to 90 °C, it uses cheaper materials with respect to SOFCs, in which the process temperature is about 800 °C. SOFC have better performance than PEMFC technology, but start-up and cooling phases take longer time. These aspects affects time and costs required for installation, maintenance, repair and durability of SOFC [3]. Due to the low temperature thermal energy requests by buildings, PEMFC are used in these simulations. In order to model the function of a micro-cogenerator based on FC, a non-linear regression method which is based on experimental data for a proton exchange membrane fuel cell (PEMFC), was used [97]. In this model the electric and thermal efficiencies are function of MCHP electrical power, cooling water flow and inlet temperature. The efficiency model consists of 8 coefficients for each equation:

$$\eta_{el}^{DC} = a_0 + a_1 \cdot P_{el} + a_2 \cdot F_w + a_3 \cdot T_{w,in} + a_4 \cdot P_{el}^2 + a_5 \cdot F_w^2 + a_6 \cdot T_{w,in}^2 + a_7 \cdot F_w \cdot T_{w,in} \quad (2.1)$$

$$\eta_{el}^{AC} = 0.8 \cdot \eta_{el}^{DC} \quad (2.2)$$

$$\eta_{th} = b_0 + b_1 \cdot P_{el} + b_2 \cdot F_w + b_3 \cdot T_{w,in} + b_4 \cdot P_{el}^2 + b_5 \cdot F_w^2 + b_6 \cdot T_{w,in}^2 + b_7 \cdot F_w \cdot T_{w,in} \quad (2.3)$$

where: $a_0 = 0.404$; $a_1 = 1.736 \times 10^{-4} [W^{-1}]$; $a_2 = -0.293 [l^{-1} \text{ min}]$; $a_3 = -0.0035 [^{\circ}C^{-1}]$; $a_4 = -4.059 \times 10^{-8} [W^{-2}]$; $a_5 = -0.0468 [l^{-2} \text{ min}^2]$; $a_6 = 6.925 \times 10^{-5} [^{\circ}C^{-2}]$; $a_7 = 0.005 [^{\circ}C^{-1} l^{-1} \text{ min}]$; $b_0 = 0.443$; $b_1 = -4.112 \times 10^{-4} [W^{-1}]$; $b_2 = 2.268 [l^{-1} \text{ min}]$; $b_3 = -0.0034 [^{\circ}C^{-1}]$; $b_4 = -8.996 \times 10^{-8} [W^2]$; $b_5 = -0.602 [l^{-2} \text{ min}^2]$; $b_6 = -4.244 \times 10^{-5} [^{\circ}C^{-2}]$; $b_7 = -0.0179 [^{\circ}C^{-1} l^{-1} \text{ min}]$.

Once the efficiencies are obtained, the required fuel input and the cooling water outlet temperature can be determined by energy balance equations. The model was experimentally calibrated and validated at CanmetENERGY laboratory in Ottawa (Canada).

The validation procedure indicated a value of the Root Mean Square Error (RMSE) and Mean Relative Error (MRE) for the thermal power output to the MCHP equal to 25.0 W and 1.9%, respectively. The RMSE and the MRE for natural gas flow input to the system are equal to 0.095 slpm and 2.0%. More detailed information about the model, its calibration and validation procedure and the experimental facility can be found in [97] [87]. Table 2.1 presents a brief description of the model “type” used in the simulation.

Table 2.1. Main TRNSYS model “type” used in the simulation.

Component	TRNSYS type	Comments
Building	Type 56	Multi zone building model
Boiler	Type 751	With variable input efficiency profile at part load
Chiller	Type 655	Performance data based
Two-speed blower/fan	Type 644	
Heating coil	Type 753	Bypass fraction approach
Cooling coil	Type 508	Bypass fraction approach
Hot/cold TES	Type 534	With option of immersed heat exchangers and auxiliary heaters
Circulation pump	Type 656	Variable speed pump
Overhang shading device	Type 34	Interact with building (type 56)
Pipe	Type 31	It uses a "plug-flow" model
Ground temperature	Type 77	Temperature of the ground that interact with the pipe (type 31)
Ground heat exchanger	Type 557	Vertical u-tube GHX. Duct ground heat storage model
Water-to-water HP	Type 668	Performance data based
PVT panels	Type 563	
PEM fuel cell		Empirical performance maps.

The end users, which consist of a house and an office building with the same floor area of 200 m² and related thermal load, were simulated using the interface “TRNBuild” of TRNSYS and its “type 56”. The building characteristics of the two users are reported in Table 2.2. According to the Standard EN 410:2011, the g value represents the total solar energy transmittance, or solar heat gain coefficient, of glazing for solar radiation in the wavelength range between 300 nm and 2500 nm [98]. The g value is essential in order to characterize the transparent surface of the building envelope. Moreover in order to reduce the solar gain in the cooling period an overhang shading device was modelled through the “type 34”. This “type” computes the solar radiation on a vertical receiver (window) shaded by an overhang and/or wingwall. Detailed description of the “type” model can be found in TRNSYS documentation [42][43].

Table 2.2. Building envelope characteristics.

	Opaque building elements			Transparent building elements		
	Roof	External walls	On ground floor	North	South	West/East
U [W/m ² K]	0.38	0.40	0.42	2.31	2.31	2.31
g [-]	-	-	-	0.60	0.60	0.60

2.3. Simulation inputs and control approach

2.3.1 Domestic hot water demand

The residential domestic hot water draw profile used in the simulation was carried out by means of a software [82] developed within the scope of the Solar Heating and Cooling Program of the International Energy Agency (IEA SHC) Task 26. In order to take into account fairly realistic DHW demand for a period of one year a time step of 6 minute was chosen. The average daily demand was assumed equal to 260 l/day for the house and 40 l/day for the office users [83]. The software carried out a DHW demand different for each day of the simulated year. In order to show a typical profile, in Figure 2.6, the DHW demand for the residential user is reported for the first week of the simulated year (for reasons of brevity). The hot water profile for an office user, in a week day, is shown in Figure 2.7. In literature, there is not detailed information about typical hot water profile for office users, therefore the hot water demand is assumed higher at lunch time and lower at other work time. This assumption represents an approximation but it does

not affect the simulation results due the low office DHW demand with respect to the total thermal energy demand of the users. In a weekend day the hot water demand for an office user is equal to zero and the temperature of the DHW demand was assumed equal to 40°C.

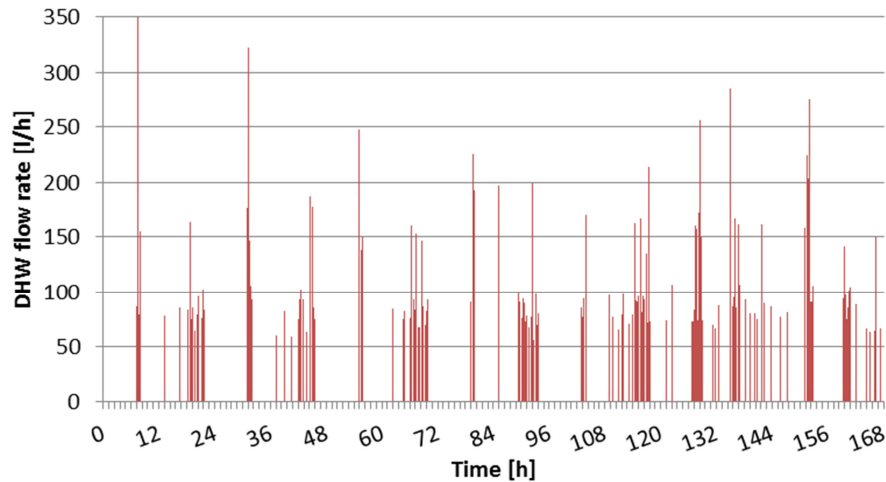


Figure 2.6. Hot water profile for residential user in the first week of the simulated year.

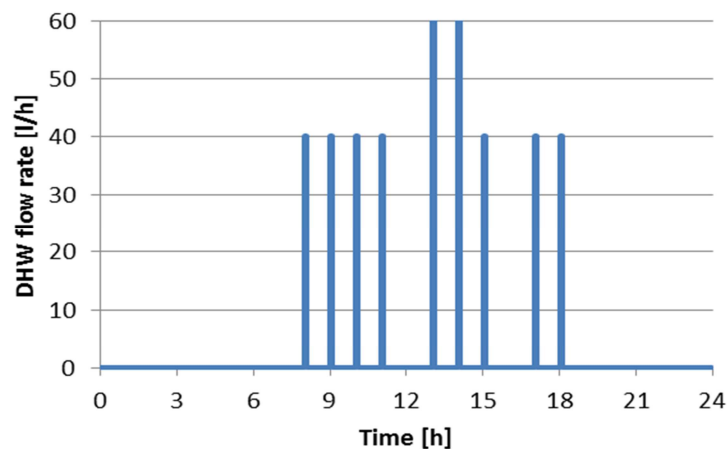


Figure 2.7. Hot water profile for an office user in a week day.

2.3.2 Electric load profile

The electric load for the residential user is defined for three different type days (Weekday, Saturday and Sunday). The electric load profiles shown in Figure 2.8 are based on real data measured in ref. [99]. The different load profile for the three type days are both due to the different occupancy and occupants behavior. In a work day the electric demand shows a morning and evening peak, while during the work time the

electric load is lower. On Saturday, the different load profile is due to the large use of household appliances in the central hours of the day. The Sunday load profile presents a smaller peak compared to the other days of the week, due to a low occupancy factor and a lower use of appliances.

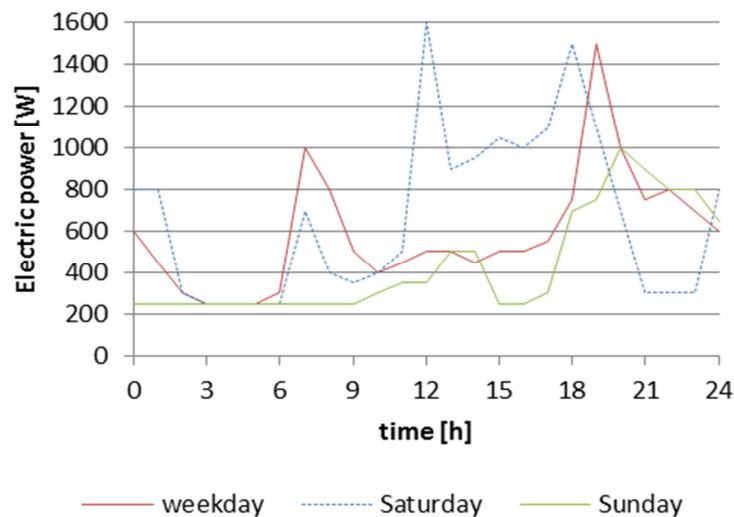


Figure 2.8. Electric load profiles for weekday, Saturday and Sunday (residential user).

The annual electric consumption of the office user is assumed equal to 50 kWh/m² [100]. The load profile is assumed constant in the weekend and during the night (0.57 kW), while on weekdays the electric demand is equal to 2.8 kW during the working hours (9-18) with a small reduction during lunch time (electric load about 2 kW).

2.3.3 Equipment capacity

The capacity and the nominal characteristics of the main components in the different cases are reported in Table 2.3. The sizing of the different components is based on the heating and cooling load of the end users. In case 3 the presence of TES allows to reduce the capacity of the GSHP with respect to the nominal capacity of boiler and chiller in case 2. Moreover an auxiliary heater is added in the TES in order to meet the peak load and the DHW demand in cooling period. In case 5, 30 PVT collectors are installed, with a total surface area of 76.8 m². Module performance is referred to standard test conditions (STC, irradiance 1000 W/m² and ambient temperature 25°C). In Table 2.3 the electrical and thermal rate capacity of PVT is referred to the total value (30 collectors)

while the PVT panels are south oriented with a tilt angle of 30 degrees (coplanar with the roof surface). The design of PVT system is based on electrical requirement of the combined user and also on considering the available surface (south oriented) of the residential user. The thermal and electric efficiency of the FC is referred to a full load condition with an inlet temperature of cooling water of 35 °C. For the cooling operation, the COP of GSHP and chiller is reported at full load condition with a load side temperature of 12/7 °C (in/out) and a source side temperature of 30/35°C (in/out), while for the heating operation the COP of GSHP is referred to a load side temperature of 40/45 °C (in/out) and a source side temperature of 10/7°C (in/out).

Table 2.3. Capacities of the main components.

	Component	Capacity	Nominal characteristics
Case 1	Boiler (house)	15.0 kW	$\eta = 0.921$
	Boiler (office)	15.0 kW	$\eta = 0.921$
	Chiller (house)	14.1 kW	COP = 3.0
	Chiller (office)	17.6 kW	COP = 3.2
	TES for DHW (house)	0.189 m ³	$U_{TES} = 0.36 \text{ W/m}^2\text{K}$
	TES for DHW (office)	0.189 m ³	$U_{TES} = 0.36 \text{ W/m}^2\text{K}$
Case 2	Boiler	25 kW	$\eta = 0.931$
	Chiller	24.6 kW	COP = 3.5
	TES for DHW	0.227 m ³	
Case 3	GSHP heating	21.03 kW	COP = 3.9
	GSHP cooling	17.66 kW	COP = 4.0
	TES (hot)	0.300 m ³	$U_{TES} = 0.36 \text{ W/m}^2\text{K}$
	TES (cold)	0.190 m ³	$U_{TES} = 0.36 \text{ W/m}^2\text{K}$
Case 4	GSHP heating	21.03 kW	COP = 3.9
	GSHP cooling	17.66 kW	COP = 4.0
	TES (hot)	0.300 m ³	$U_{TES} = 0.36 \text{ W/m}^2\text{K}$
	TES (cold)	0.190 m ³	$U_{TES} = 0.36 \text{ W/m}^2\text{K}$
	FC	1 kW _{el}	$\eta_{el} = 0.32$ $\eta_{th} = 0.53$
Case 5	GSHP heating	21.03 kW	COP = 3.9
	GSHP cooling	17.66 kW	COP = 4.0
	TES (hot)	0.500 m ³	$U_{TES} = 0.36 \text{ W/m}^2\text{K}$
	TES (cold)	0.190 m ³	$U_{TES} = 0.36 \text{ W/m}^2\text{K}$
	PVT	8.85 kW _{el} 46.1 kW _{th}	See [96]

2.3.4 Control strategy

The heating system is turned on according to the following time schedule:

- 6:00-9:00 and 17:00-22:00 for the house;
- 8:00-18:00 for the office;

The room thermostats set-point are set to 20 ± 0.5 °C for both these end users who are located in Napoli (South Italy), while the climate data that is used in the simulation are downloaded from “EnergyPlus” website [101]. The operation hours of the heating system represents the maximum limit according to Italian law [84] which is equal to 10 hours/day in Napoli but actually depends on the climatic zone of the user. The heating period is assumed to be from November 15 to March 31. The cooling system is turned on according to the following time schedule:

- 14:00-20:00 for the house;
- 8:00-18:00 for the office;

In a cooling period the room thermostats set-point are set to 25 ± 0.5 °C for both the users. The office user the heating and cooling timetable is chosen in order to ensure thermal comfort in the work time while for the residential user the heating and cooling systems are activated in the hours of higher occupation of the building.

For case 1 and case 2, the boiler is turned on when there is a heating need or when the temperature in the DHW storage tank is below than the set-point. The boiler outlet temperature is controlled to 82 ± 2 °C while the temperature of the fluid provided to the end user is set to 60 °C by a three way valve (tempering valve). The temperature of the storage tank used for DHW demand is controlled through a sensor installed in the middle of the storage tank and its temperature is kept in the range 45 ± 2.5 °C. A tempering valve is used to ensure DHW temperature is kept at 40°C. In cooling season the chiller is activated when there is cooling load by the users and the water temperature is kept at 7 ± 2 °C. The GSHP is controlled by the water temperature in the hot/cold storage tank. In particular in heating/cooling period the GSHP is turned on in order to keep the temperature of the storage tank in the range of 50 ± 2.5 °C/ 7 ± 2 °C. In case 4 the fuel cell is assumed running continuously at its maximum capacity. This choice is due to the low thermal and electric capacity of the FC (compared with the thermal and

electric load of the users). The presence of TES allows storage of surplus cogenerated thermal energy in summer period, when there is only DHW demand (with discontinuous thermal energy requirements). Moreover the high electric efficiency of the FC allows to obtain a good energy performance and also a partial utilization of the cogenerated thermal energy. In case 5 a differential control strategy is used in order to manage the activation of the PVT pump. The pump differential controller activates the PVT pump if the difference between the temperature of the heat transfer fluid outlet the PVT and the water in the TES (in proximity of the heat exchanger that thermally interacts with PVT panels) is greater than 8°C, while the PVT pump is deactivated if this difference is less than 4°C.

The introduction of hybrid energy systems bring about increased complexity in the control strategy and system configurations. Nowadays the development of control and automation systems allow to overcome these potential problems through dedicated control systems.

2.4. Energy, environmental and economic analysis methodologies

In order to evaluate the performance of the different cases an energy, environmental and economic analysis (3-E) [3] was implemented.

The energy performance of the different systems were evaluated through the Primary Energy Saving (PES) which represents the primary energy saving of the analyzed case with respect to the reference case (case 1).

The environmental performance of each case was evaluated through a simplified approach based on the evaluation of carbon dioxide equivalent emissions (CO_{2eq}). The comparison is based on the avoided CO_{2eq} emissions (ΔCO_{2eq}) of the analyzed case with respect to the reference one (case 1). The primary energy and CO_{2eq} emissions are evaluated according to the methodology described in section 1.3.

Table 2.4 reports the equation used to estimate the investment costs of every case. The cost estimation for the analyzed systems (GSHP, PVT and FC) has a large variability due to their immature market share. In our work, the evaluation of the investment costs are based on the current market price indicated in the references reported in Table 2.4.

Moreover the investment cost could be influenced by incentives mechanism and by the price reductions on equipment resulting from economy of scale and market expansion of these technologies.

Table 2.4. Investment costs estimation for each component.

Component	Investment costs [€]
Boiler	$(421 + 13.93 \cdot P_b) / 1.26$ [79]
Chiller	$5315.4 + 604.95 \cdot P_c$ [102]
TES	$500 + 1450 \cdot V_{TES}$ [102]
GHX	$67 \cdot L_{GHX}$ [103]
GSHP	$1949.5 \cdot P_{GSHP}^{0.665}$ [104]
FC	$6700 \cdot P_{FC}$ [3]
PVT	$710 \cdot S_{PVT}$ [105]
Thermal network	$40 \cdot L_{network}$ [78]

2.5. Discussion and results

The heating, cooling and DHW load is almost the same for all the cases. For this reason, only the energy demands of case 1 is reported:

- heating requirement 5,834 kWh/year;
- cooling requirement 16,729 kWh/year;
- DHW 3,065 kWh/year.

The low energy demand for heating (about 15 kWh/m²/year) is due to the good isolation of the building envelope (see Table 2.2) in addition to the “mild climatic condition” of Napoli.

The Figure 2.9 shows the electricity and primary energy related to natural gas. Moreover the electricity (el. in Figure 2.9) consumption is divided in five groups:

- el. noHVAC, represents the total electricity demand except the electricity used for the HVAC (Heating, Ventilation, and Air Conditioning) systems;
- el. fan+pump, is the electricity utilized for the pumps and the fans of the HVAC system;
- el. chiller, is the electricity used to feed the chiller during the cooling period.

- el. GSHP heating, is the electricity used to feed the GSHP in heating period;
- el. GSHP cooling, is the electricity used to feed the GSHP in cooling period;
- el. production, represents the electricity “production” used for the cases 4 and 5.

The subdivision of the final energy consumption in cases 1 and 2 are almost the same, but case 2 allows obtaining a small reduction in energy consumption (about 3.7%) with respect to case 1. The case 3 presents a good reduction (27.5%) of the energy consumption with respect to case 1, due to the high coefficient of performance of the GSHP (with respect to the conventional system used in cases 1 and 2). Particularly in this case, the natural gas is used to meet DHW demand in a cooling period and for a peak of heating load in winter. For this reason the natural gas demand is less than the demand of cases 1 and 2. In case 4 the high natural gas consumption (with respect to the case 1) is due to the introduction of an FC. The case 5 allows for a good reduction of energy consumption due to the introduction of PVT panels. Moreover in the last two cases an electricity “production” which is due to the presence of FC and PVT, is present.

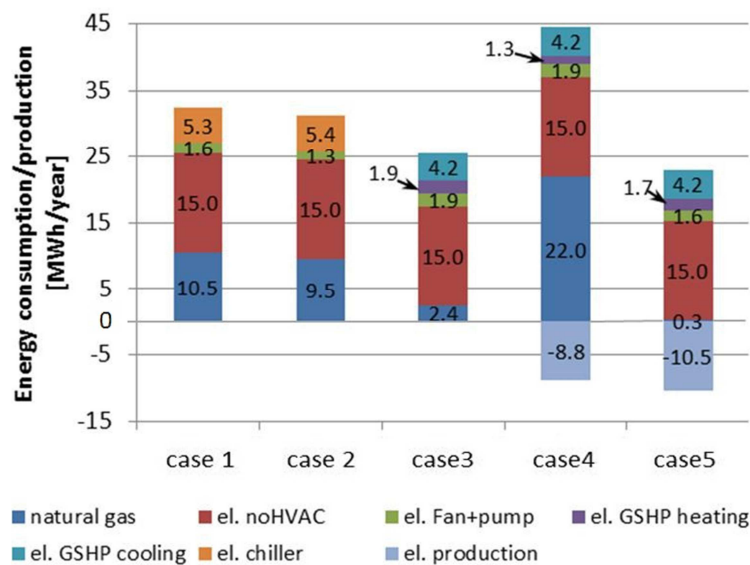


Figure 2.9. Electricity and natural gas “consumption”.

A better indication of the energy performance of the different cases is obtained by means of evaluation of primary energy consumption which is reported in Figure 2.10. The load sharing approach allows obtaining a reduction of a primary energy consumption of 2.1% (Figure 2.10) with respect to the reference case (case 1). This result

is due to the improved equipment efficiency (size factor) and also to different load conditions. The GSHP (case 3) is able to achieve a primary energy saving of 8.4%. In case 4 a GSHP and MCHP based on FC were introduced and the combination of the two devices allows improvement of the system energy performance while ensuring primary energy savings of 12.8 % with respect to the reference case. In case 5 for the calculation of the primary energy saving the solar energy input to the PVT system is not taken into account. In this case the combination of a GSHP and PVT allows to obtain a primary energy saving of 53.1%. The better energy performance of these two cases is due to the introduction of a hybrid energy system based on an MCHP. In fact the cogeneration approach allows to recover thermal energy by cooling the FC (case 4) or PVT (case 5) and it also allows utilization of a part of the produced electricity to feed the GSHP. In case 4 the FC works, at full load, for all simulations. For this reason in some operational conditions the temperature of the cooling water inlet to the FC is high (about 50 °C) so the thermal efficiency of the MCHP decreases.

Avoided $\text{CO}_{2\text{eq}}$ emissions ($\Delta\text{CO}_{2\text{eq}}$) of the analysed case in respect to the reference one are also reported in Figure 2.10. The load sharing approach (case 2) allows a reduction of $\text{CO}_{2\text{eq}}$ emissions of 1.9%. The introduction of a GSHP in load sharing (case 3) ensures a ΔCO_2 equal to 6.8%. The two hybrid cases showed good environmental performance with a $\Delta\text{CO}_{2\text{eq}}$ equal to 15.8% for GSHP-FC (case 4) and 52.0% for GSHP-PVT (case 5).

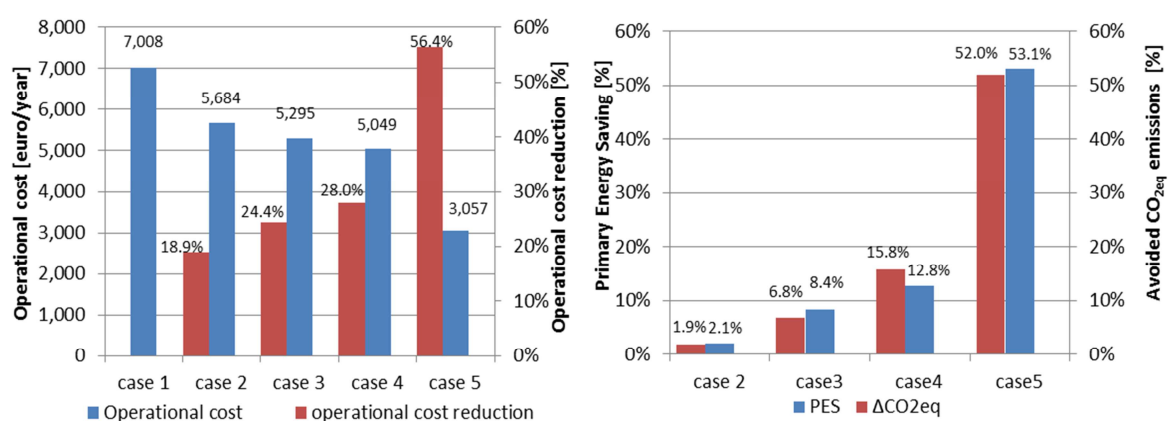


Figure 2.10. Primary Energy Saving and avoided $\text{CO}_{2\text{eq}}$ emissions with respect to the case 1 (on the right); operational cost and operational cost reduction with respect to the case 1 (on the left).

The Figure 2.10 (on the left side) reports the operational cost and the operational cost reduction with respect to the reference case. In all cases good reduction of the operational cost has been achieved which vary between 18.9% (case 2) and 56.4% (case 5).

Table 2.5 reports an overview of the economic analysis, such that the additional cost and the operational cost reduction reported in therein are evaluated with respect to the reference case (case 1).

Table 2.5. Economic analysis.

	Case 1	Case 2	Case 3	Case 4	Case 5
Investments cost [€]	32,355	23,637	50,648	57,348	105,466
Additional cost [€]	-	-8,719	18,293	24,993	73,111
Operational cost [€]	7,007	5,683	5,295	5,048	3,057
Operational cost reduction [€]	-	1,324	1,712	1,959	3,950
SPB [years]	-	-	10.7	12.7	18.5

It is interesting to analyze the economic results of case 2, wherein the introduction of a small thermal network allows to reduce not only the operation cost but also the investment cost. Indeed the presence of a thermal network allows to install a centralized heating and cooling plant, with advantages in terms of investment cost because the costs associated to the realization of thermal network are low (about 2000 €) for this size. For this case is not possible to evaluate the SPB due to the negative value of additional cost. In the case 3 the introduction of a GSHP allows the obtaining of a good reduction of the operation cost, but the high investment cost associated to the GHX constructions leads to a high value of SPB (10.7 years). For both hybrid systems, the SPB value is higher than the case 3. Moreover the Italian law provides an economic support for the installation of systems feeds on renewable energy or energy efficient. For example the introduction PVT and GSHP in the residential sector allow to obtain a tax deduction equal to 65% of the investment cost. In this way the SPB index could achieve interesting values.

In conclusion, a set of different energy systems, conventional system with boiler and chiller, conventional system in load sharing operational mode, GSHP system, hybrid GSHP-FC and hybrid GSHP-PVT, were modelled and analyzed in TRNSYS simulation

environment. 3-E analysis was performed in order to evaluate the energy, environmental and economic performance of the studied systems. This analysis highlights the validity of the load sharing approach, as it allows an improvement of the systems' performance due to improved equipment efficiency and load factor operation. The economic analysis shows that this approach could reduce the investment cost due to the installation of one less expensive centralized system with respect to different systems (two in this case). Moreover the cost for the construction of thermal micro-grid could offset this effect, especially if the dimension of the thermal micro-grid grows. The introduction of a GSHP system ensured a PES equal to 8.4% in respect to the reference case. Without economic incentive the SPB is equal to 10.7 years, but this value could be reduced through support mechanisms. The hybrid micro-cogeneration systems showed good improvements both in terms of energy and environmental performance. In particular the GSHP-FC allows a PES of 12.8%, a $\Delta\text{CO}_{2\text{eq}}$ equal to 15.8% and a reduction of operational costs (28%). The hybrid GSHP-PVT obtained the best performance in relation to the other cases, with a PES equal to 53.1%, a $\Delta\text{CO}_{2\text{eq}}$ equal to 52.0% and a reduction of operational cost equal to 56.4%. The SPB is equal to 12.7 years in case 4 and 18.5 years in case 5, however in this case this value could be improved by means of an economics incentive and price reductions on equipment resulting from economy of scale and market expansion of these technologies. In future work, the introduction of hybrid micro-cogeneration systems which serve a greater group of different users will be evaluated so as to investigate the advantages of these systems in a micro-grid set up with multiple end users. Further improvement could be achieved by developing predictive control strategy to optimize the hybrid systems performance under variety of conditions and applications.

CHAPTER 3: Energy planning by means Urban Energy Maps: CCHP for small urban districts

This chapter shows a methodology and its application aimed for optimizing both energy generation and use in urban areas. The study has been applied to the Historical centre of Benevento, an Italian southern city. A geo-referenced energy model of the ancient town is showed, allowing evaluation of energy demands for both heating and cooling, with reference to each building. In addition, also the electric demands of buildings have been quantified, carefully considering the various energy uses, as well as the necessary installed power.

A Geographic Information System (GIS) techniques have been applied for geo-referencing the energy necessities, then permitting the definition of Urban Energy Maps (UEMs). UEMs have been used for evaluating present criticalities, and thus in order to design possible urban retrofits, as installation of combined cooling, heat and power systems (CCHP), in order to satisfy the various energy demands. Finally, the entire procedure, in terms of coupled information referred to thermal, cooling and electric load profiles, allows a more rational energy use, cost optimization and reduction of polluting emissions. The presented methodology can be easy implemented and repeated, and could be adopted as new tool for proper energy planning.

Therefore, with reference to an Italian historical city centre (i.e., most buildings are protected as Cultural Goods), high-efficiency cogeneration systems are proposed for improving the energy uses, by coupling Combined Heat and Power (CHP) to district heating, cooling and energy nets. These intentions are presently supported by European Institutions, that promote the building connection to grid system for electricity, when produced by high-efficiency cogeneration, especially with reference to small scale and micro-cogeneration units [106][107].

More in deep, the aim of this chapter is to develop and apply a geo-referenced model suitable in order to:

- estimate the energy demand of the existing building stock,
- explore energy and environmental effects of particular energy efficiency measures,

- identify benefits derived by "CHP-based" district heating and cooling technologies as well as distributed electric energy generation.

According to this aim, it is presented a case study regarding the historical centre of Benevento, an Italian town located in the Mediterranean area.

3.1 Energy planning of urban districts: methodology

Geographic Information Systems (GIS) are computer tools suitable for assembling, manipulating and displaying a lot of geo-referenced information [108]. Xu and Coors [109] propose integration of System Dynamics models and GIS technology: indeed, this could be an interpretative method for evaluating future assessment of sustainability [109]. In the same directions, various other studies [110] [111] recur to GIS for collecting and improving the building energy performances of entire urban areas.

This study couples potentiality of GIS and a new model for evaluating energy performances of buildings. The aim is the development of a tool for investigating efficient energy measures, in order to reduce urban energy consumption and polluting emissions. In particular, the proposed methodology joins investigations of single buildings and statistical data, for creating large database of building energy performances, with reference to entire city districts. The searched outcome, suitable for a comprehensive view of the city energy performances, are the so-called "urban-energy maps" (i.e. "UEM", in the following) [112]. In particular, these thematic maps could assist planners and stakeholders in identifying social, environmental and economic effects of energy improving measures, by considering, at the same time, also efficiency and refurbishing possibilities for the energy generation and distribution. The data insert in the geo-referenced model, can be easily updated and improved. It isn't difficult integrate the created database with other information as, for instance, the energy labeling of buildings, or data obtained by energy distributors and inserted directly by citizens in a web platform.

The proposed study will be divided into three main steps: 1) creation of a global database of energy performances of buildings, 2) definition of urban energy maps and analysis of possible energy efficiency measures, 3) planning and evaluation of district

heating, cooling and electrical nets based on Combined Cooling, Heating and Power (CCHP) generation systems. The logic of the approach is shown in Figure 3. 1.

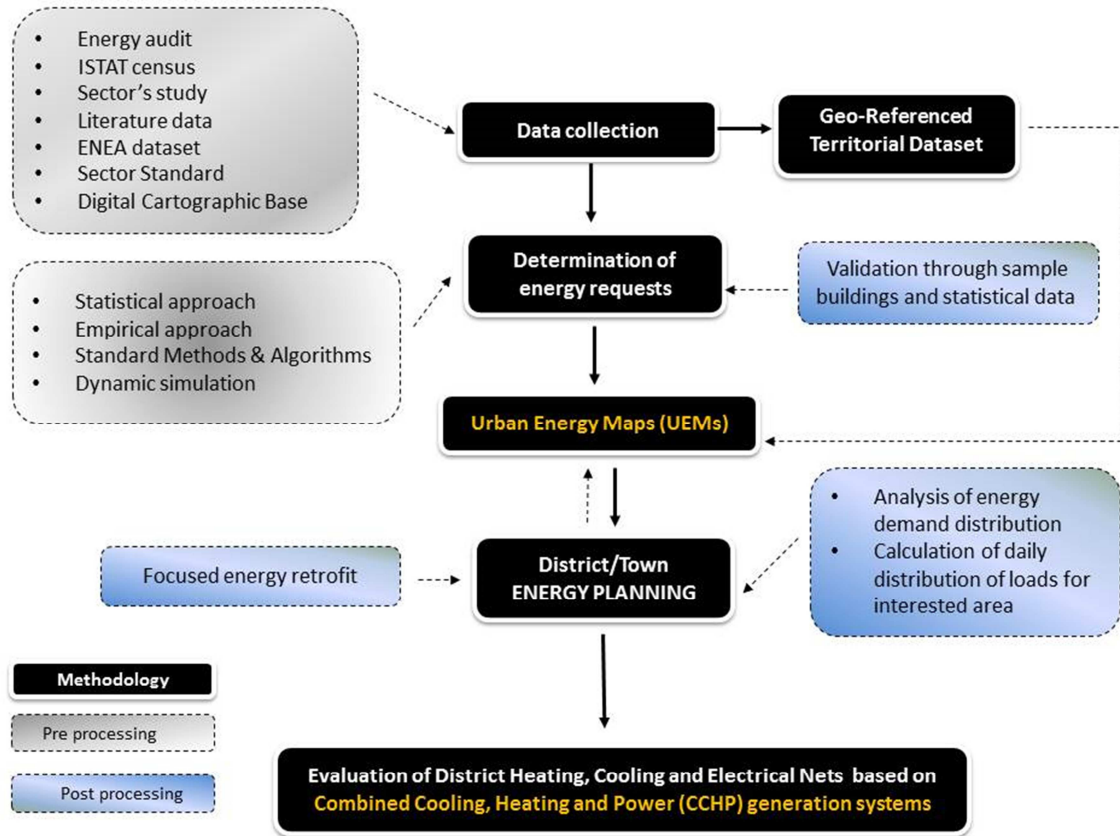


Figure 3. 1. Flowchart of the proposed methodology

3.2 Evaluations of building energy performances

The first step requires two main activities: a) buildings' energy audit, b) determination of energy requests and validation of results' reliability. These will be described in the next rows.

With reference to each building, direct census and surveys [88] provided input data for the energy calculations. In addition, further information has been derived by statistical evaluations, already discussed in [40]. The European standard EN 13790 [113], as well as the Italian version UNI TS 11300 [114] [115], evaluates the primary energy demand for the building heating (i.e., EP_i kWh/m²) as the "energy need ($E_{H,nd}$)" to "seasonal energy efficiency of the heating system (η_{sys})" and "overall floor area (S_T)" ratio. Equation 3.1 summarizes the method.

$$EP_i = E_{H,nd} / \eta_{sys} \cdot S_T \quad (3.1)$$

In particular:

$$E_{H,nd} = (E_{H,tr} + E_{H,ve}) - \eta_{H,gn} \cdot (E_{sol} + E_{end}) \quad (3.2)$$

where $E_{H,tr}$ and $E_{H,ve}$ are respectively heat losses due to energy transmission and ventilation, $\eta_{H,gn}$ is the utilization factor of free-gains: E_{end} (i.e., endogenous gains) and E_{sol} (solar free-gains). With reference to each term, [40] shows the entire calculation procedure, by evaluating, with reference to the case study here presented, a reliable average value of seasonal energy efficiency ratio of heating systems equal to around 0.75.

Diversely, in regards to the summer cooling, the energy performance index ($EP_{e,envlope}$ kWh/m²) of buildings can be calculated by means of a simplified approach. This method is fully described in [40]. It is based on solution of equation 3, where the cooling load (L_C), at the summer peak, is determined.

$$L_C = \left(L_{C,tr} + L_{C,w} \right) \cdot \gamma_C + L_{C,gr} + L_{C,sol} + L_{C,end} + L_{C,ve} \quad (3.3)$$

Starting from L_C , this has been multiplied for the length of the cooling season, and then corrected in order to evaluate, by means of a semi steady-state approach, the cooling energy need for the entire cooling periods ($E_{C,nd}$ in equation 3.4), by considering the mean monthly solar radiation and monthly-averaged air temperatures.

It should be pointed that, in the evaluation of the seasonal energy demand for the building cooling, by means of wide regression studies, they estimated that the solar radiation affects the cooling loads for around the 80%, while the remaining 20% is due to the outdoor air temperatures.

With the aim to identify the reduction of cooling need due to shading effects induced by other buildings and surrounding, the most common situations in the historical center of Benevento have been investigated. Several different percentage reductions (ΔR) have been identified, depending on the street width, the building height, the number of surrounding constructions. At the end, knowing $E_{C,nd}$ and by using ΔR , the energy performance index for the summer cooling was calculated according to equation 3.4.

$$EP_{e,enveloe} = E_{C,nd} \cdot \Delta R / S_T \quad (3.4)$$

Table 3.1 – referred to the entire physical methodology proposed in [40]- shows the input parameters and their sources with reference to the proposed equations.

Table 3.1. Input parameters and relative sources.

Heating demand		
Equation parameters	Sources	
Equation 1	Overall seasonal energy efficiency of the heating systems	UNI/TS 11300-2 [115]
	Total floor area	Calculated
Equation 2	Basement thermal transmittance	Crossing "Construction period" and [111]
	Building type	Audit data
	Construction period	Audit data
	Endogenous gains	Crossing "Kind of use" and data by [114]
	Heating need	UNI/TS 11300-1 [114]
	Heat losses due to transmission	UNI/TS 11300-1 [114]
	Heat losses due to ventilation	UNI/TS 11300-1 [114]
	Heated/cooled volume	Calculated
	Kind of use	Audit data
	Lateral surface	Calculated
	Liveableness	Audit data
	Number of floors	Audit data
	Perimeter	Calculated (average polygonal geometry)
	Solar free-gains	UNI/TS 11300-1 [114]
	Solar factor of window glass	0.75 for a normal double glazing [114]
	Solar Irradiation	UNI 10349 [116]
Surface area of the building	Istat data [117]	
Surface of glazed components	Estimated 12% of the vertical walls	

	Surfaces' orientation	Derived from the cartographies
	Utilization factor	Estimated: 0.80
	Utilization factor of free-gains	UNI/TS 11300-1 [114]
	Wall thermal transmittance	Crossing "Construction period" and [111]
	Window thermal transmittance	Crossing "Construction period" and [111]
Cooling demand		
	Equation parameters	Sources
Equation 3	Equivalent temperature difference	Derived [118]
	External temperature	Assumed 32°C UNI 10339 [119]
	Ground's temperature	Assumed: 13°C [116]
	Internal temperature	Assumed 26°C [114]
	Seasonal mean temperature	UNI 10349 [116]
	Seasonal mean solar radiation	UNI 10349 [116]
	Seasonal peak temperature	UNI 10349 [116]
	Seasonal peak solar radiation	UNI 10349 [116]
	Thermal bridges factor	Estimated: 15%
	Type of solar shadings	Audit data
Equation 4	Percentage Reduction	Estimated using dynamic energy simulation [120]

The energy need for the summer cooling has been calculated for the each building of the city center. The obtained outcomes have been compared, for some reference buildings, to those derived by accurate simulations by EnergyPlus [120] (Table 3.2) and by experimental data from energy billings, when available [121].

Table 3.3 shows the percentage differences for five buildings, interested by long monitoring and analyses of energy billings of previous years [40]. All comparisons show very satisfactory accordance. Indeed, the gap between the proposed methodology and the reference ones is always lower than 10%.

Table 3.2. Comparison with simulation results

Building	Percentage Gap	
	EP _i	EP _{e, envelope}
Bosco Lucarelli	≈ 4%	≈ 8%
Y_70 building	≈ 6%	≈ 10%
Y_2010 building	≈ 10%	≈ 7%

Table 3.3. Comparison with the energy bills

Building	Percentage Gap	
	EP_i	$EP_{e,envelope}$
R-cost	$\approx 7\%$	$\approx 7\%$
Bosco Lucarelli	$\approx 6\%$	$\approx 7\%$
Giannone	$\approx 8\%$	$\approx 9\%$
Ex-Inps	$\approx 5\%$	$\approx 10\%$

Obviously, the methodology has been thought for large investigations. Diversely, with reference to single analyses, referred to specific buildings, energy audits characterized by higher reliability should be adopted [122][123], by considering, for instance, also the incidence of thermal bridges, that could significantly affect the energy demand of buildings [124][125].

3.3 Urban energy maps

The thematic information on individual buildings, relative to the energy requests for the winter heating and summer cooling, have been then connected to the geo-referenced territorial support, by using a digital cartographic map of the ancient center of Benevento.

Figure 3.2 shows the maps of primary energy demand for the space heating (EP_i) (Figure 3.2a) and energy performance index for the summer cooling ($EP_{e,envelope}$) (Figure 3.2b). These maps provide information useful for feasibility studies aimed to test potential energy saving derivable by energy-retrofit measures. Definitively, the procedure is aimed to identify proper strategies and priorities.

Furthermore, combined information about thermal, cooling and electric load profiles of whole city areas could be also the starting point for design and optimize hybrid generation systems, for instance by integration of renewable energy sources or by means design of energy generation systems at "district scale".

About it, the next section introduces the investigation about installation of CCHP system, designed for satisfying the overall energy demands of a city block, by means of proper heating, cooling and electrical energy nets.

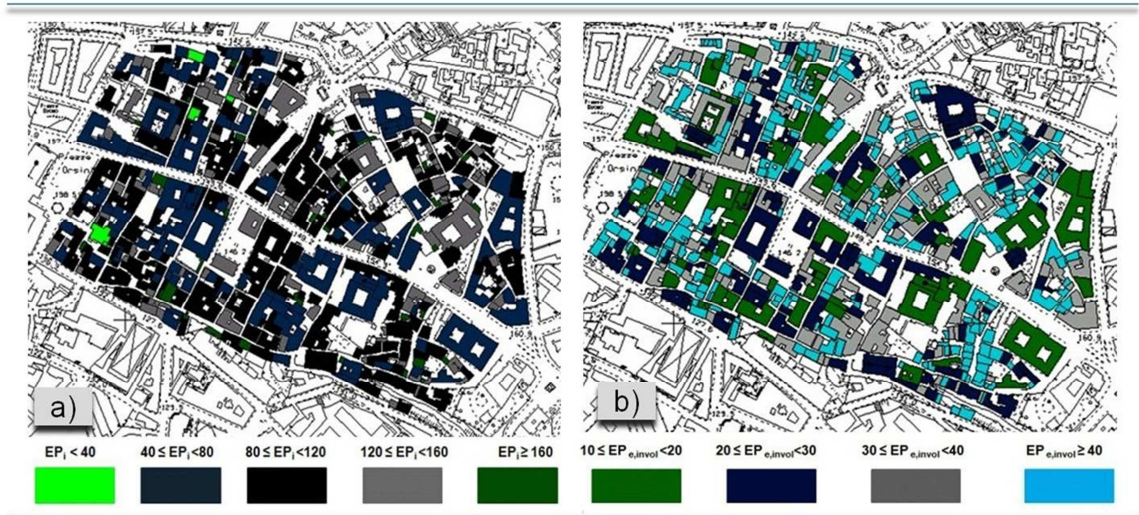


Figure 3.2. Urban Energy Map of the Benevento: Heating (a) and cooling (b) periods' performances.

The first steps of the analysis process are: a) the individuation of energy demand distribution and identification of suitable areas, b) calculation of seasonal energy demands and daily distribution of loads, with reference to each building and then for the entire chosen urban area.

With reference to the estimation of heating, cooling and electrical loads in buildings, various approaches are possible, based on statistical regression analysis, intelligent computer systems and energy simulation. In this chapter, the load profiles have been estimated by means of regression analyses, starting from the calculated energy requirements. Diversely, the electricity load distribution has been derived by typological values based on the building use.

According to the aim of the study - and thus the underlining of UEMs' capabilities in order to improve the territorial energy efficiency - the design of thermal and electric micro-grids that connect two urban cadastral sections (Figure 3.3) is described in the following sections.

The shown areas have been chosen because their buildings are characterized by well-combinable load profiles, as shown by UEMs. The main information about each building is reported in Table 3.4.

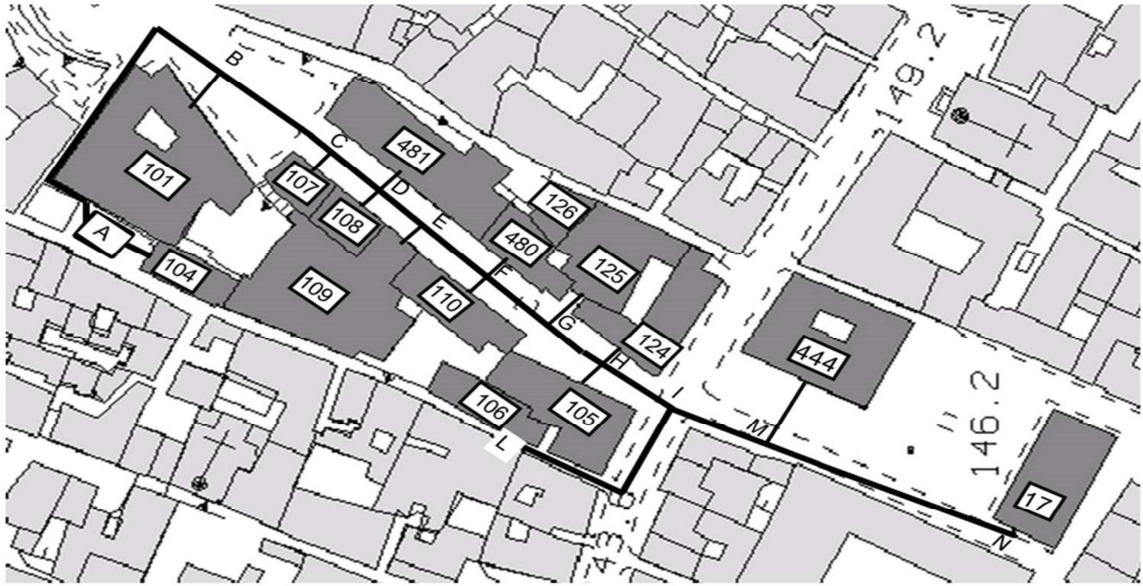


Figure 3.3. Allocation of thermal power plant and extension of thermal micro-grid.

Table 3.4. Main building information.

Building	Kind of use	S_T [m ²]
17	University - Office	1700
101	Office	1226
105	Bar - Restaurant	345
	Residential	690
106	Residential	802
107	Shop	166
	Residential	498
108	Shop	393
	Residential	786
109	Cinema	2210
110	Shop	175
	Office	150
	Residential	519
124	Office	1396
125	Residential	1506
126	Residential	434
444	Bar	293
	Shop	586
	University - Office	1762
480	Shop	508
	Residential	766
481	Office	3884

The monthly heating and cooling load profiles are diversified for weekdays, weekends and holidays. Moreover, also the electric loads and needs are diversified for winter and summer days. Figure 3.4 shows the cumulative load profiles for a typical working day.

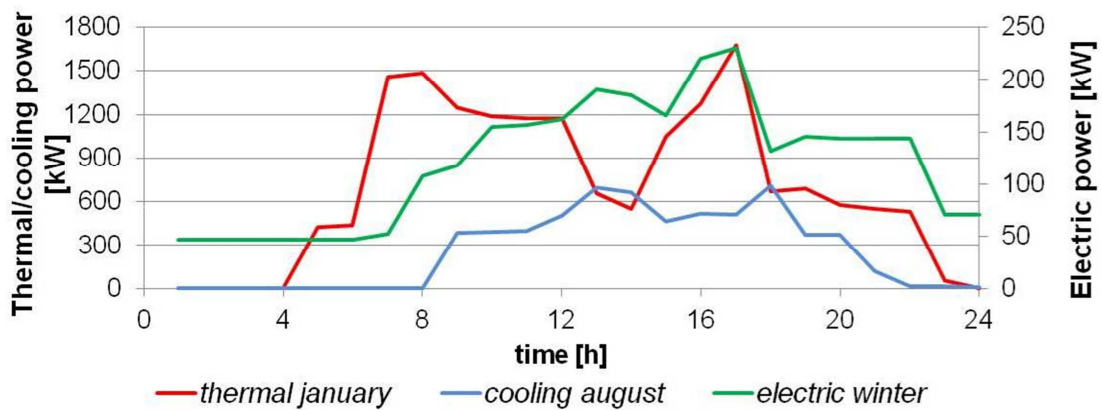


Figure 3.4. Example of cumulative load profile for a type day.

3.4 The polygeneration equipment

Thermal and electric micro-grids connect all buildings to a centralized polygeneration system, designed in order to meet the electric, heating and cooling loads. More in detail, the thermal micro-grid is a radial network, with pipes sized in order to operate during both heating and cooling periods. The diameters of ducts have been carefully sized once known the maximum power to be supplied, by ensuring velocities of fluid in the typical range $1.0 \div 2.5$ m/s. The overall heat loss coefficient of the thermal micro-grid is equal to $0.7 \text{ W/m}^2\text{K}$ [71]. During the heating period, the supply temperature of the fluid inside the plant loop is 80°C , with a loop difference temperature equal to 10°C .

In summer time, the supply temperature is 7°C , with a temperature difference - between return and supply - equal to 5°C in rated conditions. The hot water generation system is a CHP plant with an integrative gas-fired hot water boiler. The technology of CHP is quite common, based on the internal combustion engine fired by natural gas. The CHP has a rated power equal to 400 kW, with an electrical efficiency around 0.38. The rated efficiency of the integrative boiler is 0.90.

In the heating period, the CHP system provides thermal energy in order to meet the heating loads of users. Diversely, in summer, the CHP equipment is coupled to a single-stage absorption heat pump (AHP), in order to provide cold water for the space cooling, by increasing the number of operation hours per year of the CHP. In order to satisfy the peak loads during the cooling period, the CCHP plant is integrated by:

- a) an electric heat pump (EHP), (nominal capacity of the cooling equipment are 600 kW and 300 kW for the EHP and AHP respectively);
- b) to an AHP powered by a boiler (total cooling capacity of the AHP is equal to 900 kW).

Indeed, in order to optimize the entire system, both these solutions have been analyzed. In particular, energy and environmental implications of tri-generation systems has been analyzed as in [3] [52]. Also in this case, the energy consumption for pumping fluid in the micro-grid has been neglected.

Figure 3 shows location of the thermal plant (indicated with A) and the extension of the thermal micro-grid. Table 3.5 shows the physical characteristics of the micro-grid.

Table 3.5. Physical characteristics of the thermal micro-grid.

Stretch	AO	AB	BC	CD	DE	EF	FG	GH	HI	IL	IM	MN
Length [m]	14	89	36	16	13	18	20	16	21	47	20	64
Diameter [m]	0.05	0.16	0.16	0.16	0.12	0.12	0.10	0.10	0.10	0.05	0.10	0.07

The performances of the proposed system with respect to the traditional one are evaluated by means energy, economic and environmental analysis. More detailed information about this simplified approach and the parameters used in order to evaluate the different index are reported in section 1.3.

In addition to the information reported in section 1.3, this study assumes the following hypotheses, for both alternative and conventional systems:

- EHP: the seasonal energy efficiency ratio of the electric heat pump is equal to 3.0;
- the investment cost are evaluated according to [126].

With reference to the Alternative System (AS), this has been modelled by means of TRNSYS [42]. In particular, the modelling of the behaviours of the internal combustion engine, at part load conditions, adopts the performance curves inferred by ASHRAE Handbook [127] for common CHP systems based on combustion engine technology. More in detail, a set of equations is used for calculating thermal output, electric power and efficiencies when the operating conditions are different from the rated ones.

The following equations 3.5-3.9 allow calculation of distributions of primary energy input to the internal combustion engine (E^{CHP}), depending on various contributions:

- thermal energy to exhaust gases (E_{th}^{gas}) (eq. 3.5);
- thermal energy to jacket water (E_{th}^{water}) (eq. 3.6);
- thermal energy to environment ($E_{th}^{radiation}$) (eq. 3.7);
- thermal energy to lubrication oil (E_{th}^{oil}) (eq. 3.8);
- electric efficiency (η_{el}) - depending on PLR (eq. 3.9).

Moreover, equation 3.10 provides the ratio between the exhaust gas flow rate at part load conditions (\dot{m}_{PLR}^{gas}) and its nominal value (\dot{m}_{nom}^{gas}). Equation 3.10 is valid for PLR greater than 0.20.

$$E_{th}^{gas} / EP^{CHP} = -2.21 \cdot 10^{-7} \cdot PLR^3 + 4.66 \cdot 10^{-5} \cdot PLR^2 - 3.17 \cdot 10^{-3} \cdot PLR + 0.32 \quad (3.5)$$

$$E_{th}^{water} / EP^{CHP} = -3.76 \cdot 10^{-7} \cdot PLR^3 + 8.88 \cdot 10^{-5} \cdot PLR^2 - 7.15 \cdot 10^{-3} \cdot PLR + 0.41 \quad (3.6)$$

$$E_{th}^{radiation} / EP^{CHP} = -7.88 \cdot 10^{-8} \cdot PLR^3 + 2.22 \cdot 10^{-5} \cdot PLR^2 - 1.56 \cdot 10^{-3} \cdot PLR + 0.16 \quad (3.7)$$

$$E_{th}^{oil} / EP^{CHP} = -1.81 \cdot 10^{-7} \cdot PLR^3 + 4.23 \cdot 10^{-5} \cdot PLR^2 - 3.30 \cdot 10^{-3} \cdot PLR + 0.12 \quad (3.8)$$

$$\eta_{el} = -7.27 \cdot 10^{-9} \cdot PLR^4 + 2.31 \cdot 10^{-6} \cdot PLR^3 - 2.89 \cdot 10^{-4} \cdot PLR^2 + 1.68 \cdot 10^{-2} \cdot PLR \quad (3.9)$$

$$\dot{m}_{PLR}^{gas} / \dot{m}_{nom}^{gas} = 3.31 \cdot 10^{-5} \cdot PLR^2 + 4.56 \cdot 10^{-3} \cdot PLR + 0.21 \quad (3.10)$$

Figure 3.5 shows a scheme of the CHP thermal circuit [128]. The hot water used for the district heating (and as source for the AHP in summer time) is warmed by the heat exchange with the lubrication oil, the jacket water of the engine and its exhaust gas.

An efficiency of 0.80 for the exhaust gas heat exchanger has been considered, while the thermal energy of lubrication oil and jacket water is completely transferred to the district heating loop. The model of the CHP has been implemented by coupling a macro in Excel [129] and TRNSYS ("type 62", [42]). This allows also an accurate control. The admitted PLR for the CHP is in the range 0.2 ÷ 1.0.

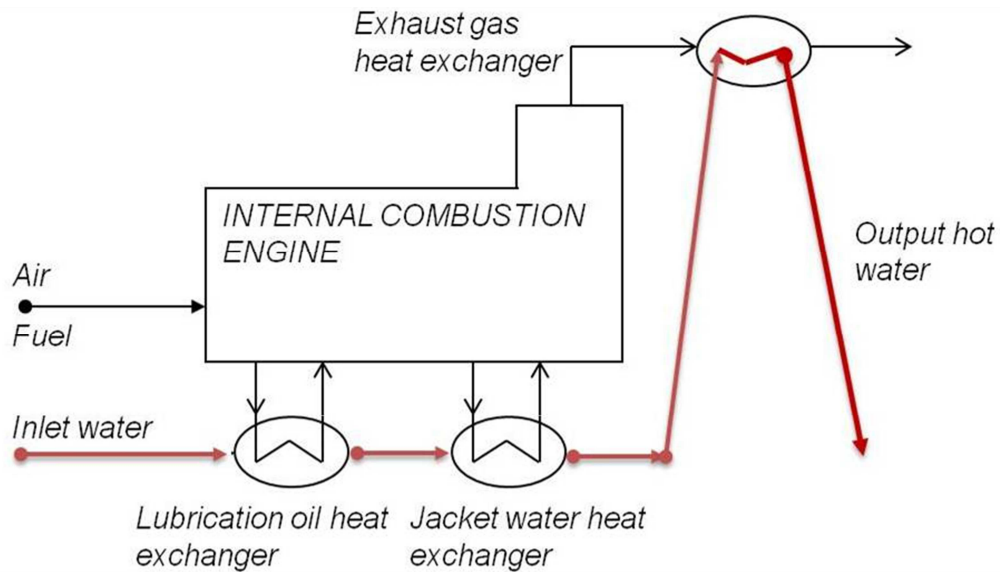


Figure 3.5. CHP thermal circuit.

The following inputs have been used: a) water mass flow rate, b) initial water temperature, c) set-point water temperature at the outlet of the CHP, d) ambient temperature. The output water temperature is calculated through mass and energy balances. The model determines, through iterative thermodynamic balances, the PLR of the internal combustion engine, in order to match the thermal load at the specific simulation time step. The auxiliary hot water boiler is automatically activated when the outlet water temperature is lower than the calculated desired value.

The hot water boiler has been simulated by means of the "type 6" of TRNSYS. Furthermore, the thermal micro-grid used the "type 31" [42]; in particular, this simulates the thermal behaviour of fluid flow in a pipe, through variable size segments. The mean exit temperature of fluid is calculated as the weighted average of temperatures of the segments that leave the pipe.

The connection of individual users to the micro-grid is modelled through the "type 649", which simulates a mixing valve through mass and energy balances. With reference to the climate conditions, an hourly weather file for Benevento has been created by means of the "Meteonorm" software [44]. In order to model the soil temperature, "type 77" has been used [42].

In TRNSYS, the heating and cooling loads, calculated according to the methods proposed in the sections 2 and 3, have been recalled through ".txt" external files.

Moreover, the absorption heat pump has been modelled by means of typical performance curves for single-stage AHP, implemented in TRNSYS by means of the "type 581" [43], that provides the coefficient of performance of the heat pump as function of the temperatures at the generator and those at the cooling tower (this last has been modelled by means of the "type 51"). In order to calculate the properties of moist air, "type 33" was used [42]. Similarly, the EHP was modelled through performance curves that provide the coefficient of performance of EHP as function of ambient air temperature, water temperature at the outlet of evaporator, part load ratio at the specific simulation time-step.

3.5 Discussion and results

The CHP has been sized in order to guarantee the thermal energy required to the users (E_{th}^{users}) and a suitable number of operating hours. The system is managed according to the heat-led control mode. Therefore, if the electricity converted by the CHP (E_{el}^{CHP}) is higher than that required by the buildings (E_{th}^{users}), the exceeding amount is sold to the electrical grid (E_{el}^{out}). Diversely, if the electricity demand is higher compared to the supplied by the CHP, a purchasing from the urban electric grid (E_{el}^{in}) is established. When the thermal energy converted by the CHP (E_{th}^{CHP}) is lower than the required, the difference is demanded to the peak boiler (E_{th}^b). The primary energy in input to CHP is indicated with E^{CHP} . The annual simulation considers three periods:

- heating period;
- intermediate period;
- cooling period.

All outcomes are reported in Table 3.6. During the heating season, the CHP operation is around 2'076 h. The energy losses through the thermal micro-grid ($E_{th}^{grid_loss}$) are equal to the 3.2% of the thermal energy delivered by the grid. In this period, compared to the conventional system, the primary energy saving (PES) is equal to 27.6%, while the corresponding reduction of CO₂ emission (ΔCO_2) is equal to 38.1%.

Table 3.6. Simulation results

	Heating period	Cooling period	Total
OH_{CHP} [h]	2'076	1'235	3'311
E_{th}^{users} [MWh]	1'288.9	-	1'288.9
$E_{th}^{grid_loss}$ [MWh]	42.8	-	42.8
E_{th}^{CHP} [MWh]	797.6	441.6	1'239.2
E_{th}^b [MWh]	534.1	181.7 ⁽¹⁾	716.8 ⁽¹⁾ 534.1 ⁽²⁾
E_{el}^{users} [MWh]	320.4	127.4	660.9
E_{el}^{CHP} [MWh]	751.7	400.3	1'157.9
E_{el}^{in} [MWh]	52.7	55.4 ⁽¹⁾ 59.8 ⁽²⁾	321.2 ⁽¹⁾ 325.6 ⁽²⁾
E_{el}^{out} [MWh]	484.1	324.6 ⁽¹⁾ 295.9 ⁽²⁾	808.6 ⁽¹⁾ 780.0 ⁽²⁾
PE^{CHP} [MWh]	1'983.3	1'075.1	3'058.4
E_C^{users} [MWh]	-	486.5	486.5
$E_C^{grid_loss}$ [MWh]	-	9.3	9.3
$E_C^{AHP(1)}$ [MWh]	-	495.7	495.7
$E_C^{AHP(2)}$ [MWh]	-	323.4	323.4
$E_C^{EHP(2)}$ [MWh]	-	172.8	172.8
$E_{el}^{tower(1)}$ [MWh]	-	3.8	3.8
$E_{el}^{tower(2)}$ [MWh]	-	2.1	2.1
PES ⁽¹⁾ [%]	27.6	4.9	18.8
$\Delta CO_2^{(1)}$ [%]	38.1	30.0	30.3
PES ⁽²⁾ [%]	27.6	10.6	20.0
$\Delta CO_2^{(2)}$ [%]	38.1	42.5	33.0

In the mid-season period, heating and cooling demands do not occur and only electrical energy is required (i.e., 213.1 MWh_{el}). Obviously, the CHP is turned off.

With reference to the cooling period, two different plants have been considered, as before already cited. In the first one, marked with the superscript (1) in the Table 3.6, the required cooling energy (E_C^{users}) is provided by an AHP (E_C^{AHP}) fired by the CHP and by the peak boiler if necessary. In the second system, marked with the superscript (2) in the Table 3.6, the integration to the chilled water provided by the AHP is achieved by using a traditional EHP (E_C^{EHP}). In both scenarios, the fan energy consumption for the cooling tower (E_{el}^{tower}) has been considered.

Compared to the conventional system, the following outcomes have been obtained (cooling period):

- Alternative System (1). The PES is equal to 4.9% while a reduction of CO₂ emission is around 30.0%.
- Alternative System (2). The use of EHP in order to integrate the AHP induces a positive value of PES (10.6%). The reduction of CO₂ emission is around 42.5%, compared to the CS.

The low value of primary energy saving for the first considered alternative system is due to the use of a boiler to feed a single stage AHP.

For both Alternative Systems considered, the CHP operation hours (OH_{CHP}) are equal to 1235 h during the cooling season. The energy losses of the district cooling micro-grid ($E_C^{grid_loss}$) are around 1.9% of the cooling energy delivered to the buildings.

All told, with reference to the entire year, the CHP operating hours are 3311 and the PES indexes are respectively around 18.8% for the Alternative System (1) and 20.0% for the AS (2). As regard the economic analysis the SPB index is evaluated. The analysis highlighted a SPB equal to 9.7 and 11.9 years for the alternative system (1) and (2) respectively. Should be pointed that the economic analysis does not take in account the possible reduction of the natural gas and additional electricity costs due to volume discounts.

Moreover, with reference to the AS (1), within a further study the CHP nominal capacity has been increased, in order to improve the energy performance of AS during the cooling season. Figure 3.6 shows the new simulation results, where the blue and red lines represent respectively the PES for the heating and cooling period and the black line refers to the annual simulation. This new configuration of CHP provides good energy performances during the cooling period, but the operating hours of CHP are lowered.

Therefore, the optimal solution is the use of an EHP in order to integrate the cooling energy, during the peak requests, in summer. Indeed, this configuration allows a long use of CHP (i.e., more than 3000 hours/year).

Future developments will combine the cogeneration system with suitable thermal storage devices. Indeed, this could allow the use of CHP in full-load conditions for longer periods, and it would induce better energy performances.

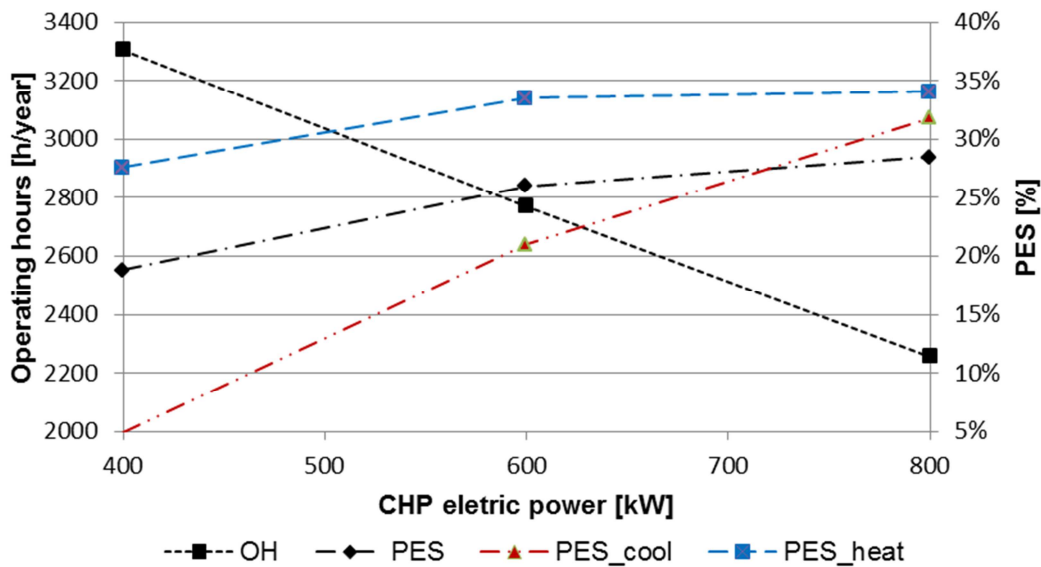


Figure 3.6. Outcomes derived by the increment of CHP system capacity.

In conclusion, with reference to an entire urban area, this chapter describes a methodology and its application for improving the building energy use and supply.

A Geographic Information System has been used for creating a global database of buildings' energy performance of the entire city centre of Benevento. In particular, asset energy ratings have been applied for the evaluation of the energy demand for the space heating of buildings, and a new calculation procedures, developed by the authors and fully described in previous studies, allowed predictions of the energy requests for the summer cooling. The methods have been applied to more than 500 buildings and the validation tests, by means of accurate dynamic energy simulations and experimental measures of energy, provided satisfactory comparisons.

Once developed suitable "Urban Energy Maps", these have been used as starting point for the evaluation of energy saving measures. In particular, urban energy maps can orient the territorial management, being a suitable tool for evidencing energy criticalities and thus in order to support planners and designers toward a sustainable urban development.

As case-study, the UEMs have been used for identifying combinable city blocks, under the point of view of the demanded energy for heating, cooling and electrical uses. By applying this methodology, combinable thermal and electrical loads have been identified for a city block. Therefore, the installation of a centralised CCHP system has been

proposed and a suitable model of district heating and cooling networks has been implemented. Various energy scenarios - on varying the designed alternative systems - show energy and environmental benefits. About it, the optimal configuration of CCHP and distributed generation allows Primary Energy Saving Index (PES) around 20%, reduction of CO₂ emissions higher than 33% and a SPB index less than 10 years.

CONCLUSION

This thesis work has dealt with polygeneration, the combined production of more than one energy vectors from a single primary energy source, in residential and tertiary sectors. In particular the thesis focuses on micro or small polygeneration systems that are placed immediately at the consumer's site. This concept, often referred as distributed polygeneration, differs from the dominant architecture of the current electricity system based on large scale centralized power generation. Compared to the separate production, polygeneration leads to primary energy saving and greenhouse gas benefits. However, in order to ensure a high market penetration of these promising technologies in residential and tertiary sector, it is essential to deal with some issues, such as the high investment payback period and the potential negative effects on the electricity network related to a large diffusion of DG.

In order to overcome this issues different possible solution were investigated:

- Load sharing approach, which consists in the introduction of a small electric and thermal micro-grid allowing the sharing of electric, thermal and cooling loads among a group of diversified end users (residential, commercial, tertiary, etc.).
- Virtual Power Plant, which consists of a number of geographically distributed power generation units that are managed by an ESCo with a centralized control system.
- Increase the share of self-consumed electricity "produced" by the MCHP. Two different strategies are analyzed in order to achieve this goal. The first consists in the careful selection of the user in which the MCHP system is installed, while the second relies on the interaction between the EVs charging and an MCHP system.
- Hybrid energy system, which combine two or more energy conversion devices, that when integrated, overcome limitations inherent in either.
- The use of Urban Energy Maps (UEMs) to locate an urban area suitable for the introduction of a polygeneration system.

All this solutions are investigated by means experimental and simulative approach. In particular, experimental and literature data were used in order to calibrate and validate the mathematical models of the system components. Once all the models were

calibrated and validated the energy, environmental and economic performances were evaluated by means dynamic simulation using TRNSYS software.

In chapter 1 a micro-cogeneration system that consists of an MCHP (electrical capacity of 6 kW), a TES and a peak boiler was analyzed in different climatic condition and serving different type of users. The analysis showed how the combined production of heat and electricity allow obtaining a primary energy saving and a CO_{2eq} emission reduction up to 23.3% and 28.0% respectively.

Moreover, the findings of this chapter highlighted the advantages of the load sharing approach, which sharing the load among different types of final users (different load profiles) allow increasing the operating hours of the MCHP system and consequently improve the economic performance. This aspect is more obvious in moderate climatic conditions, like Italian ones, typically characterized by few operating hours of heating system, where the load sharing approach can represent a key factor for the diffusion of MCHP systems.

The load sharing approach was evaluated also in case of the introduction of an Energy Service Company (ESCO), which managing a large number of systems distributed on the territory, could obtain a purchase price of natural gas and electricity lower than that applied to individual customers (section 1.4). In the analyzed case (section 1.4) the cost reduction of energy vectors was assumed equal to 20% with respect to the traditional system. This aspect leads to a good reduction of the investment payback period, which in the better case (users located in Milano and considering an economic support mechanism which can provide up to the 40% of the investment cost) reach interesting value (about 7 years).

In section 1.5, the installation of MCHP systems in buildings with low thermal energy demand with respect to the current building stock was investigated. A load sharing approach between a multifamily residential building and an office one was considered. The study showed that the introduction of a micro-grid between different users can help to have thermal and electric load profiles suitable for the MCHP application. Moreover the installation of an MCHP system in building with high level of thermal isolation allows to increase the percentage of self-consumed electricity (up to 90%) reducing the bidirectional electricity flow between the users and the network. This aspect leads to a

reduction of the impacts related to a large diffusion of distributed generation systems on the network and to economic advantages. In fact a sensitivity analysis with respect to the share of self-consumed electricity showed the influence of this parameter on the SPB, which is about 6 years in the better case.

In section 1.6 the interaction among the MCHP system, the EV charging and typical semidetached house was investigated considering two charging strategies (normal and optimized) and different daily driving distances (0÷120 km/day). In the normal charging strategy, charging occurs when the EV is parked at home until the full charge is reached, while in the optimized one charging is related to the MCHP operations in order to maximize the amount of self-consumed electricity.

Coupling EV charging with an MCHP system allows reducing the amount of “produced” electricity exported to the network with positive effects on the economic analysis and reducing the impact of large diffusion of EVs on the electric grid. The latter point is also due to the shift of electricity peaks on the network in periods of low electricity demand (i.e. during the night time).

The simulation results showed that increasing the average daily driving distance of the EV, the amount of self-consumed electricity can be increased, and consequently the operating costs decrease. Similar results could be achieved increasing the number of EVs and considering a particular charging strategy that avoids the simultaneous EVs charging.

The interaction between these two technologies involves a good reduction of the operating cost with respect to the reference system. In fact with the maximum value of the daily driving distance (120 kilometers), the increase of the operational cost reduction is equal to 61.9% for Torino and 78.3% for Napoli with respect to the base case (without EV) and considering a normal charging strategy. The introduction of the optimized charging strategy allows increasing the ΔOC , which becomes equal to 79.8% and 90.4% in Torino and Napoli, respectively.

In chapter 2, the advantages of the load sharing approach were evaluated in case of hybrid energy systems. In order to meet the energy requirements of two buildings (a residential and an office) in load sharing approach, five system configurations were defined. The first one consists of a conventional case with one boiler and one chiller for

each building (reference case), while the second represents a conventional case with a common boiler and chiller in load sharing approach. Once the advantages of load sharing approach were demonstrated, the performances of two different hybrid systems in load sharing scenario were investigated. The first hybrid system consists of a fuel cell based micro-cogenerator and a GSHP, while the second is based on PVT collectors, which represent a renewable cogeneration system, and a GSHP. The performances of these two hybrid micro-cogeneration systems were also compared to a stand-alone GSHP system.

The hybrid micro-cogeneration systems showed good improvements both in terms of energy and environmental performance. The GSHP-FC system showed a PES of 12.8%, a $\Delta\text{CO}_{2\text{eq}}$ equal to 15.8%, with an operating cost reduction equal to 28%. The hybrid micro-cogeneration system based on GSHP-PVT, using renewable energy source, obtained a PES equal to 53.1%, a $\Delta\text{CO}_{2\text{eq}}$ equal to 52.0% and a reduction of operational cost equal to 56.4%. Therefore, using renewable hybrid micro-cogeneration system is possible to improve the energy and environment performance of an MCHP system. The SPB were equal to 12.7 and 18.5 years respectively for GSHP-FC and GSHP-PVT system. The high payback period were due to the immature market share of this technologies, therefore the SPB value could be improved through economics incentive or price reductions on equipment resulting from economy of scale and market expansion of these technologies.

Chapter 3 started with a description of the methodologies used to create a global database of buildings' energy performance of the historical centre of Benevento. Subsequently, the UEM were used in order to detect an urban area suitable for the installation of a distributed polygeneration system. A trigeneration system and a district heating and cooling network able to meet the energy requirements of a cluster of users was designed. The trigeneration system is based on an internal combustion engine fired by natural gas characterized by a rated power equal to 400 kW_{el}. In cooling period the thermal energy of the CHP was used to feed an absorption heat pump. In order to satisfy the peak loads during the cooling period, two different configurations, to integrate the CCHP, are analyzed. The first consists in the installation of an electric heat pump while in the second an AHP is powered by a boiler. The simulation results showed as the first

configuration has better energy, environmental and economic performances. For this system configuration the PES was equal to 20% while the ΔCO_2 was equal to 33%. The economic analysis showed a SPB equal to 9.7 years, without take in account the possible reduction of the natural gas and electricity costs due to volume discounts. A sensitivity analysis with respect to the size of the prime mover highlighted as with increasing size the energy and environmental performance increase, while the operating hours and consequently the economic performance decrease.

In conclusion the findings of this thesis confirmed the energy and environmental advantages related to the diffusion of distributed polygeneration systems. In addition to these advantages, already shown in scientific literature, this work identified different solutions in order to overcome the main disadvantages of this promising technology. The load sharing approach, the introduction of VPP managed by an ESCo, the integration of EV charging with an MCHP, the careful selection of the end users in which the MCHP system is installed, the introduction of hybrid MCHP system, the use of UEM in energy planning problems, are promising solutions that can concur to the overcome the main issues that hinder the diffusion of distributed polygeneration system. Even though the findings of this thesis are encouraging, it is essential to reduce the installation costs of micro-polygeneration equipment in order to obtain economic results such as to ensure a high penetration of distributed polygeneration system. This result could be achieved thanks to a high market penetration of these technologies that in an early stage could be driven by economic support mechanisms.

Nomenclature

A	Area	[m ²]
a ₀ , b ₀	Regression parameters	[-]
a ₁ , b ₁	Regression parameters	[W ⁻¹]
a ₂ , b ₂	Regression parameters	[l ⁻¹ min]
a ₃ , b ₃	Regression parameters	[°C ⁻¹]
a ₄ , b ₄	Regression parameters	[W ⁻²]
a ₅ , b ₅	Regression parameters	[l ⁻² min ²]
a ₆ , b ₆	Regression parameters	[°C ⁻²]
a ₇ , b ₇	Regression parameters	[°C ⁻¹ l ⁻¹ min]
ABE	Average Absolute Error	[°C]
AE	Average Error	[°C]
C	cost	[€]
C ₁	Coefficient of equation 1.26	[-]
c	Water specific heat or specific cost	[J/kgK] [€/h] [€/Nm ³] [€/kWh]
C _{EEC}	Revenue for EEC sale	[€]
C _{EEC} ^u	Specific value of EEC	[€/tep]
CO _{2eq}	Equivalent carbon dioxide emission	[kg]
d ₀	Outside diameters of heat exchanger tubes	[m]
E	Energy	[MWh]
\dot{E}	Power	[kW]
EP _{e,invol}	Energy Performance index for the summer cooling need period	[kWh/m ² year]
EP _i	Energy Performance index for the winter period	[kWh/m ² year]
f _c	Conversion factor	[tep/kWh]
F _w	FC cooling water flow	[l/min]
g	total solar energy transmittance (or solar heat gain coefficient)	[-]
\bar{h}	mean heat transfer coefficient for internal	[W/m ² K]

	heat exchanger	
k	Water thermal conductivity	[W/mk]
L	thermal load	[W]
L_{GHX}	GHX length	[m]
$L_{network}$	Thermal network length	[m]
LHV	Lower Heating Value	[kWh/Sm ³]
m	mass	[kg]
\dot{m}	mass flow rate	
MAE	Maximum Absolute Error	[°C]
[MC]	Thermal capacity	[J/K]
MRE	Mean Relative Error	[%]
n	Exponent of Rayleigh number in equation 1.26	[-]
N	Number of measurement	[-]
\overline{Nu}	Nusselt number	[-]
OC	Operative Cost	[€]
OH	Operation Hours	[h]
P_{el}	Fuel cell DC power set-point	[W]
P_b	Nominal thermal power of boiler	[kW]
P_c	Nominal thermal power of chiller	[kW]
P_{FC}	Nominal electric power of FC	[kW]
P_{GSHP}	Nominal thermal power of GSHP	[kW]
P_{net}	Electrical power output the MCHP	[W]
PE	Primary Energy	[kWh]
PER	Primary Energy Ratio	[-]
PES	Primary Energy Saving	[-]
PLR	Partial Load Ratio	[-]
q_{gross}	Thermal power generation within the engine	[W]
q_{gen}	Thermal power input into the CHP system	[W]
R	percentage Reduction	[%]
Ra	Rayleigh number	[-]
RMSE	Root Mean Square Error	[°C] [W] [Slpm]

S	Surface	[m ²]
S _{PVT}	PVT total surface	[m ²]
SPB	Simple Pay Back period	[year]
t	time	[s]
T	Temperature	[°C]
T _{he}	Temperature of the water inside the TES near the heat exchanger	[°C]
T _{w,in}	Temperature of cooling water entering FC	[°C]
U	overall heat transfer coefficient	[W/m ² K]
[UA]	thermal conductance	[W/K]
V _{TES}	TES volume	[m ³]
x	Control variable	[-]

Acronyms

AHP	Absorption Heat Pump
AS	Alternative System
CCHP	Combined Cooling, Heat and Power
CHP	Combined Heat and Power
CS	Conventional System
DH	District Heating
DHW	Domestic Hot Water
EEC	Energy Efficiency Certificates
EHP	Electric Heat Pump
EMS	Energy Management System
EU	European Union
EV	Electric Vehicle
FC	Fuel Cell
GHX	Ground Heat eXchanger
GIS	Geographic Information Systems
GSHP	Ground Source Heat Pump
HVAC	Heating, Ventilation, and Air Conditioning

IHE1	Internal Heat Exchanger 1
IHE2	Internal Heat Exchanger 2
IHE3	Internal Heat Exchanger 3
MCCHP	Micro Combined Cool Heat and Power
MCHP	Micro Combined Heat and Power
NA	Napoli
PEMFC	Proton Exchange Membrane Fuel Cell
PVT	PhotoVoltaic Thermal
PS	Proposed System
RIC	Reciprocating Internal Combustion
SOFC	Solid Oxide Fuel Cell
STC	Standard Test Conditions
TES	Thermal Energy Storage
TO	Torino
TS	Traditional System
UEM	Urban-Energy Maps
wd	Week-day
we	Week-end day

Greek symbols

α	Experimental constant of eq. 1.27	[-]
β	Experimental constant of eq. 1.27	[°C ⁻¹]
γ	thermal bridges factor	
Δ	difference	
$\Delta\text{CO}_{2\text{eq}}$	avoided CO _{2eq} emissions	[-]
Δk	de-stratification conductivity	[W/mK]
ΔOC	operation cost difference	[€]
ΔT_{in}	logarithmic mean temperature difference of heat exchanger	[°C]
ΔU	additional thermal loss coefficient	[W/m ² K]
Δx	distance between two nodes	[m]

ε	error	[-]
η	energy efficiency	[-]
η_{el}^{AC}	DC electrical efficiency of FC	[-]
η_{el}^{DC}	AC electrical efficiency of FC	[-]

Subscripts

0	initial time
1in	inlet 1
1out	outlet 1
2in	inlet 2
2out	outlet 2
AS	Alternative System
b	bottom surface
bn	bottom node of the simulation model
C	cooling or cross-sectional
CS	Conventional System
cw	Cooling water
cw,i	Cooling water inlet
cw,o	Cooling water outlet
dh	District heating
down	down in the tank
el	electric
end	endogenous
eng	engine
env	environment
exp	experimental
f	final time
gn	gain
gr	ground
H	heating

hx	heat exchanger
i	generic node or current time step
main	maintenance
max	maximum
min	minimum
nd	need
ng	natural gas
nom	nominal
oper	operation
p	primary
PLR	Partial Load Ratio
PS	Proposed System
S	Surface
Sl,bn	lateral surface of bottom node of the model
sim	simulated
sol	solar
ss	steady-state condition
storage	storage tank
sys	heating system
T	total
tank	storage tank
tank wall	storage tank wall
th	thermal energy
tr	transmission
TS	Traditional System
up	up in the tank
ve	ventilation
w	window

Superscripts

AHP	Absorption Heat Pump
b or B	boiler
CHP	Combined Heat and Power
EHP	Electric Heat Pump
gas	exhaust gas
grid	Electric grid
grid_loss	losses by thermal micro-grid
in	in (purchased to the grid) or inlet to a system
loss	thermal losses
oil	lubrication oil
out	out (sold to the grid (if referred to the electricity)) or outlet
radiation	radiation
ref	reference
req	required
t	time
tower	cooling tower
users	users
water	jacket water

Reference

- [1] EU energy in figures, statistical pocketbook, European Union, 2012, doi:10.2833/11169. Available online at: ec.europa.eu/energy/publications/doc/2012_energy_figures.pdf, [last access 12/03/2014].
- [2] European Commission, Energy strategy for Europe, ec.europa.eu/energy/index_en.htm, [last access 12/03/2014].
- [3] G. Angrisani, C. Roselli, M. Sasso, Distributed microtrigeneration systems, *Progress in Energy and Combustion Science* 38 (2012) 502-521.
- [4] G. Allan, I. Eromenko, M. Gilmartin, I. Kockar, P. McGregor, The economics of distributed energy generation: A literature review, *Renewable and Sustainable Energy Reviews* 42 (2015) 543–556.
- [5] Directive 2004/8/EC of the European Parliament, *Official Journal of the European Union*, 2004.
- [6] M. De Paepe, P. D’Herdt, D. Mertens. Micro-CHP systems for residential applications. *Energy Conversion and Management* 47 (2006)3435–3446.
- [7] M. Pehnt, M. Cames, C. Fischer, B. Praetorius, L. Schneider, K. Schumacher, *Micro cogeneration: towards decentralized energy systems*. Nederland, Springer, ISBN 978-3-642-06498-2; 2010.
- [8] M. Dentice d’Accadia, M. Sasso, S. Sibilio, L. Vanoli, Micro-combined heat and power in residential and light commercial applications. *Applied Thermal Engineering* 23 (2003) 1247–59.
- [9] S. P. Borg, N. J. Kelly, High resolution performance analysis of micro-trigeneration in an energy-efficient residential building, *Energy and Buildings* 67 (2013) 153–165
- [10] C. Roselli, M. Sasso, S. Sibilio, P. Tzscheutschler, Experimental analysis of microcogenerators based on different prime movers. *Energy and Buildings* 43 (2011) 796–804.
- [11] A. Rosato, S. Sibilio, G. Ciampi, Dynamic performance assessment of a building-integrated cogeneration system for an Italian residential application, *Energy and Buildings* 64 (2013) 343–358.

- [12] K. Maeda, K. Masumoto, A. Hayano, A study on energy saving in residential PEFC cogeneration systems, *Journal of Power Sources* 195 (2010) 3779–3784.
- [13] S. R. Asaee, V. I. Ugursal, I. Beausoleil-Morrison, Techno-economic evaluation of internal combustion engine based cogeneration system retrofits in Canadian houses – A preliminary study, *Applied Energy* 140 (2015) 171–183.
- [14] G. Angrisani, C. Roselli, M. Sasso, F. Tariello, Dynamic performance assessment of a micro-trigeneration system with a desiccant-based air handling unit in Southern Italy climatic conditions, *Energy Conversion and Management* 80 (2014) 188–201.
- [15] S. Cho, K. H. Lee, E. C. Kang, E. J. Lee, Energy simulation modeling and savings analysis of load sharing between house and office, *Renew. Energy* 54 (2013) 70–77.
- [16] O.A. Shaneb, P.C. Taylor, G. Coates, Optimal online operation of residential μ CHP systems using linear programming, *Energy Build.* 44 (2012) 17–25.
- [17] G.M. Kopanos, M.C. Georgiadis, E.N. Pistikopoulos, Energy production planning of a network of micro combined heat and power generators, *Appl. Energy* 102 (2013) 1522–1534.
- [18] H. Cho, R. Luck, S. D. Eksioglu, L. M. Chamra, Cost-optimized real-time operation of CHP systems, *Energy Build.* 41 (2009) 445–451.
- [19] V. Curti, M. R. von Spakovsky, D. Favrat, An environomic approach for the modeling and optimization of a district heating network based on centralized and decentralized heat pumps, cogeneration and/or gas furnace. Part I: Methodology, *Int. J. Therm. Sci.* (2000) 39, 721–730.
- [20] V. Curti, M. R. von Spakovsky, D. Favrat, An environomic approach for the modeling and optimization of a district heating network based on centralized and decentralized heat pumps, cogeneration and/or gas furnace. Part II: Application, *Int. J. Therm. Sci.* (2000) 39, 731–741.
- [21] A.C.M. Ferreira, M.L. Nunes, S.F.C.F. Teixeira, C.P. Leão, Â.M. Silva, J.C.F. Teixeira, L.A.S.B. Martins, An economic perspective on the optimisation of a small-scale cogeneration system for the Portuguese scenario, *Energy* 45 (2012) 436–444.
- [22] Directive 2010/31/EU of the European Parliament and of the Council of 19 May 2010 on the energy performance of buildings (recast).
- [23] Directive 2002/91/EC of the European Parliament and of the Council of 16 December 2002 on the energy performance of buildings.

- [24] Directive 2012/27/EU of the European Parliament and of the Council of 25 October 2012 on energy efficiency.
- [25] European Commission, Reducing emissions from transport, Available online at: www.ec.europa.eu/clima/policies/transport/index_en.htm, [last access 21/11/2014].
- [26] M. Krzyzanowski, B. Kuna-Dibbert, J. Schneider, Health effects of transport-related air pollution, World Health Organization 2005, ISBN 92-890-1373-7, available online: www.euro.who.int/__data/assets/pdf_file/0006/74715/E86650.pdf [last access 22/10/2014].
- [27] K. Yabe, Y. Shinoda, T. Seki, H. Tanaka, A. Akisawa, Market penetration speed and effects on CO₂ reduction of electric vehicles and plug-in hybrid electric vehicles in Japan, *Energy Policy* 45 (2012) 529–540.
- [28] U.S. Department of Energy, Lessons Learned – The EV Project Greenhouse Gas (GHG) Avoidance and Fuel Cost Reduction, Final report, 2012, available online: http://www.theevproject.com/downloads/documents/15.%20GHG%20Avoidance_V1.1.pdf [last access 24/10/2014].
- [29] E. Akhavan-Rezai, M. F. Shaaban, E. F. El-Saadany, A. Zidan, Uncoordinated Charging Impacts of Electric Vehicles on Electric Distribution Grids: Normal and Fast Charging Comparison, *Power and Energy Society General Meeting, IEEE* (2012), doi: 10.1109/PESGM.2012.6345583.
- [30] C. Farkas, K. I. Szabó, L. Prikler, Impact Assessment of Electric Vehicle Charging on a LV Distribution System, *Energetics (IYCE), Proceedings of the 3rd International Youth Conference, Leiria, Portugal, Jun. 7–9, 2011*.
- [31] R. C. Leou, C. L. Su, C. N. Lu, Stochastic Analyses of Electric Vehicle Charging Impacts on Distribution Network, *IEEE transactions on power systems* 29 no. 3 (2014).
- [32] J. García-Villalobos, I. Zamora, J.I. San Martín, F.J. Asensio, V. Aperribay, Plug-in electric vehicles in electric distribution networks: A review of smart charging approaches, *Renewable and Sustainable Energy Reviews* 38 (2014) 717–731.
- [33] H. Ribberink, E. Entchev, Exploring the potential synergy between micro-cogeneration and electric vehicle charging, *Applied Thermal Engineering* 71 (2014) 677-685.

- [34] T. Wakui, N. Wada, R. Yokoyama, Energy-saving effect of a residential polymer electrolyte fuel cell cogeneration system combined with a plug-in hybrid electric vehicle, *Energy Conversion and Management* 77 (2014) 40–51.
- [35] A. Rosato, S. Sibilio, M. Scorpio, Dynamic performance assessment of a residential building-integrated cogeneration system under different boundary conditions. Part I: Energy analysis, *Energy Conversion and Management* 79 (2014) 731–748.
- [36] A. Rosato, S. Sibilio, M. Scorpio, Dynamic performance assessment of a residential building-integrated cogeneration system under different boundary conditions. Part II: Environmental and economic analyses, *Energy Conversion and Management* 79 (2014) 749–770.
- [37] Gary D. Burch, Hybrid Renewable Energy Systems, U.S. DOE Natural Gas / Renewable Energy Workshops August 21, 2001 Golden, Colorado, available online: <http://www.netl.doe.gov/publications/proceedings/01/hybrids/Gary%20Burch%208.21.01.pdf> [last access 10/03/2015].
- [38] N. H. Afgan, M. G. Carvalho, Sustainability assessment of a hybrid energy system, *Energy Policy* 36 (2008) 2903– 2910.
- [39] A. Hina Fathima, K. Palanisamy, Optimization in microgrids with hybrid energy systems – A review, *Renewable and Sustainable Energy Reviews* 45 (2015) 431–446.
- [40] F. Ascione, R.F. De Masi, F. de Rossi, R. Fistola, M. Sasso, G.P. Vanoli, Analysis and diagnosis of the energy performance of buildings and districts: Methodology, validation and development of Urban Energy Maps, *J. Cities* (2013), <http://dx.doi.org/10.1016/j.cities.2013.04.012>
- [41] <http://www.aisin.com>.
- [42] TRNSYS 17, a TRaNsient SYstem Simulation program, Solar Energy Laboratory, University of Wisconsin-Madison, 2010.
- [43] T.E.S.S. Component Libraries v.17.01 for TRNSYS v17.0 and the TRNSYS Simulation Studio, Parameter/Input/Output Reference Manual, Thermal Energy System Specialists, LLC, 2004.
- [44] www.meteonorm.com.
- [45] N. Kelly, I. Beausoleil-Morrison, Specifications for modelling fuel cell and combustion-based residential cogeneration devices within whole-building simulation

programs, IEA/ECBCS Annex 42 report, 2007, http://www.ecbcs.org/docs/Annex_42_Cogen_Model_Specifications.pdf.

- [46] Rosato, S. Sibilio, Calibration and validation of a model for simulating thermal and electric performance of an internal combustion engine-based micro-cogeneration device, *Appl. Therm. Eng.* 45-46 (2012) 79-98.
- [47] S. Khare, M. Dell'Amico, C. Knight, S. McGarry, Selection of materials for high temperature sensible energy storage, *Sol. Energ. Mat. Sol. C.* 115 (2013) 114–122.
- [48] Dinçer, İ. and Rosen, M. A. (2010) *Energy Storage Systems, in Thermal Energy Storage: Systems and Applications, Second Edition*, John Wiley & Sons, Ltd, Chichester, UK.
- [49] A. Sharma, V.V. Tyagi, C.R. Chen, D. Buddhi, Review on thermal energy storage with phase change materials and applications, *Renew. Sust. Energ. Rev.* 13 (2009) 318–345.
- [50] T. Nuytten, P. Moreno, D. Vanhoudt, L. Jaspers, A. Soléc, L.F. Cabeza, Comparative analysis of latent thermal energy storage tanks for micro-CHP systems, *Appl. Ther. Eng.* 59 (2013) 542-549.
- [51] F. Caresana, C. Brandoni, P. Feliciotti, C.M. Bartolini, Energy and economic analysis of an ICE-based variable speed-operated micro-cogenerator, *App. Energy* 88 (2010) 659-671.
- [52] S. Sibilio, M. Sasso, R. Possidente, C. Roselli, Assessment of micro-cogeneration potential for domestic trigeneration, *Int. J. Environ. Technol. Manage.* 7 (2007) 147-164.
- [53] A. Piacentino, F. Cardona, An original multi-objective criterion for the design of small-scale polygeneration systems based on realistic operating conditions, *Appl. Ther. Eng.* 28 (2008) 2391-2404.
- [54] A. Arteconi, N.J. Hewitt, F. Polonara, Domestic demand-side management (DSM): Role of heat pumps and thermal energy storage (TES) systems, *Appl. Ther. Eng.* 51 (2013) 155-165.
- [55] D. Haeseldonckx, L. Peeters, L. Helsen, W. D'haeseleer The impact of thermal storage on the operational behaviour of residential CHP facilities and the overall CO₂emissions, *Renew.Sust. Energ. Reviews* 11 (2007) 1227–1243;

- [56] G. Pagliarini, S. Rainieri, Modeling of a thermal energy storage system coupled with combined heat and power generation for the heating requirements of a University Campus, *Appl. Ther. Eng.* 30 (2010) 1255–1261.
- [57] A. D. Smith, P. J. Mago, N. Fumo, Benefits of thermal energy storage option combined with CHP system for different commercial building types, *Sust. Energ. Technol. Assess.* 1 (2013) 3–12.
- [58] A. Fragaki, A. N. Andersen, D. Toke, Exploration of economical sizing of gas engine and thermal store for combined heat and power plants in the UK, *Energ.* 33 (2008) 1659–1670.
- [59] E. S. Barbieri, F. Melino, M. Morini, Influence of the thermal energy storage on the profitability of micro-CHP systems for residential building applications, *Appl. Energ.* 97 (2012) 714–722.
- [60] A. C. Celador, M. Odriozola, J.M. Sala, Implications of the modelling of stratified hot water storage tanks in the simulation of CHP plants, *Energ. Convers. Manage.* 52 (2011) 3018–3026.
- [61] C. Cristofari, G. Notton, P. Poggi, A. Louche, Influence of the flow rate and the tank stratification degree on the performances of a solar flat-plate collector, *Int. J. Ther. Sci.* 42 (2003) 455–469.
- [62] W. Yaïci, M. Ghorab, E. Entchev, S. Hayden, Three-dimensional unsteady CFD simulations of a thermal storage tank performance for optimum design. *Appl. Ther. Eng.* 60 (2013) 152-163.
- [63] C. A. Cruickshank, S. J. Harrison, Heat loss characteristics for a typical solar domestic hot water storage, *Energ. Buildings* 42 (2010) 1703–1710.
- [64] Klein, S.A., "A Design Procedure for Solar Heating Systems", Ph.D. Thesis, Department of Chemical Engineering, University of Wisconsin-Madison, USA (1976).
- [65] Newton, B.J., "Modeling of Solar Storage Tanks", M.S. Thesis, Department of Mechanical Engineering, University of Wisconsin-Madison, USA (1995).
- [66] Technical data of storage tank, available from www.cordivari.it/default.aspx?lng=1 [last accessed 20/08/2013].
- [67] Wetter M. GenOpt, generic optimisation program, user manual, version 3.1.0. Lawrence Berkeley National Laboratory; 2011. Manual and program downloadable free of charge from simulationresearch.lbl.gov/GO/ [last accessed 10/08/2014].

- [68] M. Necati Özişik, Heat transfer a basic approach, McGraw-Hill , USA (1985).
- [69] G. Angrisani, et al., Load sharing with a local thermal network fed by a microgenerator: Thermo-economic optimization by means of dynamic simulations, Applied Thermal Engineering (2013), dx.doi.org/10.1016/j.applthermaleng.2013.09.055.
- [70] Technical data of solar collector, available from www.thermital.it/ [last accessed 10/01/2014].
- [71] A. Hlebnikov, N. Dementjeva, A. Siirde, Optimization of narva district heating network and analysis of competitiveness of oil shale CHP building in Narva, Oil Shale 26 (2009) 269–282.
- [72] TERNA, Statistics and forecasts, Statistical data, Production. Available online: www.terna.it/LinkClick.aspx?fileticket=axZsbhFJBW8%3d&tabid=418&mid=2501, [last access 07/04/2014, in Italian].
- [73] TERNA, Summary "Statistical data on electricity in Italy - 2011". Available online: www.terna.it/LinkClick.aspx?fileticket=b%2B6DNrXsUBA%3D&tabid=649, [last access 07/04/2014, in Italian].
- [74] Review of electricity loss factors, applied to electricity input to low and middle voltage network, Gas and Electricity Authority, Markets Department, Available online: www.autorita.energia.it/allegati/docs/12/013-12.pdf, [last access 07/04/2014, in Italian].
- [75] CO₂ emission factors in electricity sector and analysis of emissions decomposition, ISPRA, Report n. 172/2012. Available online: www.isprambiente.gov.it/it/pubblicazioni/rapporti/fattori-di-emissione-di-co2-nel-settore-elettrico-e-analisi-della-decomposizione-delle-emissioni, [last access 07/04/2014, in Italian].
- [76] Guidelines for the application of the Ministry Decree of Economic Development, September 5, 2011 - High Efficiency Cogeneration (CAR). Available online: www.gse.it/it/Qualifiche%20e%20certificati/Certificati%20Bianchi%20e%20CAR/Pages/default.aspx [last access 07/04/2014, in Italian].
- [77] AEEG resolution n. 181/06 , available online: www.autorita.energia.it/it/docs/06/181-06.htm, [last access 07/04/2014, in Italian].

- [78] E.D. Mehleri, H. Sarimveis, N.C. Markatos, L.G. Papageorgiou, Optimal design and operation of distributed energy systems: Application to Greek residential sector, *Renewable Energy* 51 (2013) 331-342.
- [79] Staffell, Purchase cost of condensing boilers in the UK, 2008. Available online: www.academia.edu/1216602/Purchase_Cost_of_Condensing_Boilers_in_the_UK [last access 15/09/2014].
- [80] Italian Legislative Decree n. 311 of December 29, 2006 (in Italian).
- [81] Richardson, M. Thomson, D. Infield, C. Clifford, Domestic electricity use: A high-resolution energy demand model, *Energy and Buildings* 42 (2010) 1878–1887.
- [82] U. Jordan, K. Vajen, Realistic Domestic Hot-Water Profiles in Different Time Scales, Universität Marburg (2001). Available online sel.me.wisc.edu/trnsys/trnlib/iea-shc-task26/iea-shc-task26-load-profiles-description-jordan.pdf [last access 28/10/1014].
- [83] UNI TS 11300-2. Energy performance of buildings. Part 2: Evaluation of primary energy need and of system efficiencies for space heating and domestic hot water production. 2008 (in Italian).
- [84] D.P.R. 26 August 1993, n. 412 (1), Regulations for the design, installation, operation and maintenance of heating systems in buildings for the purpose of reducing consumption of energy, in the art. 4, paragraph 4, of Law January 9, 1991, n. 10, [in Italian].
- [85] EL-TERTIARY, Monitoring Electricity Consumption in the Tertiary Sector. Available online www.eu.fhg.de/el-tertiary [last access 28/10/1014].
- [86] P. Caputo, G. Costa, V. Canotto, L. Pistocchini, A. Roscetti, Behavior of the platform in relation to the proper combination of demand curves and generation and control systems, Report RdS/2011/55, Electrical System research (2011), in Italian.
- [87] E. Entchev, L. Yang and M. Ghorab, Fuel Cell –Ground Source Heat Pump Simulation Study, Second Year Progress Report March 2013, Report #: CE-O-RIES-13-099.
- [88] .G.C. 12 - Economic Development- Deliberation n. 475 March 18, 2009 - Proposal for Regional Environmental Energy Plan of Campania Region and starts of consultation activities about strategic environmental assessment and drafting of the Action Plan for Energy and the Environment. In Italian, available online:

- www.enerweb.casaccia.enea.it/enearegioni/UserFiles/OSSERVATORIO/Sito/Campania/PEAR_Campania_2009.pdf [last access 28/10/2014].
- [89] V. Corrado, I. Ballarini, S. P. Corgnati, D6.2 National scientific report on the TABULA activities in Italy, May 2012, ISBN: 978-88-8202-039-2, available online: http://www.building-typology.eu/downloads/public/docs/scientific/IT_TABULA_ScientificReport_POLITO.pdf [last access 28/10/2014].
- [90] Argonne National Laboratory, Available online at: <http://www.transportation.anl.gov/D3/> [last access 27/01/1015].
- [91] Ministry of Economic Development - Ministry of the Environment and Land and Sea protection - Ministry of Infrastructure and Transport: "2012 Guide to saving fuel and CO₂ emissions from cars". In Italian, available online: http://www.sviluppoeconomico.gov.it/images/stories/documenti/GUIDA2012_CO2.pdf [last access 02/12/1014].
- [92] ISTAT, population census 2011, <http://dati-censimentopopolazione.istat.it/?lang=en&SubSessionId=84db9076-4622-4ec5-9c5e-ebc80e83019d>.
- [93] VDI 4640, Thermal use of the underground - Ground source heat pump systems, 2001
- [94] J. A. Duffie, W. A. Beckman, Solar Engineering of Thermal Processes, Wiley; 3 edition edition (2006), USA, ISBN 9780471698678
- [95] Aermec, www.aermec.com/default.htm
- [96] I. Katic, Measurement Report – Test of PV/T-module "PVtwin" , 2012, Danish Technical Institute, available online at archive.iea-shc.org/publications/downloads/DC4-1_Measurement_Report_Test_of_PVT_module_PVTwin_inkl_forside.pdf [last access 02/04/1014].
- [97] E. Thorsteinson. Performance testing of a 1 kWe PEM fuel cell cogeneration system. MICRoGen'II, 2nd international conference on microgeneration and related technologies, Glasgow (UK), April, 2011.
- [98] EN 410:2011, Glass in building - Determination of luminous and solar characteristics of glazing, 2011.

- [99] A. Borghetti, Definition of electric and thermal load for typical residential and industrial users for the design of control system of an integrated plant based on fuel cells and gas microturbine for distributed generation, (2000), available online: www.ricercadisistema.it:8080/site/binaries/content/assets/rse-sola-lettura/progresso/2002/Generazione_distribuita/a0-038094-a1.pdf [last access 02/04/2014, in Italian].
- [100] P. Caputo, G. Costa, V. Canotto, L. Pistocchini, A. Roscetti, Behavior of platform in relation to the correct matching between demand curves and generation systems and control, Report Ricerca di Sistema Elettrico (2011), available online: www.enea.it/it/Ricerca_sviluppo/documenti/ricerca-di-sistema-elettrico/efficienza-energetica-servizi/rds-55.pdf [last access 02/04/2014, in Italian].
- [101] Energy plus weather data. Available online: apps1.eere.energy.gov/buildings/energyplus/weatherdata_about.cfm [last access 04/04/2014].
- [102] H. Harb, J. Reinhardt, R. Streblow, D. Müller, OPTIMAL DESIGN OF ENERGY CONVERSION UNITS FOR RESIDENTIAL HOUSES, London (UK) 23-24 June 2014, Pro Building Simulation and Optimization BSO14.
- [103] P. Blum, G. Campillo, T. Kölbl, Techno-economic and spatial analysis of vertical ground source heat pump systems in Germany, *Energy* 36 (2011) 3002-3011.
- [104] F. Robert, L. Gosselin, New methodology to design ground coupled heat pump systems based on total cost minimization, *Applied Thermal Engineering* 62 (2014) 481-491.
- [105] N. Astea, C. Del Pero, F. Leonforte, Optimization of solar thermal fraction in PVT systems, *Energy Procedia* 30 (2012) 8 – 18.
- [106] Directive 2009/72/EC of the European parliament and of the council of 13 July 2009 concerning common rules for the internal market in electricity and repealing Directive 2003/54/EC, *Official Journal of the European Union* L 211/55 (14 August 2009).
- [107] Directive 2009/73/EC of the European parliament and of the council of 13 July 2009 concerning common rules for the internal market in natural gas and repealing Directive 2003/55/EC, *Official Journal of the European Union* L 211/94 (14 August 2009).

- [108] US Geological Survey (USGS). USGS: Science for a changing world. US Department of the Interior. Available at www.usgs.gov/research/gis. Last access of authors: June 1st, 2013.
- [109] Z. Xu, V. Coors, Combining system dynamics model, GIS and 3D visualization in sustainability assessment of urban residential development, *Build. Environ.* 47 (2012) 272-287.
- [110] S.C. Heiple, D.J. Sailor, Using building energy simulation and geospatial modeling techniques to determine high resolution building sector energy consumption profiles, *Energy Build.* 40 (2008) 1426–1436.
- [111] G. Dall’O’, A. Galante, M. Torri, A methodology for the energy performance classification of residential building stock on an urban scale *Energy Build.* 48 (2012) 211–219
- [112] F. Ascione, R.F. De Masi, F. de Rossi, R. Fistola, G.P. Vanoli, Energy assessment in town planning: Urban energy maps. In *WIT transactions on ecology and the environment*, Vol. 155 (2011) 205–216.
- [113] European Committee for Standardization. Standard ISO EN 13790: 2008, Energy performance of buildings – Calculation of energy use for space heating and cooling, 2008.
- [114] Italian Committee for Standardization. Standard UNI TS 11300 part 1: 2008, Energy performance of buildings: Evaluation of energy need for space heating and cooling, 2008.
- [115] Italian Committee for Standardization. Standard UNI TS 11300 part 2: 2008, Energy performance of buildings: Evaluation of primary energy need and of system efficiencies for space heating and domestic hot water production, 2008.
- [116] Italian Committee for Standardization (in Italian). Standard UNI 10349: 1993, Riscaldamento e raffrescamento degli edifici - Dati climatici, 1993.
- [117] ISTAT Censimento 2001- 14° Censimento della popolazione e delle abitazioni, in Italian. Available at www.dawinci.istat.it. Last access of authors: June 30th, 2013.
- [118] C. Pizzetti, Condizionamento dell'aria e refrigerazione. Teoria e calcolo degli impianti, CEA, 1986, in Italian.

- [119] Italian Committee for Standardization (in Italian). Standard UNI 10339:1995, Impianti aeraulici ai fini di benessere. Generalità, classificazione e requisiti. Regole per la richiesta d 'offerta, l' offerta, l' ordine e la fornitura, 1995.
- [120] U.S. Department of Energy (2010). Energy Plus simulation software, Version 6.0.0.
- [121] F. Ascione, F. de Rossi, G. P. Vanoli, Energy retrofit of historical buildings: Theoretical and experiment investigations for the modelling of reliable performance scenarios, *Energy Build.* 43 (No 8) (2011) 1925–1936.
- [122] Z. Ma, P. Cooper, D. Daly, L. Ledo, Existing building retrofits: Methodology and state-of-the-art. *Energy Build.* 55 (2012) 889-902.
- [123] F. Ascione, N. Bianco, R.F De Masi, G.P. Vanoli, Rehabilitation of the building envelope of hospitals: Achievable energy savings and microclimatic control on varying the HVAC systems in Mediterranean climates, *Energy Build.* 60 (2013) 125-138.
- [124] F. Ascione, N. Bianco, F. de Rossi, G.P. Vanoli, Transient heat transfer through walls and thermal bridges. Numerical modelling: Methodology and validation. In *Proceedings of the 2012 winter simulation conference*, Berlin, December 2012.
- [125] F. Ascione, N. Bianco, F. de Rossi, G. Turni, G.P. Vanoli, Different methods for the modelling of thermal bridges into energy simulation programs: Comparisons of accuracy for flat heterogeneous roofs in Italian climates, *Appl. Energy* 97(2012) 405–418.
- [126] A. Piacentino, C. Barbaro, F. Cardona, R. Gallea, E. Cardona, A comprehensive tool for efficient design and operation of polygeneration-based energy μ grids serving a cluster of buildings. Part I: Description of the method, *Applied Energy* 111 (2013) 1204–1221.
- [127] ASHRAE Handbook - Heating, Ventilating, and Air-Conditioning Systems and Equipment (I-P Edition), (2012). American Society of Heating, Refrigerating and Air-Conditioning Engineers, Inc. Available at: www.knovel.com. Last access of authors: June 30th, 2013.
- [128] A. Meybodi, M. Behnia, Impact of carbon tax on internal combustion engine size selection in a medium scale CHP system, *Appl Energy* 88 (2011) 5153-5163.
- [129] Microsoft Office, Software Excel, Office 2007, Microsoft Corporation. Available at: www.microsoft.com/it-it/default.aspx. Last access of authors: June 30th, 2013.

LIST OF FIGURES

INTRODUCTION

Figure A. Sankey diagram of energy conversion processes. 7

CHAPTER 1

Figure 1.1. System configuration..... 20

Figure 1.2. The AISIN-SEIKI micro-cogenerator. 20

Figure 1.3. Thermal recovery circuit of the AISIN MCHP. 22

Figure 1. 4. Analyzed thermal energy storage..... 23

Figure 1.5. Cogeneration model control volumes..... 26

Figure 1.6. Energy balance for the generic node i 36

Figure 1.7. Diagram showing experimental plant installed in the laboratory of University of Sannio (Italy). 37

Figure 1.8. Connections and dimensional characteristics of TES [66]..... 38

Figure 1.9. Temperature profile measured during cool-down test..... 44

Figure 1.10. Heat loss coefficient for each node as a function of the cool down test duration..... 46

Figure 1.11. Heat loss coefficient of the node 2-7 and of bottom surface as a function of cool down test duration. 47

Figure 1.12. Comparison between measured and simulated temperature for a charge test of the TES..... 48

Figure 1.13. Comparison of measured and simulated temperature for a charge test of the TES after optimization..... 49

Figure 1.14. Measured and simulated heat transfer from the water to the heat exchanger. 52

Figure 1.15. Measured and simulated temperature in a charge test with lower heat exchanger. 53

Figure 1.16. Illustrative scheme of the analyzed solar thermal system..... 54

Figure 1.17. Micro-cogeneration system..... 63

Figure 1.18. Electrical load profile for residential user (Benevento). 64

Figure 1.19. Electrical load profile for office user (Benevento). 65

Figure 1.20. Control scheme of the experimental plant at the University of Sannio. 66

Figure 1.21. Comparison between the proposed system (PS) and the traditional system (TS).....	67
Figure 1.22. Control algorithm of micro-polygeneration system.....	70
Figure 1.23. Energy, environmental and economic analysis for the analyzed system.	72
Figure 1.24 SPB in case of reduced purchasing costs of energy vectors.....	73
Figure 1.25. Residential building.	76
Figure 1.26. Daily profile of active occupants for each type of residential user.....	77
Figure 1.27. Daily electric demand for each type of residential user.	78
Figure 1.28. Hot water demand profile for residential user in the first week of year.....	79
Figure 1.29. Duration diagram of the space heating load for residential buildings.....	80
Figure 1.30. Electric load profile for office user.	81
Figure 1.31. Number of occupants for the office building in a work day.....	81
Figure 1.32. Duration diagram of the space heating load for the office building.....	82
Figure 1.33. Duration diagram of the space heating load for the two buildings in load sharing approach.....	83
Figure 1.34. System configuration.....	84
Figure 1.35. Simulation results for the users located in Napoli in a typical winter day....	86
Figure 1.36. Simulation results for the users located in Torino in a typical winter day....	87
Figure 1.37. Energy, environmental and economic analysis.....	90
Figure 1.38. SPB as function of the percentage of self-consumed electricity.....	91
Figure 1.39. Daily profile of active occupants.	96
Figure 1.40. Daily electric demand.	97
Figure 1.41. Hot water demand profile for the semidetached house in the first week of year.....	97
Figure 1.42. Duration diagram of the space heating load for the semidetached house. .	98
Figure 1.43. a) Interactions between building and MCHP plant; b) MCHP plant.....	99
Figure 1.44. Thermal load of the semidetached house and thermal power provided by boiler and MCHP for the user located in Napoli (left) and Torino (right) in a typical winter day.	101
Figure 1.45. Electric power required by the user, sold to and purchased from the electric grid for different daily driving distances with normal charging strategy in Napoli.	102

Figure 1.46. Electric power required by the user, sold to and purchased from the electric grid for different daily driving distance with optimized charging strategy in Napoli.	103
Figure 1.47. Electric power required by the user, sold to and purchased from the electric grid for different daily driving distances with normal charging strategy in Torino.	104
Figure 1.48. Electric power required by the user, sold to and purchased from the electric grid for different daily driving distances with optimized charging strategy in Torino.	104
Figure 1.49. PES and $\Delta\text{CO}_{2\text{eq}}$ (percentage and absolute values) as a function of EV daily driving distance for the two charging strategies and for the two locations.	107
Figure 1.50. Operation cost reduction of the PS with respect to CS in the two different locations and for different charging strategy.....	108
CHAPTER 2	
Figure 2.1. System configuration of case 1.....	113
Figure 2.2. System configuration of case 2.....	113
Figure 2.3. System configuration of case 3.....	114
Figure 2.4. System configuration of case 4.....	115
Figure 2.5. System configuration of case 5.....	115
Figure 2.6. Hot water profile for residential user in the first week of the simulated year.	120
Figure 2.7. Hot water profile for an office user in a week day.....	120
Figure 2.8. Electric load profiles for weekday, Saturday and Sunday (residential user).	121
Figure 2.9. Electricity and natural gas “consumption”	126
Figure 2.10. Primary Energy Saving and avoided $\text{CO}_{2\text{eq}}$ emissions with respect to the case 1 (on the right); operational cost and operational cost reduction with respect to the case 1 (on the left).	127
CHAPTER 3	
Figure 3. 1. Flowchart of the proposed methodology.....	132
Figure 3.2. Urban Energy Map of the Benevento: Heating (a) and cooling (b) periods' performances.	137

Figure 3.3. Allocation of thermal power plant and extension of thermal micro-grid.....	138
Figure 3.4. Example of cumulative load profile for a type day.	139
Figure 3.5. CHP thermal circuit.....	142
Figure 3.6. Outcomes derived by the increment of CHP system capacity.....	146

LIST OF TABLES

CHAPTER 1

Table 1.1. MCHP manufacturer data [41].....	21
Table 1.2. MCHP model parameters.	30
Table 1.3. Characteristics of measuring instruments installed in the laboratory.	39
Table 1.4. Model parameters.	39
Table 1.5. input variables of the model.....	42
Table 1.6. overall heat transfer coefficient for heat losses for each node.	46
Table 1.7. heat loss coefficient with a volume of 986 L.	49
Table 1.8. statistical index for the two value of the volume of the storage.	50
Table 1.9. Main component used in the TRNSYS model.	54
Table 1.10. Simulation results on annual basis.	55
Table 1.11. Comparison between the reference case and the other ones.....	56
Table 1. 12. Primary energy and CO _{2eq} emission factors for natural gas and electricity. .	59
Table 1.13. Natural gas costs and tax in Italy.	60
Table 1.14. Electricity costs for a residential and an office user.....	61
Table 1.15. Main characteristics of the considered building.	63
Table 1.16. Building envelope characteristics.	63
Table 1.17. Simulation results during the heating period.....	71
Table 1.18. Main characteristics of building envelope.....	75
Table 1.19. Energy simulations results on annual basis.....	88
Table 1.20. Main characteristics of building envelope [88] [89].....	94
Table 1.21. Electricity demand for EV charging as function of EV daily driving distance.	101
Table 1.22. Energy simulations results for heating period in Napoli and Torino.....	105
Table 1.23. Electricity user demand and electricity exchange between building and electric grid as a function of daily driving distance with normal and optimized charging strategy in Napoli and Torino.....	106

CHAPTER 2

Table 2.1. Main TRNSYS model “type” used in the simulation.	118
Table 2.2. Building envelope characteristics.	119

Table 2.3. Capacities of the main components.	122
Table 2.4. Investment costs estimation for each component.....	125
Table 2.5. Economic analysis.	128

CHAPTER 3

Table 3.1. Input parameters and relative sources.....	134
Table 3.2. Comparison with simulation results.....	135
Table 3.3. Comparison with the energy bills.....	135
Table 3.4. Main building information.	138
Table 3.5. Physical characteristics of the thermal micro-grid.	140
Table 3.6. Simulation results.....	144